People's Democratic Republic of Algeria
Ministry of Higher Education and Scientific Research
University of 8 Mai 1945Guelma

Institute of Telecommunications
Department of Telecommunication Systems
Laboratory of Telecommunications (LT)

Thesis

In view of obtaining the Doctorate degree in 3rd cycle

Domain: **Sciences and Technology** Field: **Telecommunications**
Speciality: **Telecommunications**

Presented by:

GUETAF Bilal

Entitled

Design of a New Antenna for Biomedical Applications

Defended on: 03/07/2024 In front of the board of examiners composed of:

Mr Abdesselam BABOURI	Professor	Univ. of 8 Mai 1945, Guelma	President
Mr Abdelhalim CHAABANE	MCA	Univ. of 8 Mai 1945, Guelma	Supervisor
Mr Abderrezak KHALFALLAOUI	MCA	Univ. of 8 Mai 1945, Guelma	Co- supervisor
Mr Sami BEDRA	Professor	Univ. of Abbas Laghrour, Khenchela	Examiner
Mr Ahcene BOUALLEG	Professor	Univ. of 8 Mai 1945, Guelma	Examiner

Academic year: 2023/2024

Acknowledgement

Above all, I offer thanks to ***Allah*** *for His blessings and the opportunity to pursue this program of study, recognizing that there are individuals unable to pursue their educational aspirations due to circumstances beyond their control.*

I want to convey my gratitude to my supervisor, Dr. ***Abdelhalim Chaabane****, a teacher at Université 8 Mai 1945 - Guelma, and my co-supervisor, Dr.* ***Abderrezak Khalfallaoui****, also a teacher at Université 8 Mai 1945 - Guelma. I appreciate their support, the confidence they have placed in me, and the constructive feedback they have provided during this academic journey.*

I express my sincere gratitude to the jury members, Prof. ***Abdesselam Babouri*** *from the University 8 Mai 1945 - Guelma, Prof.* ***Sami Bedra*** *from the University Abbas Laghrour - Khenchela, and Prof.* ***Ahcene Boualleg*** *from the University 8 Mai 1945 - Guelma, for their meticulous evaluation of the thesis and their valuable insights.*

A heartfelt appreciation to the faculty members of the Department of Telecommunications at the University 8 Mai 1945 - Guelma, for their excellent teaching, as well as to my fellow doctoral students.

I cannot conclude my acknowledgments without expressing my sincere gratitude to my parents and sisters for their unwavering support and constant belief in me. To my colleagues and friends, who have helped me and wished me well along the way.

Abstract

In the current era, antennas play a significant role in advancing biomedical engineering to enhance both health and quality of life. Various healthcare instruments, such as microwave imaging devices, magnetic resonance imaging machines, pacemakers, deep neural implants, endoscopy tools, and clinical instruments for thermal ablation, leverage the advantages of antennas. Antennas can be implanted, placed on the body, or ingested to transmit diagnostic information from the human body to external monitors and, subsequently, to healthcare professionals through the Internet. Additionally, analyzing variations in the electrical and radiation characteristics of antennas, such as near-field electromagnetic radiation, current density, electric field distribution, magnetic field distribution, specific absorption rate and reflection coefficient, enables non-ionizing and non-invasive disease detection. Important applications of antennas include the detection of brain and breast tumors, and brain strokes.

Circularly polarized (CP) antennas significantly enhance the efficiency of radar systems in medical microwave imaging by mitigating indoor multi-path effects and accommodating various body postures. They also minimize polarization mismatch losses, penetrate lossy dielectric materials in human body tissues, and ensure reliable detection of pathological tissue without being constrained by antenna orientation. While numerous antennas have been documented for biomedical applications, existing ones typically utilize linear polarization and serve a singular purpose, whether for tumor screening, stroke detection, or health-monitoring. Hence, there is a need for innovative high-performance antennas capable of addressing a variety of biomedical applications.

This thesis introduces a mono-static circularly polarized printed monopole antenna (CPPMA) with dimensions of $34 \times 28 \times 1.5$ mm^3, designed for applications in the Industrial, Scientific, and Medical (ISM) band. The proposed CPPMA is intended for use in medical microwave imaging and wearable health monitoring applications. Its capabilities include the detection of brain strokes and breast tumors at different positions with various sizes. Additionally, the CPPMA holds potential for deployment in remote health-monitoring systems due to its operation in the ISM band and CP properties.

Keywords: *Antennas for biomedical applications, breast cancer detection, brain stroke detection, medical microwave imaging and health-monitoring applications.*

Résumé

À l'heure actuelle, les antennes jouent un rôle significatif dans l'avancement de l'ingénierie biomédicale en vue d'améliorer à la fois la santé et la qualité de vie. Divers instruments de soins de santé tels que les dispositifs d'imagerie médicale par micro-ondes, les appareils d'imagerie par résonance magnétique, les stimulateurs cardiaques, les implants neuronaux profonds, les outils d'endoscopie et les instruments cliniques d'ablation thermique tirent parti des avantages des antennes. Les antennes peuvent être implantées, placées sur le corps ou ingérées pour transmettre des informations diagnostiques du corps humain à des moniteurs externes, puis aux professionnels de la santé via Internet. De plus, l'analyse des variations des caractéristiques électriques et de rayonnement des antennes, telles que le rayonnement électromagnétique en champ proche, la densité de courant, la distribution du champ électrique, la distribution du champ magnétique, le taux d'absorption spécifique et le coefficient de réflexion, permet la détection de maladies de manière non ionisante et non invasive. Les applications importantes des antennes incluent la détection des tumeurs du sein et du cerveau, ainsi que des accidents vasculaires cérébraux (AVC).

Les antennes à polarisation circulaire améliorent les performances des systèmes radar d'imagerie médicales par micro-ondes en réduisant les effets de multi-trajet en intérieur et les postures corporelles, en diminuant les pertes de désalignement de polarisation, et en pénétrant les matériaux diélectriques absorbants des tissus du corps humain, et assurent une détection fiable des tissus pathologiques sans être contraintes par l'orientation de l'antenne. Bien que de nombreuses antennes aient été documentées pour des applications biomédicales, celles existantes utilisent généralement une polarisation linéaire et servent à un seul but, que ce soit pour le dépistage du cancer, la détection des AVC, ou la surveillance de la santé. Il existe donc un besoin d'antennes innovantes et performantes capables de répondre à diverses applications biomédicales.

Cette thèse présente une antenne monopôle imprimée à polarisation circulaire avec des dimensions de 34 $\times$ 28 $\times$ 1,5 mm^3, conçue pour des applications dans la bande industrielle, scientifique et médicale (ISM). L'antenne proposée est destinée à être utilisée dans l'imagerie médicale par micro-ondes et les applications de surveillance de la santé portable. Ses capacités incluent la détection de tumeurs du sein et d'AVC de différentes tailles à des positions différentes. De plus, L'antenne proposée présente un potentiel de déploiement dans les systèmes de surveillance de la santé à distance en raison de son fonctionnement dans la bande ISM et de ses propriétés de polarisation circulaire.

Mots clés: *Antennes pour les applications biomédicales, détection du cancer du sein, détection des AVC, imagerie médicale par micro-ondes et applications de surveillance de la santé.*

ملخص

تُعتبر الهوائيات في العصر الحالي عنصرًا بارزًا في تقدم الهندسة الطبية الحيوية، بهدف تحسين الصحة وجودة الحياة. تستفيد أدوات الرعاية الصحية المختلفة، مثل أجهزة التصوير بالميكروموجة وأجهزة التصوير بالرنين المغناطيسي، وأجهزة تنظيم ضربات القلب، والمزروعات العصبية العميقة، وأدوات التنظير، والأدوات السريرية للاستئصال الحراري، من مزايا الهوائيات. يمكن زرع الهوائيات أو وضعها على الجسم أو ابتلاعها لنقل المعلومات التشخيصية من جسم الإنسان إلى أجهزة المراقبة الخارجية، وبالتالي إلى المتخصصين في الرعاية الصحية عبر الإنترنت. بالإضافة إلى ذلك، فإن تحليل الاختلافات في الخصائص الكهربائية والإشعاعية للهوائيات، مثل الإشعاع الكهرومغناطيسي القريب، وكثافة التيار، وتوزيع المجال الكهربائي، وتوزيع المجال المغناطيسي، ومعدل الامتصاص المحدد ومعامل الانعكاس، يتيح اكتشاف الأمراض بطريقة غير مؤينة وغير جراحية. وتشمل التطبيقات الهامة للهوائيات الكشف عن أورام الثدي والدماغ، والسكتات الدماغية.

تعمل الهوائيات المستقطبة دائريًا على تعزيز كفاءة أنظمة الرادار بشكل كبير في التصوير الطبي بالميكروموجة عن طريق تخفيف تأثيرات المسارات المتعددة الداخلية واستيعاب أوضاع الجسم المختلفة. كما أنها تقلل من خسائر عدم تطابق الاستقطاب، وتخترق المواد العازلة الخاسرة في أنسجة الجسم البشري، وتضمن الكشف الموثوق عن الأنسجة المرضية دون التقيد بتوجيه الهوائي. ورغم وجود العديد من الهوائيات الموثقة للاستخدام في التطبيقات الطبية الحيوية، إلا أن هذه الهوائيات غالبًا ما تستخدم الاستقطاب الخطي وتخدم غرضًا فريدًا، سواء الكشف عن السرطان أو السكتة الدماغية أو مراقبة الصحة. وبالتالي، هناك حاجة ملحة إلى هوائيات مبتكرة ذات أداء عالي قادرة على التعامل مع مجموعة متنوعة من التطبيقات الطبية الحيوية.

تقدم هذه الأطروحة هوائيًا أحادي القطب مطبوعًا مستقطبًا دائريًا بأبعاد 34 × 28 × 1.5 ملم^3، مصمم للتطبيقات في النطاق الصناعي والعلمي والطبي .تم تصميم الهوائي المقترح للاستخدام في التصوير الطبي بالميكروموجة وتطبيقات مراقبة الصحة القابلة للارتداء. وتشمل قدراته الكشف عن أورام الثدي والسكتات الدماغية بأحجام مختلفة وفي مواقع مختلفة. بالإضافة إلى ذلك، يتيح الهوائي المقترح إمكانية استخدامه في أنظمة مراقبة الصحة عن بعد بسبب تشغيله في نطاق الصناعي والعلمي والطبي، مع خاصية الاستقطاب الدائري.

الكلمات المفتاحية: الهوائيات للتطبيقات الطبية الحيوية، الكشف عن سرطان الثدي، الكشف عن سكتات الدماغ، التصوير الطبي بالميكروموجة، وتطبيقات المراقبة الصحية عن بعد.

Contents

List of Figures

List of Tables

Abbreviations and Acronyms

< **5G** > < fifth Generation >

< **AR** > < Axial Ratio >

< **BANs** > < Body Area Networks >

< **BAT** > < Brown Adipose Tissue >

< **BW** > < bandwidth >

< **CAD** > < Computer-aided Design >

< **CP** > < Circularly Polarized >

< **CPPMA** > < Circularly Polarized Printed Monopole Antenna >

< **CPW** > < Coplanar Waveguide >

< **CRT** > < Cardiac Resynchronization Therapy >

< **CST** > < Computer Simulation Technology >

< **CT** > < Computed Tomography >

< **DBS** > < Deep Brain Stimulation >

< **ECC** > <Electronic Communication Committee >

< **ECG** > < Electrocardiogram >

< **EEG** > < Electroencephalogram >

< **EIRP** > < Equivalent Isotropically Radiated Power >

< **EM** > < Electromagnetic >

< **EMG** > < Electromyogram >

< **FCC** > < Federal Communications Commission >

< **FDTD** > < Finite Difference Time Domain >

< **FEKO** > < Feldberechnung bei Körpern mit beliebiger Oberfläche >

< **FEM** > < Finite Element Method >

< **GEHC** > < General Electric Healthcare >

< **HCC** > < Hepatocellular Carcinoma >

< **HFSS** > < High Frequency Structure Simulator >

< **ICD** > < Implantable Cardioverter Defibrillators >

< **ICNIRP** > < International Commission on Non-Ionizing Radiation Protection >

< **IEEE** > < Institute of Electrical and Electronics Engineers >

< **IMDs** > < Implantable Medical Devices >

< **ISM** > < Industrial, Scientific and Medical >

< **LHCP** > < Left-Hand Circularly Polarized >

< **LPPMA** > < Linearly Polarized Printed Monopole Antenna >

< **MBANs** > < Medical Body Area Networks >

< **MDRC** > < Medical Device Radio Communication >

< **MI** > < Microwave Imaging >

< **MICS** > < Medical Implant Communications System >

< **MMNs** > < Medical Micropower Networks >

< **MNM** > < Multiport Network Model >

< **MoM** > < Method of Moments >

< **MR** > < Magnetic Resonance >

< **MRI** > < Magnetic Resonance Imaging >

< **MWR** > < Microwave Radiometry >

< **MWT** > < Microwave Tomography >

< **OGIB** > < Obscure Gastrointestinal Bleeding >

< **PET** > < positron emission tomography >

< **PPG** > < Photoplethysmogram >

< **RF** > < Radio Frequency >

< **RHCP** > < Right-Hand Circularly Polarized >

< **SAR** > < Specific Absorption Rate >

< **SDT**> < Spectral Domain Technique >

< **SPECT-CT** > < Single Photon Emission Computed Tomography-Computerized Tomography >

< **SPO2** > < Blood Oxygen Saturation >

< **SRD** > < short-Range Devices >

< **TLM** > < Transmission Line Model >

< **TSAR**> < Tissue Sensing Adaptive Radar >

< **TUMT** > < Transurethral Microwave Thermotherapy >

< **ULP-AMI-P** > < Ultra Low Power Active Medical Implant and Peripheral >

< **ULP-WMCE** > < Ultra Low Power Wireless Medical Capsule Endoscopy >

< **UWB** > < Ultra Wide Band >

< **VSWR** > < Voltage Standing Wave Ratio >

< **WBAN** > < Wireless Body Area Networks >

< **WiMAX** > < World Interoperability for Microwave Access >

< **WMTS** > < Wireless Medical Telemetry Services >

General Introduction

Antennas in medical applications are specialized devices that transmit or receive electromagnetic signals, enabling a variety of functions crucial to modern healthcare. These functions include medical imaging, wireless communication with implants, therapeutic applications, and real-time monitoring of physiological parameters [1].The unique challenges presented by the human body, such as tissue absorption and reflection characteristics, have led to the development of antennas specifically tailored for medical use [2].

In the mid-20th century, researchers began exploring the use of microwaves for medical imaging. Antennas designed for microwave tomography contributed to imaging techniques based on the interaction of microwaves with biological tissues [3]

The development of Magnetic Resonance Imaging (MRI) introduced the use of radiofrequency (RF) antennas. RF antennas play a critical role in MRI systems by transmitting RF pulses and receiving signals to create detailed images of internal structures [1].

Antennas became integral components in implantable medical devices, such as implantable cardioverter-defibrillators (ICDs) and pacemakers, allowing for wireless communication with external devices [4].

The rise of wearable health devices led to the integration of antennas for wireless telemetry. Antennas in wearables enable the real-time transmission of health data to external monitoring systems [5].

Antennas are employed in therapeutic applications, such as radiofrequency ablation and hyperthermia, delivering targeted electromagnetic energy for treating conditions like tumors [6].

Antennas are utilized in wireless capsule endoscopy, allowing for both wireless communication and imaging within the digestive tract [1].

Ongoing research explores the use of advanced antenna technologies in emerging medical applications, including non-invasive sensing and imaging techniques [1].

The evolution of antennas in medical applications has been marked by continuous innova-

tion, driven by the need for more precise, non-invasive, and patient-friendly healthcare solutions. As technology progresses, we can anticipate further advancements in antenna design and applications, playing a pivotal role in shaping the future of medical diagnostics, treatments, and monitoring.

The primary motivation for this work within the scope of this thesis is the design of a new antenna tailored for biomedical applications: medical microwave imaging (MI) and health monitoring. This antenna is characterized by its compact size, a stable radiation pattern offering good gain and efficiency, high sensitivity to detect the location and size of tumors and strokes, as well as the highest possible depth of body penetration.

In general, our thesis is structured into four chapters, and each of them is detailed in the following paragraphs.

In the first chapter1, we will provide basic concepts about antennas, including their characteristics such as reflection coefficient, radiation pattern, directivity, gain, etc. Microstrip antennas are generally described, covering their advantages and limitations, applications, feeding techniques, and radiation mechanisms. A brief overview of microstrip antenna analysis methods will be discussed at the end of the chapter.

In the second chapter2, we will explore the critical role of antennas in various biomedical engineering devices, emphasizing their strategic placement on, within, or near the human body for diagnostic or therapeutic purposes. The text highlights the challenges posed by physical limitations and the impact of the human body's characteristics on antenna design and performance. Specifically, it focuses on the complex interplay between antennas and biological tissues, addressing factors such as human body effects on antenna performance, radiation antenna effects on the human body, authorized operating frequency ranges for wireless medical applications, and models of the human body. The chapter aims to delve into these key factors, recognizing the intricate relationship between antenna design and the diverse characteristics of the human body in biomedical applications.

In the third chapter3, we will discuss the current emphasis on advancing medical applications through microwave techniques, highlighting the crucial role of antennas in diagnostics, biomedical telemetry, and therapeutic applications. Conventional diagnostic technologies, such as MRI and Computed Tomography (CT) scans, face limitations in terms of accessibility, risks, and discomfort. In contrast, microwave techniques offer non-ionizing electromagnetic waves, providing less detrimental alternatives with superior tissue penetration and high-resolution imaging. Microwave applications extend to therapeutic interventions, leveraging heat to treat abnormal tissues with heightened sensitivity and efficacy. With rising healthcare costs, there

is a growing interest in leveraging emerging wireless technologies for cost-effective remote patient monitoring. Wireless Body Area Networks (WBANs) emerge as promising technologies, utilizing miniature sensors as intelligent patch antennas for affordable and efficient healthcare solutions. WBANs enable healthcare professionals to securely monitor patients' health, offering continuous tracking of vital signs and environmental parameters. Collected data can be transmitted to a centralized repository, allowing remote access for evaluation and issuing alerts to patients through various means.

In the fourth chapter4, we propose a CPPMA designed for applications in health-monitoring and medical MI. The designed CPPMA is specifically optimized for operation within the ISM band. We fabricate a prototype of the antenna on a cost-effective FR-4 substrate, featuring a compact dimension of $34 \times 28 \times 1.5$ mm^3. Simulations reveal that the proposed CPPMA operates effectively between 2.425 GHz and 2.475 GHz, and experimental measurements cover the range of 2.32 GHz to 2.515 GHz. Furthermore, the designed CPPMA demonstrates CP performance at 2.45 GHz (ranging from 2.4386 GHz to 2.4633 GHz). We confirm the CPPMA's suitability for MI by evaluating its capacity to detect brain strokes and breast tumors. The antenna exhibits a high detection capability for strokes and tumors of various sizes placed at different positions, showcasing sensitivity to anomalies or changes in the dielectric properties of human tissues. Additionally, we experimentally validate the CPPMA's utility for wearable applications, and we observe excellent agreement between simulated and measured results.

We will conclude our manuscript with a general conclusion and perspectives.

List of Publications

Journal Papers

1. Bilal GUETAF, Abdelhalim CHAABANE, Abderrezak KHALFALLAOUI, Hussein ATTIA, "Narrow-band Circularly Polarized Antenna for Medical Microwave Imaging and Health Monitoring Applications," Applied Computational Electromagnetics Society Journal, 2023, vol. 38, no 6. https://doi.org/10.13052/2023.ACES.J.380607.

Chapter 1

Antennas: Introduction and Generalities

Contents

1.1 Introduction

An antenna is a metallic device that is used to radiate or receive radio waves. It acts as a transitional component between free space and guiding devices, such as a coaxial line and a waveguide, which are used for transferring electromagnetic (EM) signals generated by the transmission sources to the antennas or from the antennas to the receiving device, as shown in **Figure 1.1**.

Thereby, a transmitting antenna is used to send radio waves, and a receiving antenna is used to receive them [7].

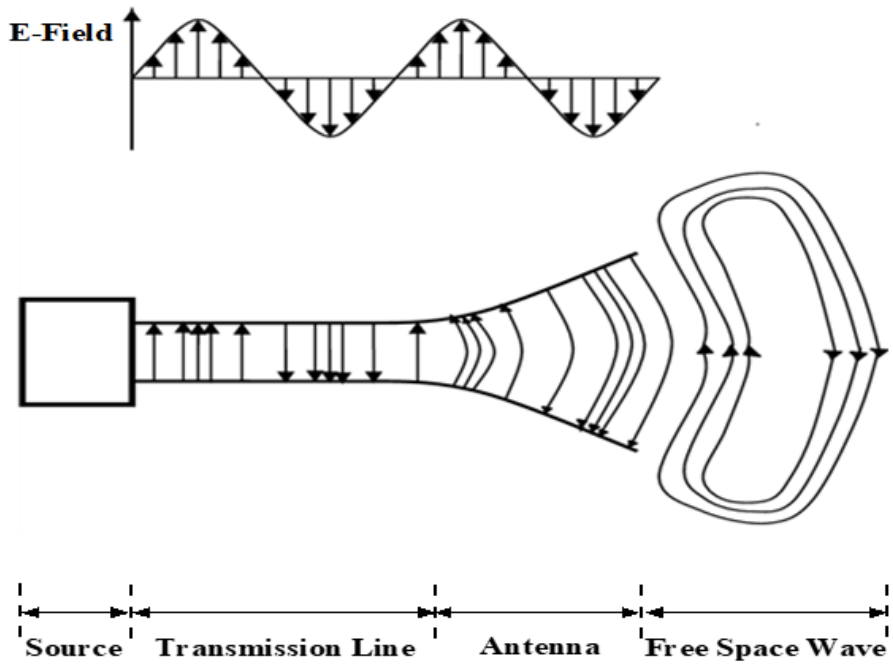

Figure 1.1: Antenna as a transitional device [7].

To understand how an antenna radiates, it is important to understand how radiation occurs in the first place. When a conducting wire experiences a time-varying current or experiences acceleration (or deceleration) of charge, radiation will occur. However, if there is no motion of charges, no radiation takes place. Even with charges moving at uniform velocity along a straight wire, radiation will not happen. But if the same charges move with uniform velocity along a curved or bent wire, radiation will occur. Finally, when a charge is oscillating with time, even a straight wire will produce radiation, as clarified by Balanis [7].

Understanding antenna radiation is facilitated by **Figure 1.1**, depicting a voltage source linked to a two-conductor transmission line. Applying a sinusoidal voltage across the transmission line produces a sinusoidal electric field (E-field). This E-field gives rise to tangential electric lines of force, and their clustering indicates the electric field's intensity. The motion of free electrons on the conductors is influenced by these lines, resulting in a current that generates a magnetic field (H-field).

As the sinusoidal source consistently generates an electric disturbance, it leads to the continuous generation of electromagnetic waves. These waves travel through the transmission line and extend beyond the antenna into free space. Within the transmission line and the antenna, charges sustain these EM waves. However, upon entering free space, the waves take the form of closed loops and undergo radiation [7]

In order to measure and describe the performance of an antenna, various parameters must be defined. While some of these parameters are interconnected, not all of them need to be

specified for a full understanding of how the antenna works. In this chapter, we will provide definitions for these parameters. Then we introduce the technology of printed antennas (microstrip antennas), their applications, feeding techniques, the mechanism of radiation, and different analysis techniques encompassing both analytical and numerical methods. In the last part of this chapter, we explore the advantages and disadvantages of microstrip patch antennas.

1.2 Properties and Characteristics of Antennas

Many parameters have been defined to account for the electrical and electromagnetic properties of antennas. Generally, antennas are characterized by considering the properties related to the associated electrical circuit, such as voltage standing wave ratio (VSWR), reflection coefficient, input impedance, and bandwidth, as well as those related to electromagnetic radiation, like the directivity, gain, efficiency, antenna polarization, and radiation pattern.

1.2.1 Electrical Characteristics

- **a. Input Impedance:**

  The input impedance is essential to match the antenna to the generator that powers it, or in reception, to ensure maximum transfer of active power between the feed and the antenna [8]. The input impedance, denoted as Z_{in}, is characterized as the impedance that an antenna presents at its feed point, or the ratio between the voltage and current at this feed point. Typically, the input impedance is a complex number that varies with frequency. It can be mathematically represented as follows:

$$Z_{in} = R_{in} + jX_{in} \tag{1.1}$$

  The actual component of the impedance, represented by R_{in} ,encompasses both the radiation resistance R_{r} responsible for the power emitted by the antenna and the loss resistance R_{L}. The radiation resistance is associated with the power radiated by the antenna, while the loss resistance pertains to the energy dissipated within the antenna, accounting for losses in dielectric materials, antenna conductor losses, and similar factors. X_{in} is the reactance of antenna [9].

- **b. Reflection Coefficient and Return Loss:**

  The antenna's input impedance should match the characteristic impedance of the connected transmission line at its feed point, typically utilizing a $50\,\Omega$ cable. When the antenna's input impedance deviates from $50\,\Omega$, it results in an impedance mismatch at the feed point, potentially causing signal reflections. In this scenario, some signals sent to the antenna may be reflected back to their sources.

  The reflection coefficient, symbolized by Γ, indicates the proportion of the reflected wave's voltage to that of the incident wave. This coefficient at the antenna's feed point correlates with the antenna input impedance through the subsequent equation [10]:

$$\Gamma = \frac{Z_{in} - Z_0}{Z_{in} + Z_0} \tag{1.2}$$

  In the given equation 1.2, Z_0 and Z_{in} represent the characteristic impedance of the transmission line connected to its feed point and the input impedance of the antenna, respectively. It is observed that when Z_{in} equals Z_0, the reflection coefficient becomes zero; consequently, the incident wave is completely absorbed, and it is said that there is adaptation.

  The return loss represents the power lost or reflected due to an improperly matched load. For an optimally designed antenna, the desired return loss should typically be at least 10 dB, and can be calculated by:

$$RL = -20\ log\,|\Gamma| = -10\log|\Gamma|^2\,[\text{dB}] \tag{1.3}$$

- **c. Voltage Standing Wave Ratio (VSWR):**

  VSWR (Voltage Standing Wave Ratio, also known as Standing Wave Ratio) is the ratio of the maximum voltage V_{max} to the minimum voltage V_{min} on the transmission line. It can be mathematically defined by the reflection coefficient (Γ) as follows.

$$VSWR = \frac{V_{max}}{V_{min}} = \frac{1 + |\Gamma\ |}{1 - |\Gamma\ |} \tag{1.4}$$

  The VSWR ranges from 1 to infinity ($1 \leq$ VSWR $\leq \infty$). In the case of an optimal antenna, the VSWR is 1.0, indicating that no power is reflected back. An antenna with a VSWR between 1.0 and 2.0 is deemed high-performing.

- **d. Bandwidth:**

  The antenna's bandwidth is described as "the range of frequencies within which the performance of the antenna, with respect to some characteristic, conforms to a specified standard" [11]. Generally, the bandwidth is established by the frequency range in which the principal parameters of the antenna meet some criterion, such as ensuring a minimum return loss of 10 dB and a maximum VSWR of 2.0. The bandwidth (BW) may be evaluated by measuring the highest frequency f_{H} and the lowest frequency f_{L} achieved in its range.

$$BW\ \ (Hz) = \ f_H - f_L \tag{1.5}$$

- **e. Antenna Efficiency:**

  The efficiency of an antenna takes into account losses at the input terminals and within the structure of the antenna which are caused by reflection loss due to mismatch between the transmission line and the antenna, as well as conduction and dielectric losses. In general, the overall efficiency can be expressed as [12]

$$e_0 = e_r e_c e_d \tag{1.6}$$

  Where

  e_0 = total efficiency

  e_{r} = reflection (mismatch) efficiency = $1 - |\Gamma|^2$

  e_{c} = conduction efficiency

  e_{d} = dielectric efficiency e_{c} and e_{d} are usually difficult to calculate, but can be determined experimentally. Since it is impossible to separate them through measurements, equation (1.6) is typically written in a more convenient form [7]

$$e_0 = e_r e_{cd} = e_{cd}(1 - |\Gamma|^2) \tag{1.7}$$

  Antenna radiation efficiency, represented by e_{cd} or η, which is used to correlate the directivity and gain [7].

1.2.2 Radiation Characteristics

- **a. Radiation Patterns:**

  The antenna's radiation pattern depicts how radiated power is dispersed in space. This may be represented in a spherical coordinate system by plotting the radiation power according to the elevation angle (θ) or azimuth angle (φ).

  Figure I.2 (a) is a visualisation of the radiation pattern in the elevation plane, showing the main lobe having the greater portion of radiating power, the back lobe emitting in the backward direction, and the side lobes that are smaller-sized. The 3-dB beamwidth represents the angular span between two points where the radiated power is equal to half of the maximum radiated power. The azimuth-plane radiation pattern can be visualized by plotting the radiated power against the azimuth angle (φ) [9].

  Antenna patterns can be classified into three distinct types [9]:

  - **Isotropic patterns:** Isotropic patterns are homogeneous in all directions but do not exist in reality.
  - **Directional patterns:** The majority of the radiated power is concentrated in a single direction, as depicted in **Figure 1.2(a)**, with the most significant radiation occurring along the x-axis.
  - **Omni-directional patterns:** Omni-directional patterns: The antenna exhibits a non-directional pattern within a specific plane, radiating uniformly in all directions around it, forming a complete 360-degree pattern. The omni-directional pattern is illustrated by **Figure 1.2(b)**, which has a donut-shaped pattern.

- **b. Field Regions:**

  The area surrounding an antenna frequently divides into three (3) regions: the far-field (Fraunhofer), radiating near-field (Fresnel), and reactive near-field (Rayleigh), as seen in **Figure 1.3**. The three regions are designated to characterize the field structure in each. There aren't any abrupt changes when moving between each region, though there are still differences among them. The exact boundaries between these regions aren't definite, but there are accepted criteria that can be used to identify them [7, 13].

  - **Reactive near-field (Rayleigh) region:** The region of the near field immediately around the antenna in which the reactive field is dominant is referred to as the reactive

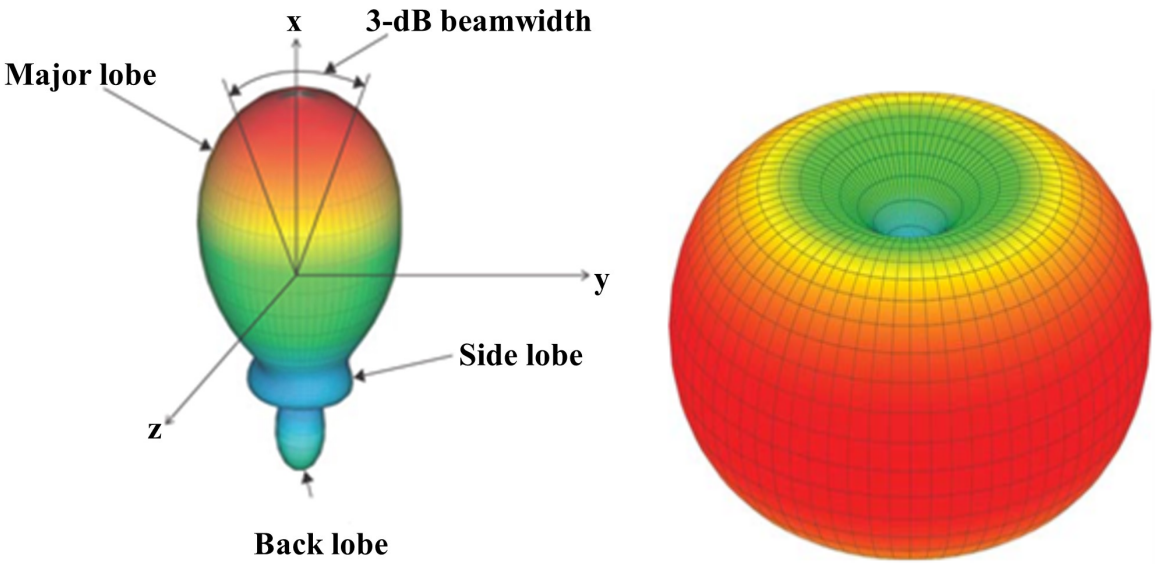

(a) (b)

Figure 1.2: (a) A directional radiation pattern observed in the elevation plane, (b) Omni-directional pattern [9].

near field region. For most antennas, it is usually assumed that the outer boundary of this region exists at a distance of $R < 0.62\sqrt{D^3/\lambda}$ from the antenna surface; where λ represents the wavelength in this case, while D is the largest dimension of the antenna [7].

- **Radiating near-field (Fresnel) region:** The region of the antenna's field located between the reactive near field and the far field regions, where the radiation fields are dominant and the angular field distribution is determined by the distance from the antenna, is the radiating near field region $0.62\sqrt{D^3/\lambda} \leq R < 2D^2/\lambda$. If the antenna's largest dimension is not very large when compared to the wavelength, this region may not be present. For an antenna focused at infinity, this area is sometimes called the Fresnel region due to its similarity to optical terminology [7].
- **Far-field (Fraunhofer) region:** In this region, the field components are predominantly transverse and the angular distribution doesn't depend on the radial distance at which the measurements are taken. The inner boundary is typically assumed to be at a distance of $R = 2D^2/\lambda$, with the outer boundary assumed to be at infinity. The far field region of an antenna that is focused at infinity is sometimes referred to as the Fraunhofer region due to its relation to optical terms [7].

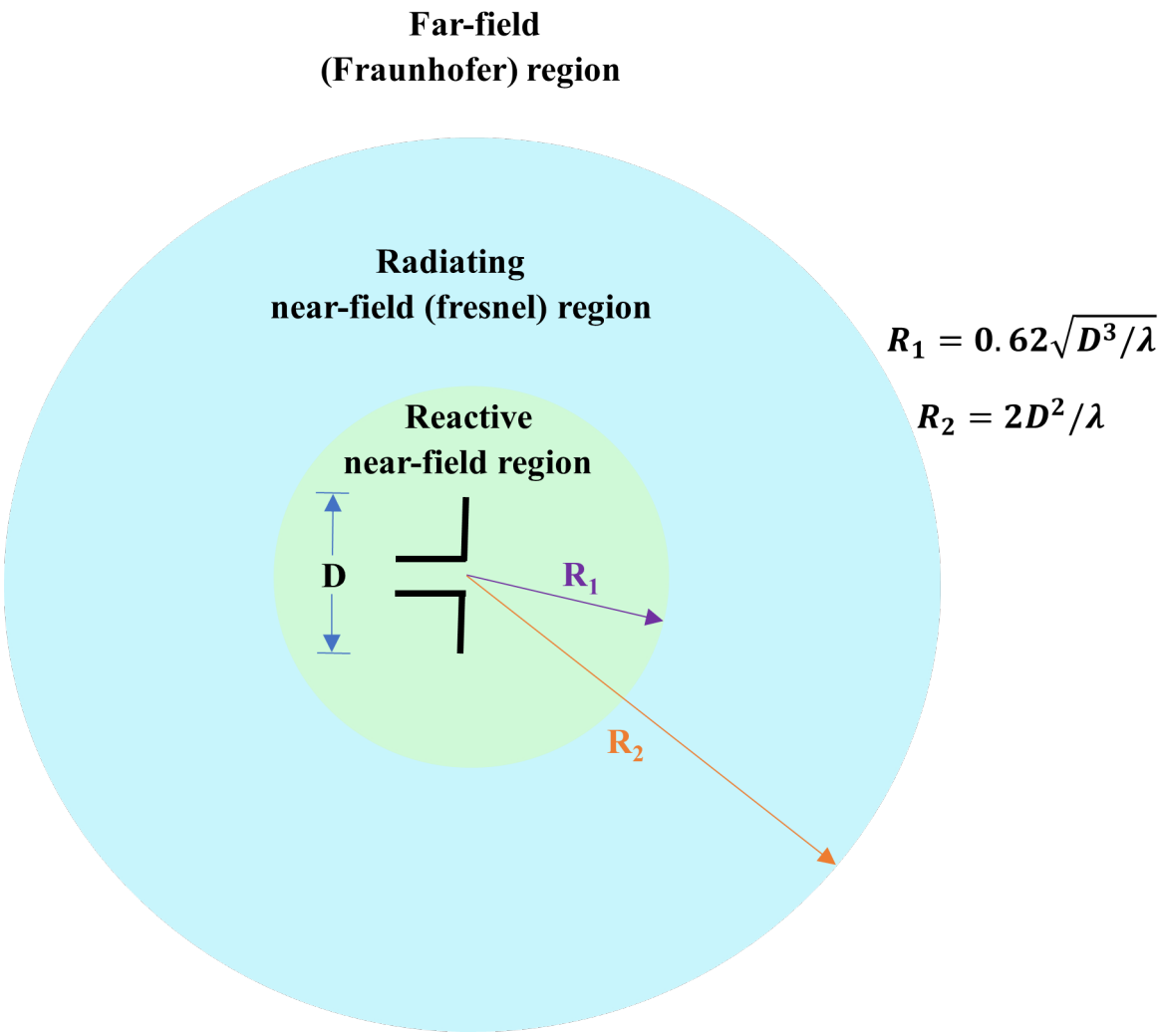

Figure 1.3: Regions of an antenna field[7].

- **c. Directivity and Gain:**

  The directivity function, $D\ (\theta,\ \varphi)$ quantifies the power emitted by an antenna in a specific direction $(\theta,\ \varphi)$ relative to the power emitted by an isotropic radiator in the identical direction [14].

  The power emitted in a particular direction by an isotropic radiator is equivalent to the power emitted in all other directions combined. This power is calculated as $P_t/4\pi$, where P_t represents the total transmitted power, and $P_t/4\pi$ denotes the radiation intensity of the isotropic radiator (The value 4π represents the solid angle of an entire sphere in three-dimensional space) [14].

  Consequently

$$D\ \ (\theta,\ \varphi) = \frac{P(\theta,\varphi)}{P_t/4\pi} \tag{1.8}$$

  Where, $P(\theta,\varphi)$ refers to the power emitted by the real antenna in the specific direction (θ,φ). Therefore, we can compare the power emitted by the real antenna to the power

that would have been emitted by an isotropic radiator, which would distribute the same total power [14].

The directivity, represented by D, is known as the maximum value achieved by the directivity function [14]:

$$D = Max\ [D\ (\theta,\ \varphi)] \tag{1.9}$$

However, in most cases, an antenna's total transmitted power is either unknown or challenging to determine accurately. Hence, a second function called the gain function, denoted as $G\,(\theta,\ \varphi)$, is introduced. The gain function shares similarities with the directivity function, except that it replaces the total radiated power with the total accepted power, P_{in}.

$$G\,(\theta, \varphi) = \frac{P\ (\theta,\ \varphi)}{P_{in}/4\pi} \tag{1.10}$$

P_{in} is more readily evaluated or determined compared to the total radiated power.

The gain function does not consider the impact of impedance mismatch on the antenna terminals. In situations where 99% of the power delivered to the antenna terminals is reflected, the gain function provides insights into the spatial distribution of the remaining 1% of power, which is the accepted power. The gain, denoted as G, represents the maximum value obtained from the gain function [14].

$$G = Max\ [G\ (\theta,\ \varphi)] \tag{1.11}$$

The ratio of gain to directivity is equivalent to the ratio of total radiated power to total accepted power, which is known as the radiation efficiency, denoted as η [14].

$$\eta = \frac{G}{D} = \frac{P_t}{P_{in}} \tag{1.12}$$

When all the accepted power by the antenna is radiated, the efficiency reaches its maximum value ($\eta = 100\%$).

- **d. Polarization and Axial Ratio:**

An antenna's polarisation is dependent on the orientations of the E-fields that it radiates. Polarisation may be categorised into three types: elliptical, circular, or linear[9, 15].

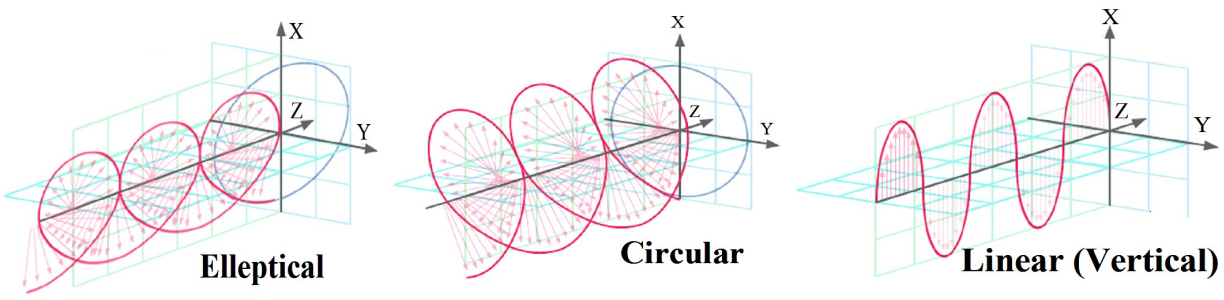

Figure 1.4: Different types of antenna polarization [16].

When a half-wavelength dipole is positioned vertically above the Earth, it generates far-field radiated fields that are predominantly represented by $E_\theta(\theta,\ \varphi)$. In this scenario, the dipole's polarisation is referred to as vertical polarisation. On the other hand, when a half-wavelength dipole is oriented horizontally above the Earth, the far-field radiated E-fields of the antenna are primarily represented by $E_\varphi(\theta,\ \varphi)$. The antenna's polarisation is then known as horizontal polarization. Both horizontal and vertical polarizations belong to the category of linear polarizations [9].

In order to generate circular polarization, it is necessary to have two perpendicular components of E-fields in the far-field region. The E-fields radiated by an antenna can be expressed as:

$$\vec{E}\,(\theta,\varphi) = \vec{\theta}\,E_\theta\,(\theta,\ \varphi)\,e^{j\phi_1} + \vec{\varphi}E_\varphi(\theta,\varphi)e^{j\phi_2} \tag{1.13}$$

In this context, $E_\theta\,(\theta,\ \varphi)$ and $E_\varphi(\theta,\varphi)$ represent the amplitudes of the E-field components in the far-field of the antenna. The variables ϕ_1 and ϕ_2 indicate the phase shifts associated with each field component.

To achieve circular polarisation, the total E-field must consist of two orthogonal components of equal amplitudes ($E_\theta\,(\theta,\ \varphi) =\ E_\varphi(\theta,\varphi)$) and a phase difference of 90° between them ($\phi_2 - \phi_1 = \pm\frac{\pi}{2}$) [9].

In the case of a CP wave, the E-field vector at a specific point in space traces out a circular path over time. By observing the direction of the field's temporal rotation while looking at the wave along its direction of propagation, we can determine the sense of rotation. If the field rotation is in a clockwise direction, the wave is classified as right-hand circularly polarized (RHCP), whereas if the field rotation is counterclockwise, the wave is classified as left-hand circularly polarized (LHCP) [9, 15].

In practice, achieving perfect circular polarization is not feasible, resulting in the traced

curve at a specific position as a function of time usually being an ellipse, as depicted in **Figure 1.5**. Lines a and b illustrate the main and minor axes of the polarization ellipse, respectively. The axial ratio (AR) is the ratio of the main axis to the minor axis of an ellipse [9].

$$AR = \frac{a}{b} \tag{1.14}$$

The AR is an important metric for assessing circular polarization. It is generally recommended to have an AR below 3 dB for a CP antenna.

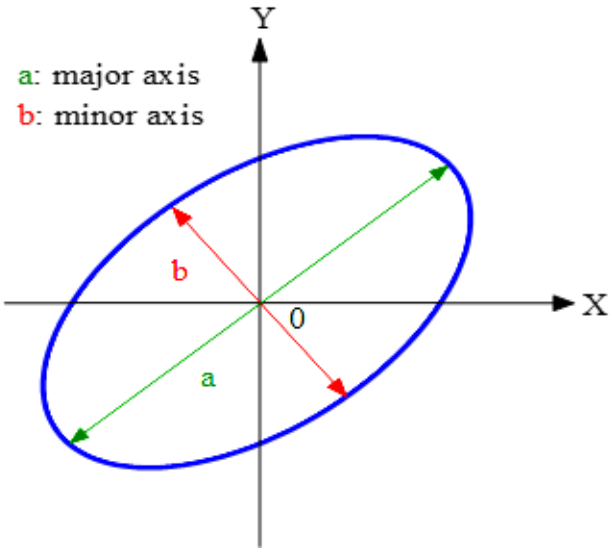

Figure 1.5: Polarization ellipse generated at a specific position as a function of time [9].

1.3 Microstrip Antennas

1.3.1 Introduction

Microstrip antennas, also known as patch antennas, are a popular type of antenna widely used in various applications. They were initially proposed by G. A. Deschamps in 1953, but their practical implementation and widespread use came about in the 1970s when Robert E. Munson and some of his fellow researchers developed them using low-loss substrates [17–19]. Since its inception, this category of antennas has undergone extensive research and development. Advancements have been made in various aspects of microstrip antenna design, aiming to enhance its performance. These developments encompass expanding the bandwidth, minimizing the physical dimensions, mitigating mutual coupling and surface-wave excitation, and enhancing the diversity and reconfigurability of the antenna element [20].

Due to the numerous distinctive and appealing characteristics of microstrip antennas, it is highly likely that they will continue to be extensively utilized in various applications in the future. These properties encompass a low profile, lightweight design, compactness, and compatibility with mounting structures. Additionally, their easy fabrication and seamless integration with solid-state devices further contribute to their advantages. The combined impact of these properties has played a significant role in the success of microstrip antennas, not only in military applications and in commercial domains but also in medical domains. These applications include WBAN, health monitoring, MRI, deep neural implants, clinical instruments for thermal ablation, pacemakers, medical microwave imaging, and endoscopy [1].

1.3.2 Basic Structure

A microstrip antenna is made of an extremely thin metallic patch ($t \ll \lambda_0$, where λ_0 is the free-space wavelength) placed on top of a dielectric substrate ($h \ll \lambda_0$, usually $0.003\lambda_0 \leq h \leq 0.05\lambda_0$) which has a ground plane on the opposite side, as depicted in **Figure 1.6**. Typically, the patch and the feed lines are fabricated through a photoetching process on the dielectric substrate. The radiating patch is usually in the shape of a square, rectangle, or circle, although other geometries can also be used. The patch is commonly constructed from a conductive material like gold or copper, while the dielectric substrate, in some cavity models, is a low-loss material with a permittivity usually in the range of $2.2 \leq \varepsilon_r \leq 12$.

The most desirable substrates for optimal antenna performance are those with larger thickness and lower dielectric constants within the given range. These substrates offer wider bandwidth, improved efficiency, and loosely bound fields to ensure effective radiation into space. However, they require larger element sizes. On the other hand, for microwave circuitry, thin substrates with elevated dielectric constants are preferred. They enable tightly bound fields, minimizing undesired radiation and coupling, and allowing for smaller element sizes. However, they exhibit reduced efficiency, greater losses , and relatively smaller bandwidths. Since microstrip antennas are often integrated with other microwave circuitry, a compromise must be reached to balance antenna performance and circuit design considerations [7].

LP and CP can be obtained using either individual microstrip antennas or arrays of microstrip antennas. Arrays of microstrip elements, equipped with either single or multiple feeds, can also be employed to enable scanning capabilities and enhance directivity [7].

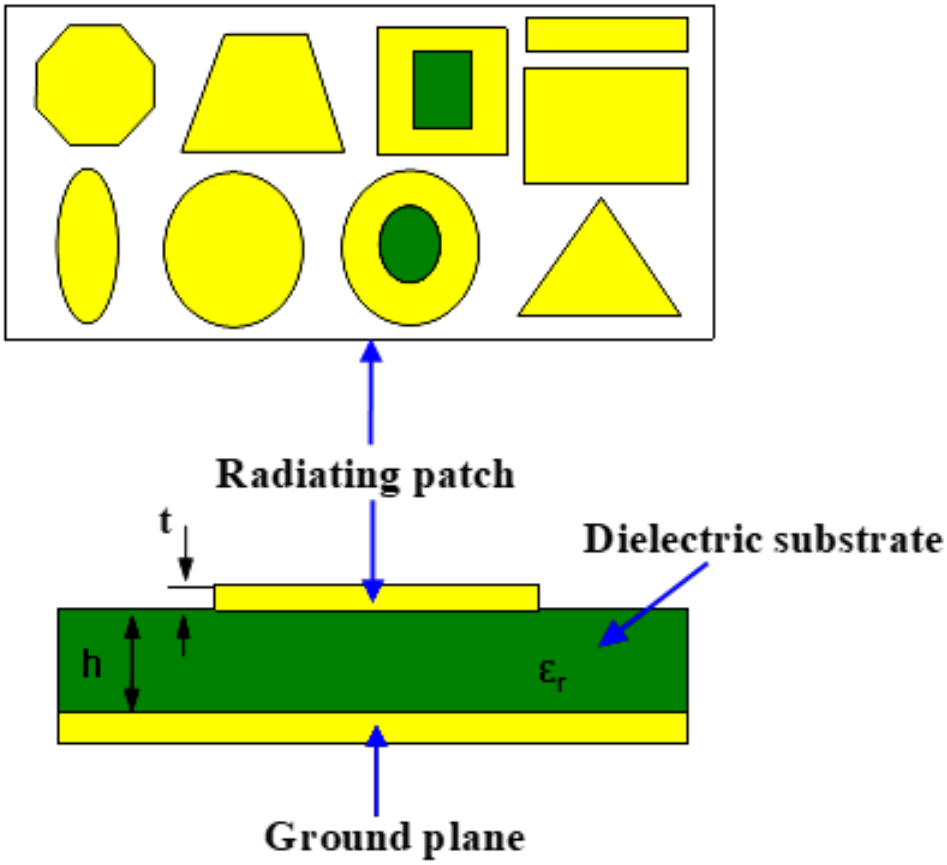

Figure 1.6: Structure of a Microstrip Antenna [21].

1.3.3 Types of Feeds

Various techniques are available for transmitting EM energy to a microstrip patch antenna. The feeding process is crucial for ensuring efficient antenna operation and improving impedance matching. The feeding techniques employed in microstrip antennas can be broadly categorized into two main classes: Contacting Feed and Non-Contacting Feed Methods.

The contact feeding method involves directly supplying power to the patch through a direct path, while the non-contact feeding method achieves power transmission through magnetic coupling. Contact feed methods encompass microstrip Line Feeding, Coaxial Feeding and Fiber optic feeding techniques, while non-contact methods encompass Aperture-Coupled Feeding and Proximity-Coupled Feeding techniques.

- **Line Feeding technique:**

  This technique involves connecting the antenna's conducting strip directly to the edge of the microstrip patch, with the width of the conducting strip being smaller than that of the patch as demonstrated in **Figure 1.7**. The significant advantage of this approach is the ability to etch the feed on the same substrate, simplifying the fabrication process and making it straightforward to implement [22–24].

  The feeding can be done through a connection directly to a microstrip line, where the point of junction is either on the element's symmetry axis (**Figure 1.8(a)**) or offset from this symmetry axis (**Figure 1.8(b)**), if it allows for better impedance matching [12].The main objective of incorporating an inset cut in the printed patch antenna is to achieve impedance matching between the line feed and the antenna structure, eliminating the requirement for additional matching components. This may be achieved by properly controlling the width, length, and placement of the inset, as illustrated in **Figure 1.8(c)** [25, 26].

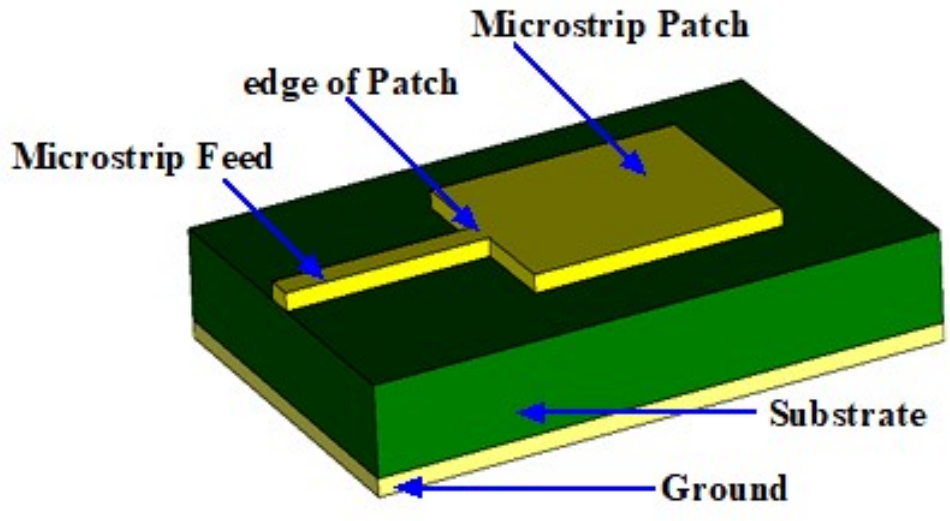

Figure 1.7: Line Feeding technique [27].

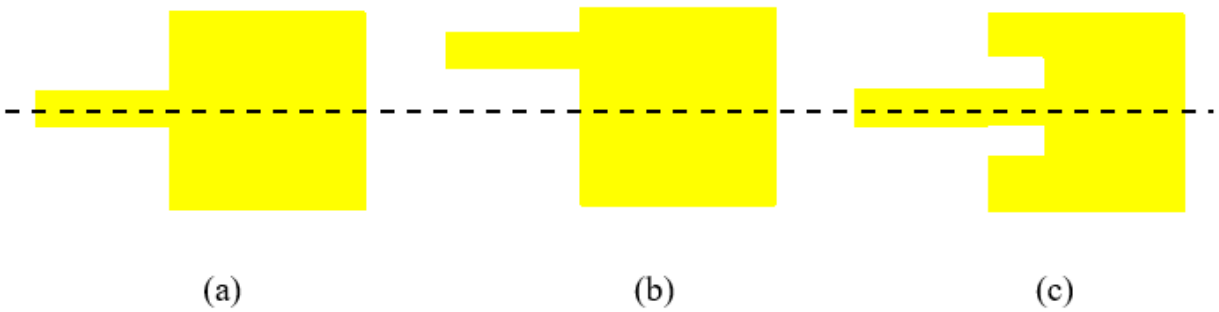

Figure 1.8: Line Feeding technique: (a) axial, (b) offset, (c) axial with inset [28].

- **Coaxial Feeding or Probe Feeding technique:** The Coaxial feed, also known as the probe feed, is a widely employed method for providing power to Microstrip patch antennas.

In this approach, depicted in **Figure 1.9**, the central conductor of the coaxial connector passes through the dielectric material and is joined to the radiating patch using solder. Meanwhile, the outer conductor of the coaxial connector is connected to the ground plane [22–24].

One of the key benefits of utilizing the Probe Feeding technique is its flexibility in inserting the feed at any desired position inside the patch, enabling proper matching with the input impedance. This method is relatively simple to fabricate and minimizes unwanted radiation. However, it does come with certain limitations. Firstly, it has a narrow bandwidth and can be challenging to model accurately, especially for thicker substrates where a hole must be drilled, and the connector protrudes outside the ground plane, compromising planarity (for substrates with a thickness greater than $0.02\lambda_0$) [25]. Additionally, as the probe length increases for thicker substrates, the input impedance becomes more inductive, resulting in matching difficulties. As observed, both the microstrip line feed and coaxial feed encounter several drawbacks when applied to thicker dielectric substrates that offer wider bandwidths.

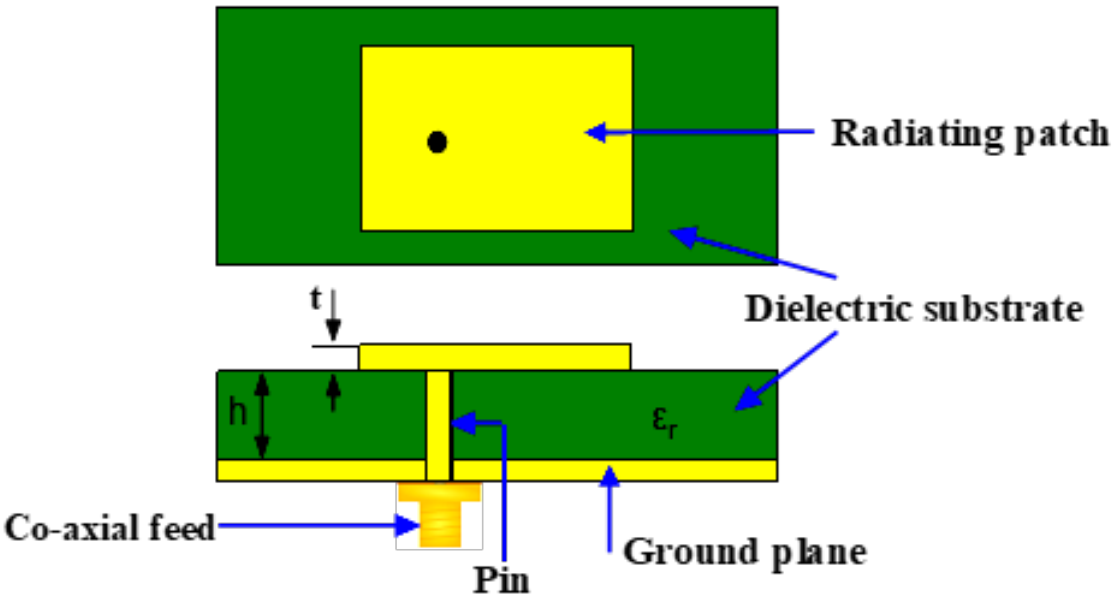

Figure 1.9: Coaxial Feeding technique [7].

- **Fiber Optic Feeding techniques:**

  One way to overcome the limitations of metallic microwave links is to replace them with optical fiber connections. This type of connection offers several advantages, such as a wide bandwidth, strong link, high immunity to electromagnetic noise, lightweight, and compact size.

The concept of such a feeding system is as follows: a laser diode is modulated using a microwave source, and the signal is then coupled to the antenna substrate through an optical fiber. On the antenna substrate, a photodiode demodulates the optical signal, which is then coupled to the printed antenna through an adaptation circuit [29].

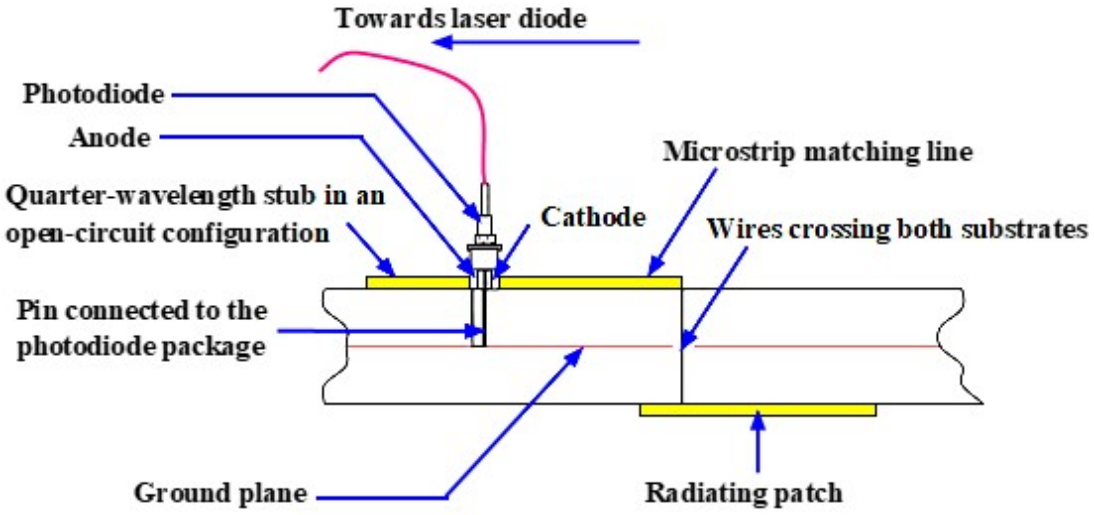

Figure 1.10: Fiber optic feeding technique [29].

- **Aperture-Coupled Feeding technique:** In this particular feeding technique, the ground plane serves as a separator between the radiating patch and the microstrip feed line, as depicted in **Figure 1.11**. The patch and feed line are coupled via an aperture or a slot in the ground plane [25]. Typically, the coupling aperture is positioned centrally beneath the patch, which promotes lower cross-polarization by virtue of the configuration's symmetry. The aperture's shape, size, and placement determine the extent of coupling from the feed line to the patch. As the ground plane acts as a barrier between the patch and the feed line, the occurrence of spurious radiation is minimized. To optimize the radiation emitted by the patch, a highly dielectric material is often used for the bottom substrate, while a thick substrate with lower dielectric constants is employed for the top substrate. However, it is important to note that this feeding technique poses some drawbacks. It is challenging to fabricate due to the involvement of multiple layers, resulting in increased antenna thickness. Additionally, this feeding scheme tends to offer a narrow bandwidth [25, 30, 31].

- **Proximity-Coupled Feeding technique:** The proximity coupled feeding technique can be employed, which involves utilizing a two or multilayer substrate composition, as depicted in **Figure 1.12**. In this design configuration, a microstrip line is positioned on the bottom substrate, while the patch antenna element is placed on the upper substrate.

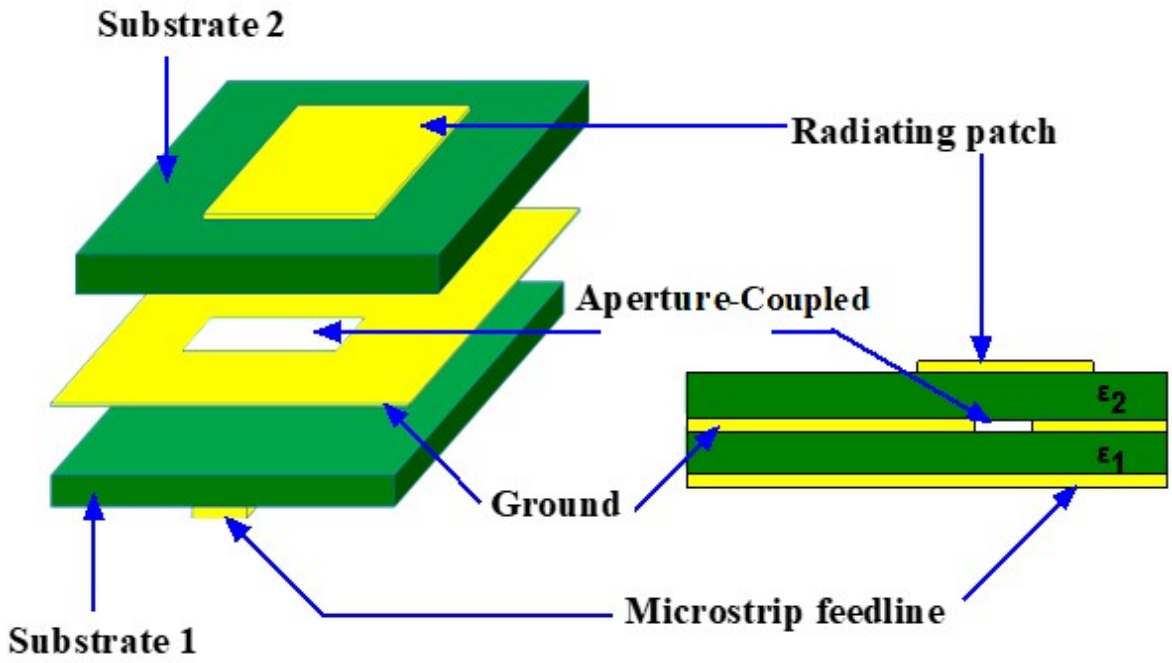

Figure 1.11: Aperture-Coupled Feeding technique [32].

Another term for this feeding technique is EM attachment, as it facilitates EM coupling. Capacitive interaction is observed between the feed line and the antenna patch in this design arrangement [33, 34]. The proximity coupled feeding technique offers a distinct advantage, as it effectively eliminates spurious feed radiation and provides a remarkably high bandwidth (up to 13%) [33]. This is achieved through an overall increase in the thickness of the printed patch antenna. Furthermore, this design configuration offers the flexibility of choosing between two distinct dielectric media, one for the feed line and a second for the radiating layer, to optimize the antenna's individual performance. Achieving accurate pattern and impedance matching is possible by adjusting the feed line's length, the gap between the line feed and patch antenna, and the width ratio of the line feed to the patch [25].

- **Coplanar waveguides feeding technique:** Coplanar Waveguide (CPW) is a widely used transmission line for feeding printed antennas. The concept of this technique is to avoid soldering and drilling on the substrate. The advantage of this type of feeding is that the ground plane and the feeding line are located on the same side of a dielectric substrate, as shown in **Figure 1.13**. The radiating element is fed by a central metallic strip placed between two parallel ground planes [32].

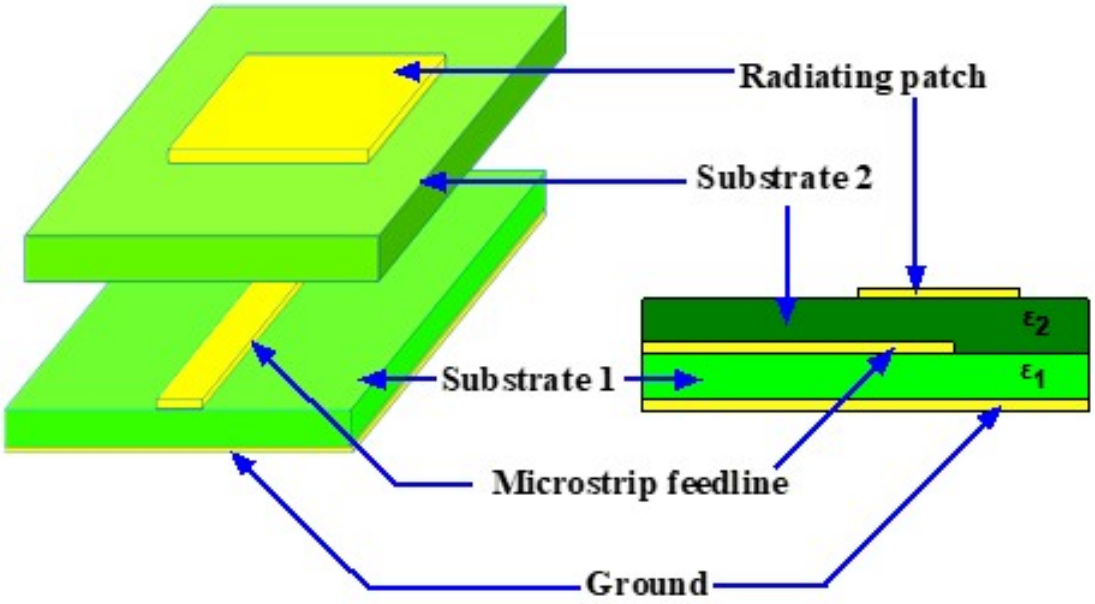

Figure 1.12: Proximity-Coupled Feeding technique [35].

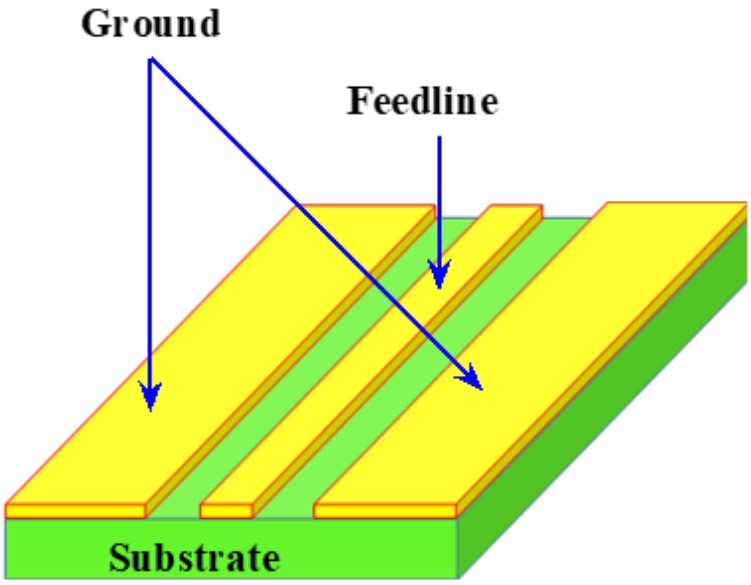

Figure 1.13: Coplanar waveguides feeding technique (CPW) [32].

1.3.4 Microstrip Patch Antenna's Radiation Mechanism

The fringing fields around the edges of a microstrip patch antenna cause it to radiate, As shown in **Figure 1.14**. Charges between the ground plane and the metallic patch's underside are distributed when the patch is excited. The region below the patch carries a positive charge, while the ground plane becomes negatively charged, creating attractive forces between the patch and ground plane [36, 37]. The analysis of the patch considers it a resonant cavity with electric walls composed of metal (including the patch and ground plane) and magnetic or impedance walls along the edges. Impedance matching occurs when the patch resonates

as a cavity, allowing the antenna to achieve maximum efficiency. The width of the field lines is uniform, but they vary sinusoidally along their length. The E-field is strongest at the two radiating edges, although the current is highest in the patch's centre [36, 38].

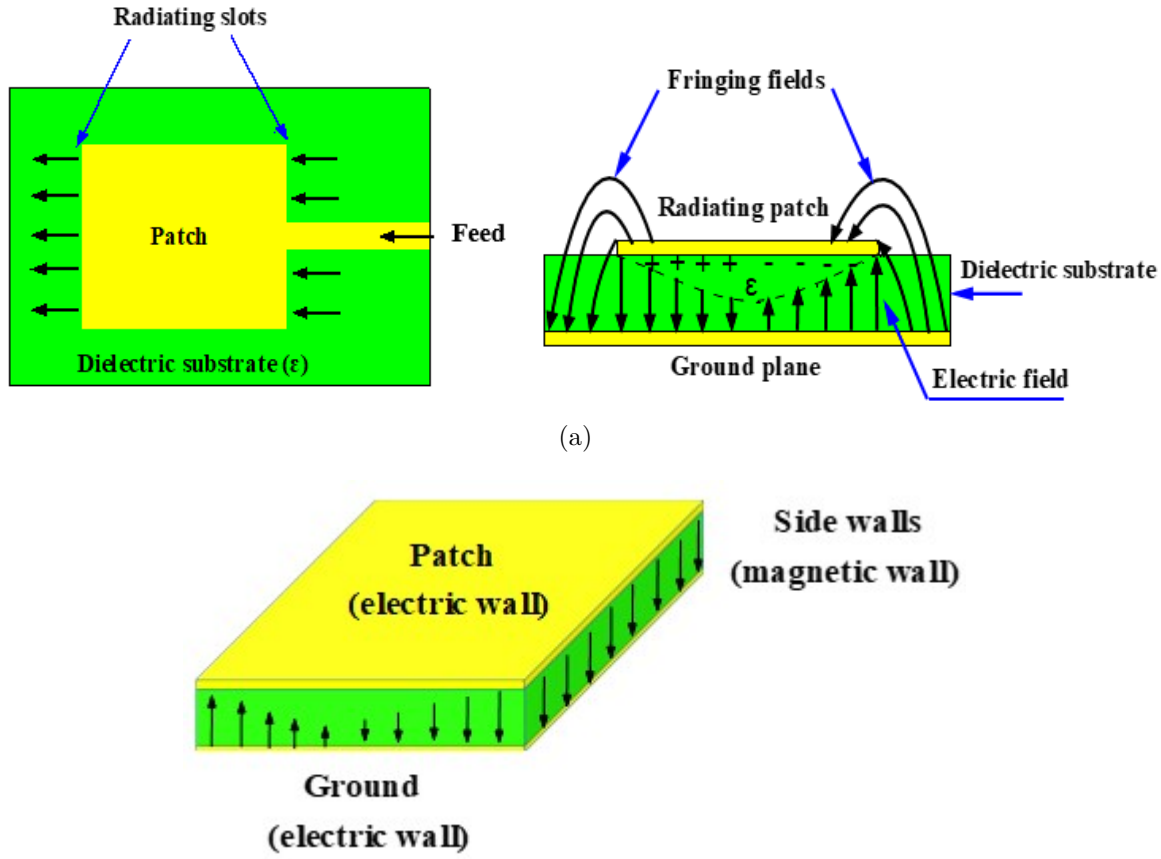

Figure 1.14: (a) The microstrip patch antenna's radiating mechanism and (b) a cavity model representation [39].

In contrast, a regular transmission line emits a reduced amount of power as the fringing fields are nullified by nearby opposing fields. The emission of power occurs from open circuits and discontinuities, with the quantity relying on the radiation conductance load concerning the patches. The edges of the patch serve as slots, and their stimulations hinge on the internal fields of the cavity. Optimal antenna design favors the utilization of a thick dielectric substrate with a lower dielectric constant, offering enhanced efficiency, a broader bandwidth, and superior radiation. However, a larger antenna is the result of this design. Higher dielectric constants, which are less efficient and result in a narrower bandwidth, are required in the design of a miniature microstrip patch antenna. As a result, performance and antenna size must be compromised[36].

1.3.5 Methods of Analysis

Creating an analytic model for the microstrip antenna serves two primary purposes. Firstly, it offers a cost-effective and efficient alternative to the time-consuming process of experimental iteration in antenna design. Secondly, it enables the designer to gain insights into the underlying physical mechanisms governing the operation of the microstrip antenna. By employing this analysis technique, engineers can accurately predict various antenna performance attributes, including resonant frequency,input impedance, bandwidth, efficiency, and radiation patterns [40]. Several analysis methods have been used for modeling the microstrip antennas. These analysis methods can be categorised into two different groups: analytical methods and numerical methods.

- **Analytical Methods:** Analytical methods are based on the distribution of the equivalent magnetic current around the radiating element. In this method, three models are distinguished among them [17, 41]:
  - Transmission Line Model
  - Multimode Cavity Model
  - Multiport Network Model

  - Transmission Line Model (TLM): An equivalent circuit network can be used to describe a microstrip patch, which is fundamentally understood as a $\lambda/2$ long microstrip transmission line. Since the two sides of a rectangular patch are represented by equivalent slots along the resonating dimension, the radiation of the patch originates predominantly from these edges (refer to **Figure 1.15**). Each of the two slots of this microstrip radiator, which are divided by a gearbox line, is represented by a parallel circuit with conductance (G) and susceptance (B). A representation of the total patch antenna can be found in the analogous network shown in **Figure 1.15**.This TLM has certain accuracy constraints, despite being theoretically obvious, computationally efficient, and simple. For instance, it neglects the radiation from the patch's non-radiating edges and the mutual coupling between the two radiating slots [36, 40].

  - Multimode Cavity Model: Although it is straightforward to use, the TLM has some drawbacks. Indeed, it only applies to rectangular patches, and it neglects the variations of the field along the radiating edges. These drawbacks can be addressed by employing the cavity model proposed by Lo et al [42]. As seen in **Figure 1.14(b)**, the cavity model views the space between the ground plane and the patch as a cavity surrounded by electric

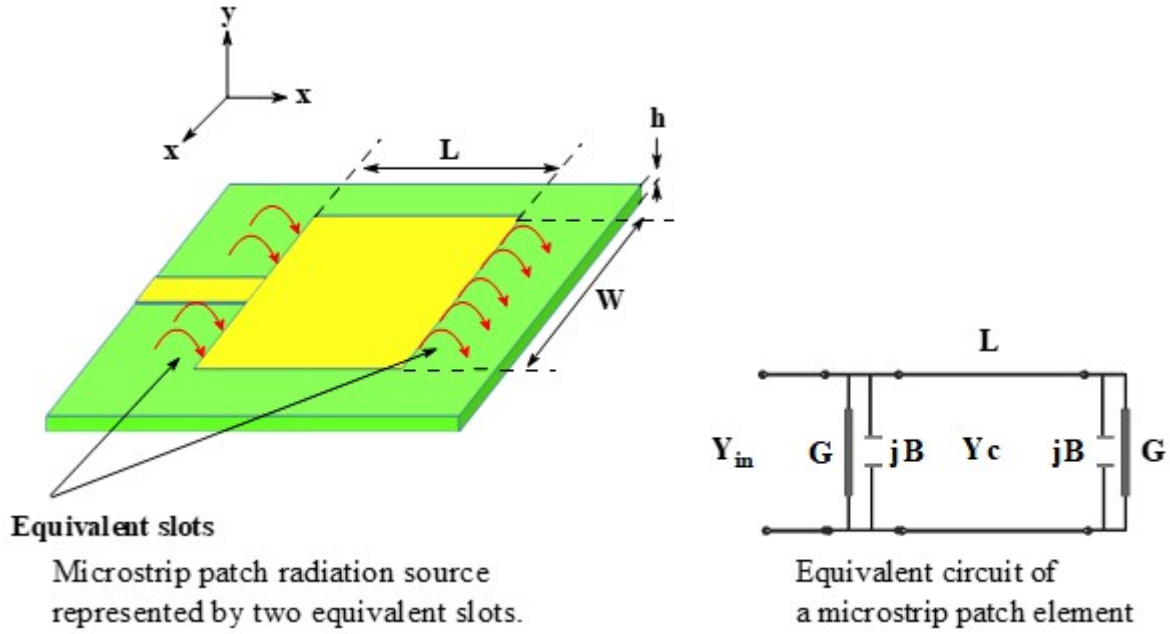

Figure 1.15: TLM of microstrip patch antenna [36].

walls at the top and bottom and magnetic walls on the sides. The field within the cavity stays uniform throughout the substrate's thickness when sinc-thin substrates are utilised. The fields beneath the patch can be described by summing up the several resonant modes of the two-dimensional resonat for regular shapes such as sectoral, triangle, circular, and rectangular shapes [43]. The patch boundary is extended outward to make sure that the effective dimensions are greater than the patch's actual dimensions in order to account for the fringing fields surrounding the edges. By adding conductor and antenna losses to the dielectric substrate's loss tangent, the effects of radiation from these sources are taken into account. Then, using the equivalent magnetic current along the cavity's perimeter, the radiated power and far-field are computed [44]. Adding an impedance boundary condition at the cavity's walls is an alternative approach for considering radiation effects into account in the cavity model. By using this method, the radiated power and fringing fields are localised at the cavity's boundaries rather than inside. On the other hand, evaluating the far-field solution with admittance walls can be challenging [41].

- Multiport Network Model (MNM): The MNM used to analyse the microstrip antenna is an extension of the cavity model. In this approach, the EM fields beneath and above the patch's surface are treated independently. The patch is analysed as a two-dimensional planar network with multiple ports along its perimeter. The two-dimensional Green's function of the patch is employed to compute the multiport impedance matrix. An analogous edge admittance network is incorporated to consider the fringing fields and

radiated fields around the periphery [45, 46]. The segmentation approach is then used to generate the overall impedance matrix, and the radiated fields are estimated using the voltage distribution around the perimeter. All of the analytical approaches discussed above give both physical insight and simplicity. In the last two approaches, the radiation of the Microstrip Antenna is computed by employing the equivalent magnetic current distribution surrounding the radiating patch, derived from the corresponding voltage distribution. As a result, the analysis problem of the Microstrip Antenna is simplified to determining the edge voltage distribution for a specific excitation and mode. While these methods are precise for conventional patch geometries, except for MNM with contour integration techniques, they prove inefficient for patch configurations with arbitrary shapes [17]. For intricate geometries, the numerical approaches outlined below are employed.

- **Numerical Methods:** Numerical methods are based on the distribution of electric current on the conductor (the radiating patch element and the ground plane). Additionally, these methods allow for the study of antennas with various shapes, but they involve more complex formulations or calculations and significant computation times. The most commonly used numerical methods for microstrip antennas are [41]:
  - Method of Moments (MoM).
  - Finite-Element Method (FEM).
  - Spectral Domain Technique (SDT).
  - Finite-Difference Time Domain (FDTD) method.

- Method of Moments (MoM): The MoM originated in the field of mathematics. Its fundamental concept involves converting an integral or differential equation into a system of simultaneous linear algebraic equations (or a matrix equation), Which may then be resolved through numerical approaches [47]. This method primarily operates in the frequency domain, considering one frequency at a time. The primary factor used to determine various parameters of the antenna is the current density of the antenna. The process involves replacing the antenna with an equivalent surface current density, which is then divided into a set of current-density components known as basis functions or variable-amplitude expansions. Using Green's function, the E-fields and/or H-fields throughout the space may be represented in terms of these current-density components located on the antenna's surface. Harrington invented the use of testing functions or weighted functions to apply the boundary conditions for both fields on the antenna's surface in order to solve

EM difficulties. An illustration of the MoM-based mesh on a microstrip line and the current distribution on the line is provided in **Figure 1.16** [36].

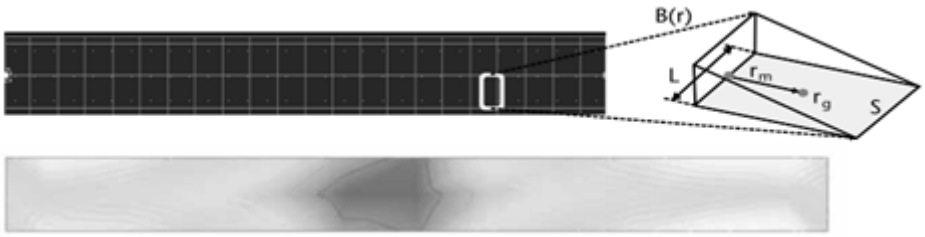

Figure 1.16: The MoM mesh applied to a microstrip line, and the resulting simulated current distribution along the line [36].

All methods that use weighted residuals commence by defining a group of experimental solution functions that include a few parameter variables. The residual represents the discrepancy between the trial and the actual solutions.The variable parameters are determined in a way that ensures the best fit of the trial functions through minimizing the residuals. In general, the equations addressed by the moment-method approach are integral equations for magnetic or electric fields. When considering the field distribution by either a perfect conductor or a lossless dielectric, these equations may be derived from Maxwell's equations. The MoM approach can be applied to configurations with conductors alone, configurations with homogeneous dielectrics only, or configurations with certain conductor-dielectric geometries, depending on the specific field integral equation used. However, these equations are not suitable for handling complex or inhomogeneous dielectrics, nor are they effective for arbitrary configurations involving conductive enclosures or thin plates [36].

- Finite-element Method (FEM): FEM, primarily a frequency domain approach, is favored for its potential to model inhomogeneous media. It is a mathematical technique used to analyze intricate structures by dividing them into numerous small elements, where some elements may be small to capture geometry details while others are larger. These elements can take various shapes, such as triangles and squares in 2D or tetrahedrals and cuboids in 3D. Within each element, the field is estimated using mathematical formulas derived from solutions of the Helmholtz equations in their weak version (Silvester et al.). A node corresponds to any edge of an element, and it is at each node that the E-field and H-field are evaluated. The complete problem is then numerically solved. However, FEM may not be as effective as MoM techniques in modeling unbounded radiation problems. In FEM simulation, the EM field solution is determined using the finite element method,

and S-parameter data is subsequently derived. The entire problem space is subdivided into smaller regions or elements, as depicted in **Figure 1.17** [36]. For every subregion (element), local functions are used to compute the EM fields. The geometric model is automatically split into tetrahedron cells in FEM-based computer-aided design (CAD) tools. Each tetrahedron is made up of four equilateral triangles. A sample of discretizing a structure using finite elements is illustrated in **Figure 1.17**. Important details about excitation, boundary restrictions, device shape, and material constants are included in the model.

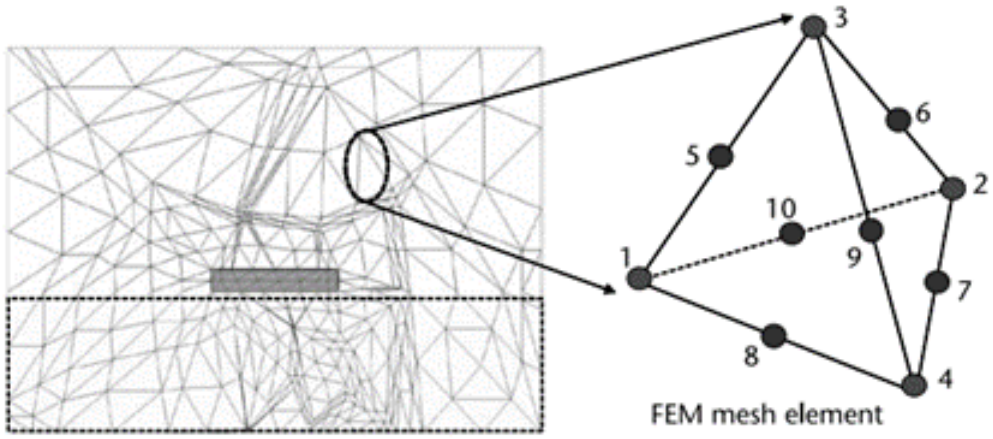

Figure 1.17: FEM mesh for simulating a microstrip line model and a tetrahedral mesh element [36].

- Spectral Domain Technique (SDT): The SDT involves applying a two-dimensional Fourier transform to the patch's two orthogonal orientations inside the substrate plane. The Fourier transform plane has boundary requirements put upon it. The current distribution on the conducting patch is represented using selected basis functions, and a matrix equation is solved to determine the distribution of the E-field on the patch and the corresponding distribution of the H-field on the substrate surface. Subsequently, the antennas' various parameters are assessed [41, 48].

- Finite-difference Time Domain (FDTD) method: The FDTD method, introduced by Yee in 1966, is a widely employed modeling technique in various engineering applications. It offers the advantage of simplicity in formulation and geometry definition (grid-layout), as it does not require complex and time-consuming mesh generation. Similar to FEM, FDTD divides the entire volume into a mesh, which is typically homogeneous but can be adjusted based on applications and geometry. FDTD operates in the time domain and proves to be effective in numerical modeling of complex inhomogeneous configurations. It often outperforms finite element modeling in handling unbounded problems.The FDTD

approach is particularly popular for computer-aided designs of printed antennas and arrays. It enables the solution of complex microstrip antenna characteristics, considering parasitic elements and aperture-coupled feeds. FDTD mesh and Yee cells are depicted in **Figure 1.18** [36]. Addressing mutual coupling effects between elements in array antenna design can be challenging, and FDTD serves as a useful solver for such cases. An advantage of the FDTD approach is its ability to provide broadband output from a single execution. Additionally, it exhibits excellent scaling performance as the problem size increases, making it suitable for large problem sizes.

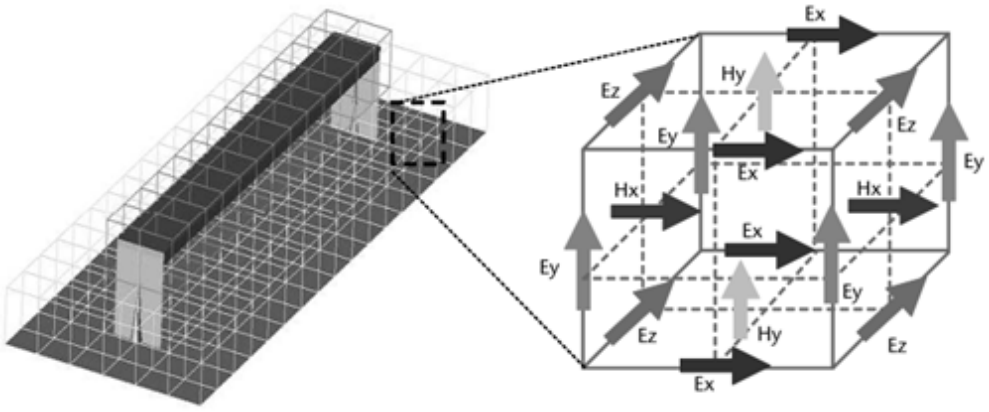

Figure 1.18: FDTD mesh for a simulation model of a microstrip line and a Yee cell [36].

1.3.6 Advantages and Disadvantages

- **Advantages of Microstrip Patch Antennas:**

  Microstrip antennas offer numerous advantages over traditional microwave antennas. The primary advantages of microstrip antennas include the following [25, 40, 41]:

  1. Lightweight and Compact: Microstrip antennas are lightweight with a small volume and possess a low-profile planar configuration.

  2. Cost-effective Mass Production: Microstrip antennas can be mass-produced with ease using printed-circuit technology, resulting in a low fabrication cost.

  3. Ideal for Mobile Communication: They can be designed in compact sizes, making them well-suited for utilization in personal mobile communication devices.

  4. Conformal Design: They can be readily designed to conform to the surface of the host, enabling seamless integration into curved or irregularly shaped structures.

  5. Polarization Versatility: Microstrip antennas allow for both linear polarization and CP, providing flexibility in polarization selection.

6. Integration Flexibility: They are more straightforward to integrate with other Microwave Integrated Circuits (MICs) on the same substrate, facilitating complex system designs.

7. Multi-Frequency Capabilities: Microstrip antennas support dual- and triple-frequency operations, offering versatility in different frequency bands.

In summary, microstrip antennas provide several key benefits, including their lightweight and compact design, ease of integration, cost-effectiveness, adaptability to various applications with different polarization and frequency requirements, making them highly advantageous over conventional microwave antennas.

- **Disadvantages of Microstrip Patch Antennas:**

  Microstrip antennas exhibit certain drawbacks when compared to conventional microwave antennas. These disadvantages include the following [25, 40, 41]:

  1. Limited Bandwidth: Microstrip antennas have a narrow bandwidth, which may restrict their ability to operate over a wide band of frequencies.

  2. Lower Gain: They generally have lower gain compared to conventional microwave antennas, impacting their ability to transmit and receive signals over long distances.

  3. Environmental Sensitivity: Microstrip antennas are sensitive to environmental factors such as humidity and temperature, which can influence their performance and stability.

  4. Limited Power-handling Capability: Microstrip antennas have lower power-handling capability, which may limit their usage in high-power applications.

  In summary, while microstrip antennas offer numerous advantages, they do have limitations in terms of bandwidth, gain, and power-handling capability when compared to traditional microwave antennas.

1.4 Conclusion

The first chapter provided a comprehensive overview of the electrical and electromagnetic characteristics of antennas. We focused specifically on microstrip antennas, delving into their applications, primary feeding methods for radiating elements, radiation mechanisms, and different

analysis techniques encompassing both analytical and numerical methods. Lastly, we explored the advantages and disadvantages of microstrip patch antennas.

Chapter 2

Microstrip Antennas in the Presence of a Human Body

Contents

2.1 Introduction

An antenna stands as a pivotal component within numerous Biomedical engineering devices, offering the flexibility to be situated nearby, within, or upon the human body [49, 50]. When dealing with devices for diagnostic or therapeutic purposes, it is common practice to strategically position one or more antennas in the proximity of the human body. For instance, applications like MRI and MI diagnosis, as well as hyperthermia treatment, necessitate the

careful placement of antennas [51]. Moreover, antennas can be implanted directly into the human body, either through direct insertion or via a capsule traversing the body's internal pathways [52]. Alternatively, they can be positioned atop the human body, whether integrated within garments or directly mounted over the torso. Such configurations enable the creation of a bio wireless sensing and communication system, capable of facilitating transmission links either on-body or off-body [49]. However, the design of most of these antennas is subject to physical limitations encompassing factors such as size, power, and safety, collectively exerting an influence on the overall efficiency of the Biomedical engineering device itself.

When focusing on antennas deployed across various regions of the human body (referred to as on-body and wearable antennas), whether integrated into the skin or within clothing materials (like textile antennas), further design complexities arise due to the intimate adjacency to the human body. The role of the human body takes on a paramount significance in the process of designing and characterizing antennas for biomedical applications. Its intricate, dispersive, and lossy characteristics considerably impact antenna performance and the propagation of EM fields. Additionally, the presence of anatomical variations among patients amplifies the intricacies associated with devising an appropriate design tailored to a specific application. Consequently, the design process for an antenna intended for use within or in close proximity to the human body demands careful consideration of multiple factors. This chapter centers its attention on the key factors associated with the interaction between antennas and biological tissues. The primary aims encompass:

- **Impact of the Human Body on Antenna Performance**
- **Radiation Antenna Effects on the Human Body**
- **Authorized Operating Frequency Ranges for Wireless Medical Applications**
- **Models of the Human Body**

2.2 Impact of the Human Body on Antenna Performance

The human body's surroundings constitute an essential component of implantable or wearable medical devices. This environment is characterized by high levels of attenuation than in free space [53], where the dielectric properties of tissues such as the electric conductivity (σ) [Siemens per metre, S/m] and relative permittivity constant (ε_r) [Farads per metre, F/m] vary with shifts in operational frequencies, as demonstrated in **Figure 2.1** [54].

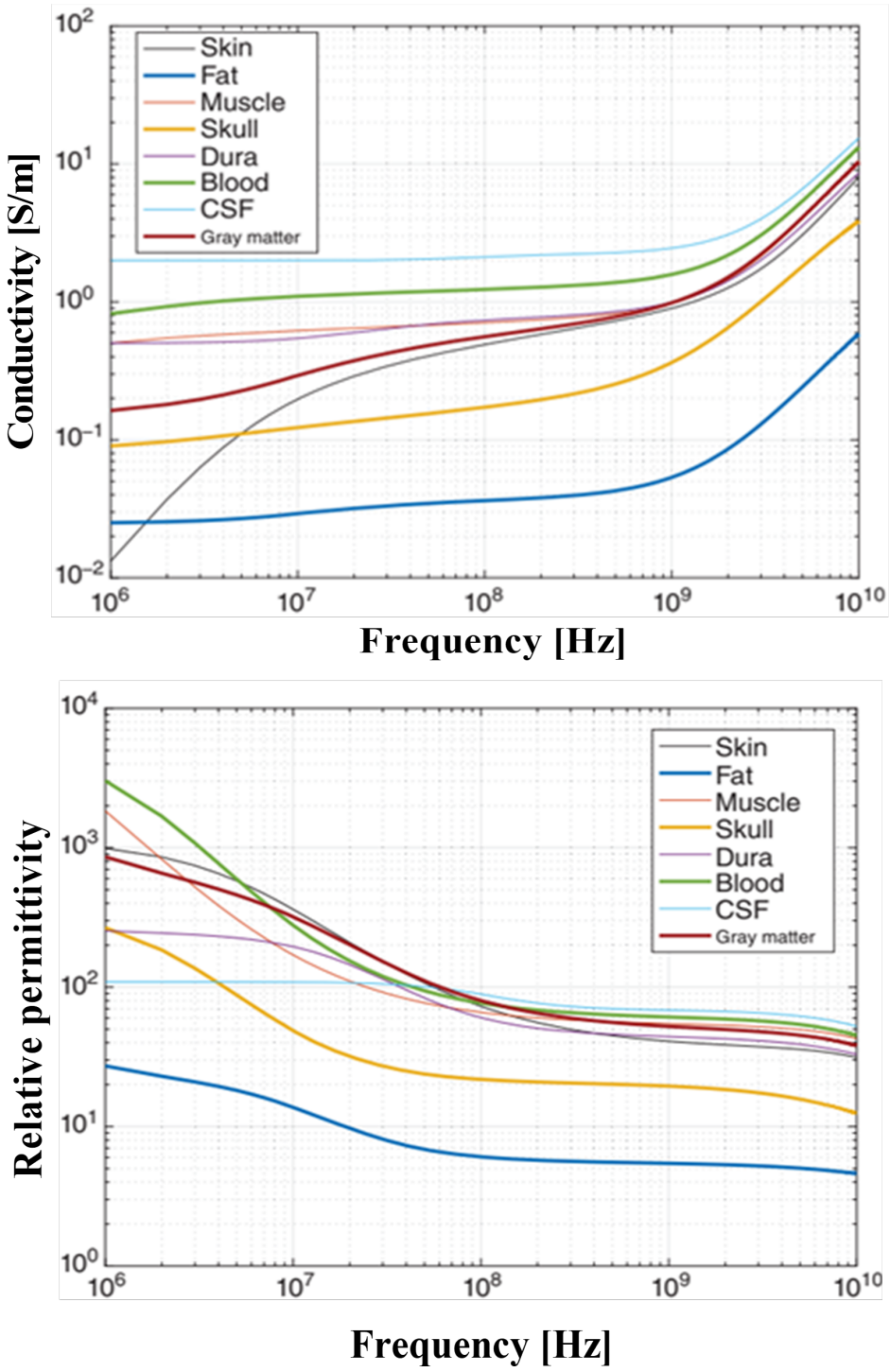

Figure 2.1: The electrical conductivity and permittivity properties of human body tissues [54].

The dielectric properties of biological tissue, such as the electrical permittivity (ε) and electrical conductivity (σ), determine how it interacts with an EM field that exists alongside it [53]. In the case of a uniform, homogeneous, and isotropic medium, the absolute permittivity and conductivity may be represented as complex values, which are specified by Equation (2.1) and Equation (2.2) [55].

$$\varepsilon(\omega, T) = \varepsilon_0(\varepsilon'_r - j\varepsilon''_r) \tag{2.1}$$

$$\sigma(\omega, T) = \sigma' - j\sigma'' \tag{2.2}$$

$$\omega = 2\pi f \tag{2.3}$$

Here, ε_0 denotes the permittivity of the vacuum ($\varepsilon_0 = 8.8541878176 \times 10^{-12}\,\mathrm{F/m}$). It should be noted that these values are influenced by both the frequency f and the temperature T. The concept of electrical permittivity explains the occurrence of induced polarization and the alignment of pre-existing dipoles when an E-field is present. The real part (ε'_r) signifies the component of the medium that does not experience losses and is associated with polarization effects. Conversely, the imaginary part (ε''_r) characterizes the energy losses resulting from the damping of vibrating dipole moments and the delayed response exhibited by the medium. On the other hand, electrical conductivity assesses a material's ability to enable the circulation of freely moving electric charges. By referring to Equation (2.1) and Equation (2.2), we can represent the relative effective permittivity (ε'_e) and conductivity (σ'_e) as follows [55, 56]:

$$\varepsilon'_e = \varepsilon'_r - \frac{\sigma''}{\omega\varepsilon_0} \tag{2.4}$$

$$\sigma'_e = \sigma' - \omega\varepsilon_0\varepsilon''_r \tag{2.5}$$

Considering Maxwell's equations in mind, the complex effective permittivity (ε_e) may be reformulated as follows:

$$\varepsilon_e = \varepsilon_0(\varepsilon'_e - j\varepsilon''_e) = \varepsilon_0(\varepsilon'_e - j\frac{\sigma'_e}{\omega\varepsilon_0}) \tag{2.6}$$

The loss tangent ($\tan\,\delta$) provides insights into the extent to which a medium may be described as "lossy". It represents the correlation between the imaginary and real parts of the complex effective permittivity:

$$\tan\delta = -\frac{\mathrm{Re}(\varepsilon_e)}{\mathrm{Im}(\varepsilon_e)} = -\frac{\varepsilon''_e}{\varepsilon'_e} = \frac{\sigma'_e}{\omega\varepsilon_0\varepsilon'_e} \tag{2.7}$$

Considering an angular frequency $\omega[rad/m]$, the efficient wavelength λ_e of a medium may be defined as:

$$\lambda_e = \frac{2\pi}{\omega\sqrt{\varepsilon_0\mu_0}}\Re\left\{\sqrt{\frac{\omega\varepsilon_0}{\omega\varepsilon_0\varepsilon'_e - j\sigma'_e}}\right\} \tag{2.8}$$

It is important to emphasize that the effective wavelength is influenced by the effective permittivity. When an EM field is involved, the effective wavelength in a medium is generally smaller compared to that in a vacuum. This aspect holds significant importance in the context of miniaturizing implantable antennas [56].

Gabriel et al. conducted a survey of biological tissues to determine their dielectric properties [57], where they extensively analyzed and documented these characteristics.

The influence of high conductivity and permittivity predominantly results in more substantial attenuation losses within human tissues, a factor determinable through the utilization of [58]:

$$L_\alpha = 20\log_{10}(e^{-\alpha l})\,[\text{dB}] \tag{2.9}$$

Here, $\alpha\,[\text{N}_p/\text{m}]$ denotes the attenuation coefficient, and l [m] signifies the distance within the tissue.

The formula to compute the attenuation coefficient is as follows [58]:

$$\alpha = \omega\sqrt{\frac{\mu\varepsilon}{2\left(1+\left(\frac{\sigma}{\omega\varepsilon}\right)^2\right)-1}} \tag{2.10}$$

Here, $\mu[H/m]$ denotes tissue permeability which is equivalent to the permeability of free space $\mu_0 = 4\pi \times 10^{-7}$ henry/m for all non-magnetic human body tissues.

Permeability and permittivity are complicated quantities in the preceding equations. Because human tissues are nonmagnetic, the imaginary part of permeability equals zero. Within the human body, there are supplementary signal losses arising from reflections occurring at tissue interfaces during signal propagation. These losses can be quantified by applying Equations (2-11) to (2-13), assuming that the angle of incidence specified in Equation (2-13) is normal or perpendicular [59]:

$$L_R = -20\log_{10}(\Gamma)\,[\text{dB}] \tag{2.11}$$

$$Z = \sqrt{\frac{j\omega\mu}{\sigma + j\omega\varepsilon}} \tag{2.12}$$

$$\Gamma = \frac{Z_2 - Z_1}{Z_2 + Z_1} \tag{2.13}$$

Where $Z[\Omega]$ represents the intrinsic impedance and Γ represents the reflection coefficient at the boundary between tissues. The boundary between the outer layer of the skin and free space causes the reflected signal to bounce back as they possess different impedances and EM properties. To calculate the power received by an external receiver, apply the equation below [60]:

$$P_{\mathrm{RX}} = P_{\mathrm{TX}} + G_{\mathrm{TX}} + G_{\mathrm{RX}} - \mathrm{Loss} \tag{2.14}$$

$$\mathrm{Loss} = L_P - e_P - \mathrm{ML}_{\mathrm{TX}} - \mathrm{ML}_{\mathrm{RX}} \tag{2.15}$$

$P_{\mathrm{RX}}[dBm]$ represents the received power, and $P_{\mathrm{TX}}[dBm]$ represents the transmitted power. $G_{\mathrm{TX}}[dB]$ is the gain of the transmitter antenna. For implantable antennas, this gain value is typically negative due to losses caused by in-body attenuation and reflections. $G_{\mathrm{RX}}[dB]$ refers to the gain of the receiver antenna. Loss$[dBm]$ is the total loss. $e_P[dBm]$ is the factor representing polarization mismatch. $\mathrm{ML}_{\mathrm{TX}}[dBm]$ represents the loss due to transmitter impedance mismatch, while $\mathrm{ML}_{\mathrm{RX}}[dBm]$ represents the loss due to receiver impedance mismatch. $L_P[dBm]$ denotes the path loss, which can be determined using [60]:

$$L_P = 10n \log_{10}\left(\frac{d}{d_0}\right) + 10 \log_{10}\left(\frac{4\pi d_0}{\lambda_0}\right)^2 + S \tag{2.16}$$

In the equation (2.16), there is a component called "n" which represents the path loss component. The value of "n" depends on the type of propagation. For line-of-sight indoor propagation, "n" is equal to 1.5. For non-line-of-sight indoor propagation, "n" is equal to 3. And for free space propagation, "n" takes a value of 2. The distance between the transmitter and the receiver is represented by the variable "d". λ_0 is represents the wavelength in free space. Lastly, S [dB] represents the random scatter.

The equation (2-16) can be simplified for loss in free-space propagation when "n" is equal to 2, resulting in the following equation [61]:

$$L_f = 20 \log_{10}\left(\frac{20\pi d}{\lambda_0}\right) \tag{2.17}$$

The ratio between the radiation intensity in a specific direction and the total input power

defines the free space gain, denoted as G. This mathematical formula represents the relationship between the two variables [14]:

$$G = \frac{4\pi P}{P_{\text{in}}} \tag{2.18}$$

Where P represents the radiation intensity measured in watts per unit solid angle, while P_{in} stands for the total input power measured in watts. The relation between radiation intensity and average radiated power intensity $S_{\text{av}}[W/m2]$ is determined by the square of the distance r [m] that is [62]:

$$P = r^2 S_{av} \tag{2.19}$$

The conductive medium's gain G_{con} can be determined through the following equation [63]:

$$G_{\text{con}} = \frac{4\pi R g^2}{R_r} \tag{2.20}$$

Where $R[\Omega]$ represents the intrinsic resistance and $R_r[\Omega]$ represents the radiation resistance. The following equation may be used to compute the intrinsic resistance:

$$R_{\text{intrinsic}} = \sqrt{\frac{\omega\mu}{2\sigma}} \tag{2.21}$$

The function g is defined taking into consideration the parameters of the medium. Its value can be obtained using the given equation:

$$g = \frac{|H| d e^{d/\delta}}{I_i^2} \tag{2.22}$$

The magnetic field is represented by |H| [A/m], the distance in meters by d, and the input current in amperes by I_i. Whereas δ indicates the depth of the skin.

2.2.1 Human Body Effects on Antenna Impedance and Antenna Reflection Coefficient

In **Figure 2.2**, there is a representation of an equivalent circuit for a transmitting antenna. As shown in Chapter 1, this antenna is connected to a feed line with a specific characteristic impedance denoted as Z_0. The antenna's impedance may be described as follows [53, 63]:

$$Z_{\text{in}} = R_L + R_{\text{rad}} + jX_{\text{in}} \tag{2.23}$$

R_L and R_{rad} represent the antenna's loss resistance and radiation resistance, respectively, while X_{in} signifies the reactance of the antenna.

The antenna is positioned within a lossy medium of infinite extent, as delineated by the spherical coordinates illustrated in **Figure 2.3**. As per the definition applicable to antennas in free space, the radiation resistance can be adjusted concerning the radiated power P_{rad} in the far-field and the input current I_i [64].

$$R_{\text{rad}} = \frac{P_{\text{rad}}}{I_i^2} = \frac{\iint S_L \sin\theta r^2 \, d\theta \, d\phi}{I_i^2} \tag{2.24}$$

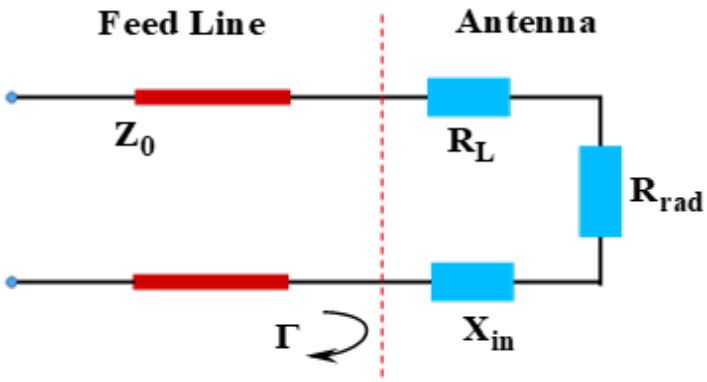

Figure 2.2: Transmission-line Thevenin equivalents of an antenna in transmission mode [53].

In the case of a lossy medium, the power density denoted as S_L can be formulated as follows [64]:

$$S_L = \text{Re}\left\{\frac{\left|\vec{E}\right|^2}{Z_m}\right\} e^{-2\alpha r} \tag{2.25}$$

This modification involves the introduction of a decay factor $e^{2\alpha r}$ (where α is a negative value in a lossy medium), to counteract the attenuation induced by the lossy medium (where Z_m represents the wave impedance in the lossy medium). Even though the attenuation of waves in the lossy medium is mitigated, the radiation resistance and the E-field still exhibit disparities in comparison to those of an antenna operating in free space. This discrepancy arises from the alteration in the antenna's current distribution caused by the presence of a lossy medium with a high relative permittivity [53].

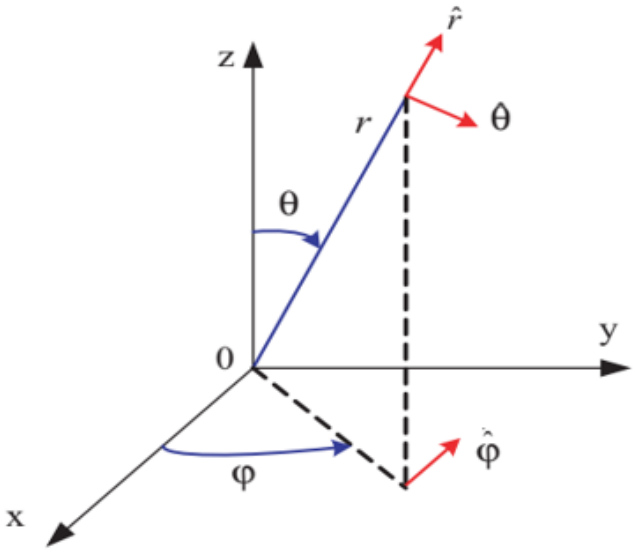

Figure 2.3: The spherical coordinate system [65].

By taking into account the R_{rad} and reactance values X_{in} of the body-matched antenna, you can calculate both the antenna's efficiency η and the reflection coefficient Γ in the following manner:

$$\eta = \frac{R_{\text{rad}}}{R_{\text{rad}} + R_L} \tag{2.26}$$

$$\Gamma = \frac{Z_{\text{in}} - Z_0}{Z_{\text{in}} + Z_0} \tag{2.27}$$

In order to minimize the Γ, it is necessary to align the impedance of the power source with that of the antenna. Ideally, the line impedance Z_0 should be the complex conjugate of the antenna's impedance Z_{in}. To achieve this in real-world applications, various methods such as employing matching networks are commonly utilized [53].

2.2.2 Human Body Effects on Antenna Bandwidth

Implantable antennas are typically miniature in size, which naturally limits their bandwidth. However, this bandwidth tends to expand due to losses and tuning issues within the human body. When implanted, not all of the radiated power from these antennas reaches the receiver because of absorption and reflection by bodily tissues. The absorbed power significantly surpasses the reflected power in the case of implantable antennas, resulting in a wider bandwidth at the expense of reduced radiation efficiency. To mitigate these losses, various techniques like impedance matching and bio-encapsulation can be employed. These methods have the

potential to reduce losses, thus achieving a narrower bandwidth. However, it's important to note that implantable antennas with narrow bandwidths often experience frequency detuning within the human body. Consequently, careful consideration is required to address this challenge effectively [55, 61].

2.2.3 Human Body Effects on Antenna Radiation Pattern

The radiation pattern of an antenna illustrates how the antenna's emitted field changes with the angle at a set distance, as discussed in Chapter 1. In contrast, the radiation pattern of implantable antennas or antennas in close proximity to the body is entirely distinct from that of a conventional antenna operating in free space. This difference is attributed to the human body's lossy properties, which can potentially cause the radiation pattern to widen. Furthermore, when electromagnetic waves interact with the human body, they can undergo reflection and refraction. These phenomena can cause the radiation pattern to be redirected or distorted, leading to variations in different directions. The positioning and orientation of the antenna relative to the human body are critical considerations. Even slight adjustments in antenna placement or orientation and thickness of human tissue can result in significant alterations to the radiation pattern. For instance, in the case of implantable antennas, factors such as implant depth and orientation within the body can profoundly affect radiation patterns [66–70].

2.2.4 Human Body Effects on Antenna Directivity and Antenna Gain

Directivity is an additional parameter used to describe antennas, and it is closely connected to the radiation pattern. It quantifies the highest power intensity radiated in a specific direction when compared to the radiation intensity of a standard isotropic antenna operating with the same input power [Chapter 1]. In the context of IMDs (Implantable Medical Devices), it is advantageous to design an implanted antenna that exhibits high directionality, with its primary radiation lobe directed away from the body's biological tissues. This design approach aims to establish an efficient through-body communication link [71].

As discussed in Chapter 1, The term antenna gain (G) shares a similar definition with antenna directivity (D), and when determining it, the influence of antenna radiation efficiency (η) is taken into consideration as follows:

$$G = \eta D \tag{2.28}$$

In simpler terms, antenna gain assesses the power transmitted in the direction of maximum radiation in comparison to that of an isotropic or reference antenna. Furthermore, for a more precise assessment of the antenna's characteristics, the analysis factors in the impedance mismatch between the antenna and the power source, resulting in the introduction of a parameter known as realized gain G_r [7, 72]:

$$G_r = G(1 - |\Gamma|^2) \tag{2.29}$$

In this context, Γ corresponds to the reflection coefficient of the implantable antennas or antennas in close proximity to the body. Consequently, an antenna that achieves a suitable impedance match attains a realized gain near the local maxima in proximity to the desired frequency bands of operation, all while maintaining its antenna gain intact.

2.3 Radiation Antenna Effects on the Human Body

Another crucial aspect to consider when designing wearable and implantable antennas is the impact EM radiation on the human body. Despite non-ionizing radiation lacking the requisite energy to alter atoms or human cells, it possesses sufficient energy to agitate human cells and raise their temperature. The temperature increase is a significant factor since a substantial rise in temperature could potentially have harmful effects on human tissues. The most prominent effect associated with non-ionizing radiation is dielectric heating. Dielectric heating is a thermal phenomenon stemming from microwave radiation, occurring when a dielectric material heats up due to the rotation of polar molecules induced by the EM field [73].

The increase in the temperature of human tissue cells can be attributed to the absorption of a portion of the microwaves emitted by an antenna as they are absorbed by the body. The tool used to quantify the rate at which energy is absorbed by human tissues is referred to as the Specific Absorption Rate (SAR) [1, 73, 74].

The SAR is a widely employed metric for evaluating the potential health risks associated with RF signals on the human body. SAR can be calculated for the entire body or for specific localized areas. When assessing localized SAR, it is typically computed for tissue volumes of either 10 g or 1 g. The SAR is represented by the following formula [67, 69, 75]:

$$\text{SAR} = \frac{\sigma}{\rho}|E|^2 = \frac{J^2}{\rho\sigma} \quad [\text{W/kg}] \tag{2.30}$$

Where, E represents the electric field strength measured in volts per meter $[V/m]$, J stands for the current density, which is measured in amperes per meter $[A/m]$, σ signifies the electrical conductivity of the tissue, expressed in siemens per meter $[S/m]$, and ρ represents the tissue's mass density, which is denoted in kilograms per cubic meter $[Kg/m^3]$.

Various standardization organizations establish specific SAR limits for wireless devices to ensure the safety of users. These limits vary depending on whether the exposure conditions are controlled (occupational) or uncontrolled (public) when it comes to RF energy. For public safety standards, the Federal Communications Commission (FCC) utilizes a SAR value of 1.6 watts per kilogram (W/kg), averaged over $1g$ of tissue volume. In contrast, the International Commission on Non-Ionizing Radiation Protection (ICNIRP) and The Institute of Electrical and Electronics Engineers (IEEE C95.1-2019) have adopted a SAR value of 2 W/kg, averaged over $10g$ of tissue volume [67, 76].

For safety considerations and applications involving thermal treatments like the development of microwave hyperthermia devices, monitoring the temperature changes within biological tissues is essential. The assessment of thermal fluctuations in biological tissue can be accomplished through the utilization of the bioheat equation, denoted as Equation (2.31) and originally formulated by Pennes [77, 78]:

$$\rho C\frac{\partial T}{\partial t} = \nabla \cdot k\nabla T + Q - B(T - T_{\text{bl}}) + A_0 \tag{2.31}$$

In this equation, C represents the specific heat capacity of the tissue (measured in joules per kilogram per degree Celsius, J/kg℃), T signifies the temperature (in degrees Celsius, ℃) at a given time t (in seconds, s), k denotes the thermal conductivity (in watts per meter per degree Celsius, W/m℃), B stands for the blood perfusion coefficient (in watts per cubic meter per degree Celsius, W/m^3 ℃), T_{bl} indicates the blood temperature (in degrees Celsius, ℃), A_0 represents the heat generated by metabolism (in watts per cubic meter, W/m^3), In the Pennes equation, Q represents the deposition of volumetric power or the heat source (measured in watts per cubic meter, W/m^3) and is determined from the EM fields employing the following equation [77, 78]:

$$Q = J \cdot E \tag{2.32}$$

2.4 Authorized Operating Frequency Ranges for Wireless Medical Applications

The allocation of radio spectrum for wireless medical applications differs across regions governed by various accredited regulatory bodies. Moreover, within each region, the spectrum allocation is categorized based on licensing approaches tailored to specific medical uses and the sharing of radio spectrum with other applications.

The choice of the operating frequency band for an antenna engineer is contingent upon the specific application. Opting for lower frequencies can result in reduced signal losses when they penetrate biological tissues, attributed to their lower conductivity. Conversely, higher-frequency biotelemetry necessitates smaller antenna dimensions and can lead to improved communication speed.

Figure 2.4 provides a summary of the bands [79]. Some of the accessible frequency bands are as follows:

- **Medical Implant Communications System (MICS) Bands:** This licensed band is employed for implant communication and has a frequency range of 402–405 MHz, which is utilized in most countries, including the USA, Europe, Japan, Australia, Korea, and others. It offers 10 channels with a bandwidth of 300 kHz, adaptive frequency agility, and a maximum effective isotropic radiated power (EIRP) of 25 μW [4, 80–82].

- **Industrial, Scientific and Medical (ISM) Bands:** Frequencies within the ranges of 5725–5850 MHz, 2400 - 2500 MHz, 902.8 - 928 MHz, 868 - 868.6 MHz, and 433.1 - 434.8 MHz are also considered for biotelemetry in implantable and wearable medical devices in some countries. The ISM band supports high data rate applications [1, 80, 83].

- **Medical Device Radio Communication Service (MDRC):** The frequency ranges of 401 - 402 MHz and 405 - 406 MHz have been allocated for wearable medical applications. The channel bandwidth limit for these bands is 100 kHz. Regulations in the USA and Europe mandate the utilization of these bands for medical applications [52, 79].

- **Medical Micropower Networks (MMNs):** The FCC has allocated a 24 MHz frequency spectrum within the 413 - 457 MHz range for IMD applications. There are 4 segments to this spectrum: 413 - 419 MHz, 426 - 432 MHz, 438 - 444 MHz, and 451 - 457 MHz [52, 84].

- **Ultra-wide Band (UWB):** UWB is a developing wireless frequency range for medical applications, operating in the 3.1 - 10.6 GHz range. Wireless medical devices using UWB can achieve high data transfer rates, up to 1 Gbps, for short-ranging communication (typically less than 1 meter) [1, 80, 84].

- **Medical Body Area Networks (MBANs):** In the USA, according to the General Electric Healthcare (GEHC) proposal, the FCC has designated a frequency spectrum in the 2360 - 2400 MHz band for monitoring human body conditions using MBANs [80, 84]. Additionally, in Europe, the 2483.5–2500 MHz frequency range allotted to MBANs is used by indoor communications systems for patient monitoring devices. For a 3 MHz channel bandwidth, the EIRP set for MBANs devices is 1 mW [52, 85].

- **Wireless Medical Telemetry Services (WMTS):** The FCC has designated three frequency bands: specifically, 608 - 614 MHz, 1395 - 1400 MHz, and 1427 - 1432 MHz [52, 86]. In Japan, two bands, 420 - 429 MHz and 440 - 449 MHz, have been allocated. Additionally, there are accessible frequency bands in Europe and Australia, namely 433 - 435 MHz and 868 - 870 MHz, as shown in **Figure 2.4**. It's worth noting that these bands are designated for short-range devices (SRD). WMTS devices play a crucial role in monitoring a patient's health condition through a bidirectional wireless link [79].

- **World Interoperability for Microwave Access (WiMAX):** WiMAX operates within the 2.5 GHz frequency band in the U.S, following the IEEE 802.16 standard. WiMAX technology can transmit data at speeds of approximately 70 Mbps, making it highly efficient for data transfer. It is often utilized for transmitting information from ambulances to hospitals [84].

- **Ultra Low Power Active Medical Implant and Peripheral (ULP-AMI-P) devices:** As per the Electronic Communication Committee (ECC) guidelines, the frequency spectrum ranging from 9 kHz to 315 kHz is employed for active IMDs with ultra-low power requirements. Additionally, the frequency range spanning from 30 MHz to 37.5 MHz is designated for ultra-low-power blood pressure measurement devices. Lastly, the frequency band between 2483.5 MHz and 2500 MHz is reserved for IMDs [52, 87].

- **Ultra-Low Power Wireless Medical Capsule Endoscopy (ULP-WMCE):** The 430–440 MHz frequency range is reserved for wearable ULP–WMCE applications. The efficient channel bandwidth equals 10 MHz, and the EIRP is -50 dBm [52, 88].

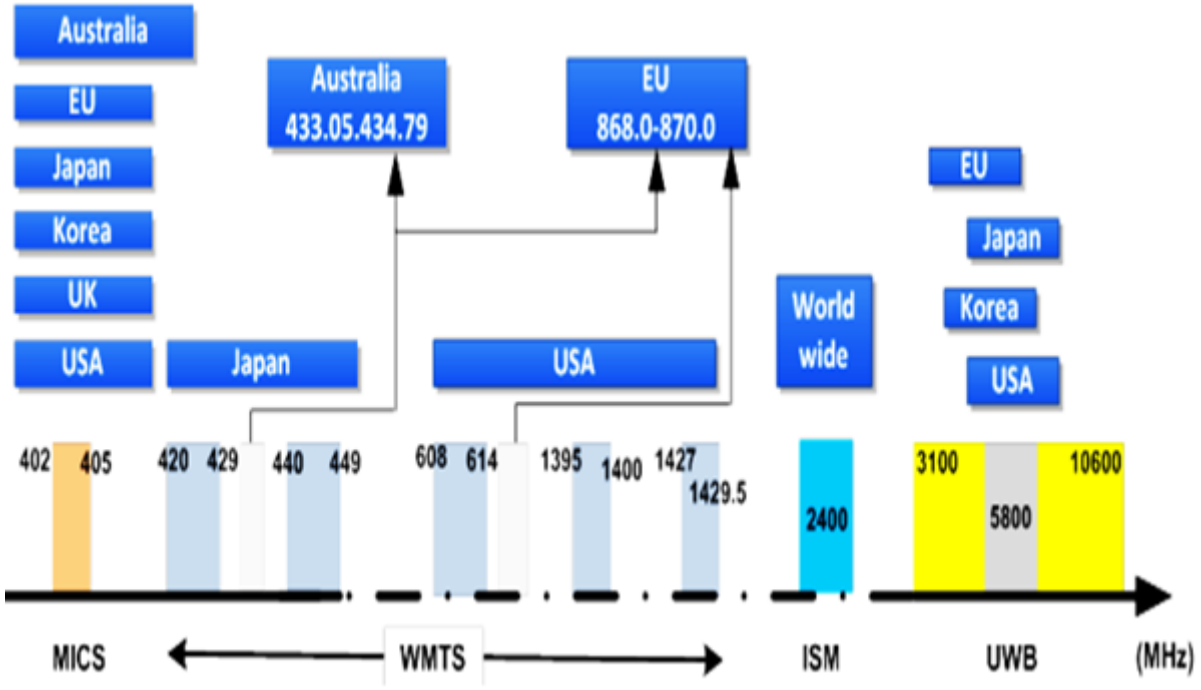

Figure 2.4: Allocating the radiofrequency spectrum for wireless medical applications [79].

2.5 Models of the Human Body

The presence of a human body near an antenna affects its efficiency because, as mentioned earlier, the near-field is closely linked to the surrounding lossy medium. Therefore, the careful choice of human models or phantoms during antenna design is essential for assessing an antenna suggested for specific applications.

The interaction between EM-fields and biological tissue is defined by the frequency-dependent complex permittivity. Various advanced simulation models, such as the FEM [89, 90], or the FDTD method [86,89,91], have been developed to computationally investigate how EM signals propagate through tissues. The accuracy of these simulation models depends on the precision of the dielectric tissue models. Extensive research has been conducted for determining the dielectric properties of various tissues across a wide frequency range [92–94]. One of the most extensive and thorough studies on the dielectric properties of human body tissues was carried out by Gabriel et al [57, 95, 96].

Parametric models have been created to incorporate measured dispersive dielectric properties into EM numerical models. Two prominent models in this context are the Debye and Cole-Cole models [91, 97, 98]. The Debye model is extensively utilized due to its versatility, allowing for convenient representation in both the frequency and time domains. In both the Debye and Cole-Cole models, optimization of model parameters is conducted to achieve the

most accurate alignment with the measured data.

Choosing a specific body model is influenced by multiple factors, including the intended application and the availability of time and resources. Typically, during the initial phases of antenna design, opting for a theoretical or standard phantom is a common practice. This choice is driven by two primary reasons: to conserve time and computational resources, and to facilitate experimental validation using a consistent model. However, as the validation process progresses to a more advanced stage, realistic or voxel phantoms become necessary. It's crucial not to underestimate simulations within these highly accurate phantoms, as even minor fluctuations in tissue dielectric properties can lead to unexpected alterations in antenna performance [67, 99].

2.5.1 Debye and Cole-Cole equations

The fundamental aspects of the tissue dielectric spectrum are widely recognized, thoroughly examined, and documented by Geddes and Baker (1967) and Foster and Schwan (1989), representing some of the most comprehensive articles on this subject [100, 101]. The dielectric spectrum of tissue is delineated by three principal relaxation segments labeled α, β, and γ, associated with low, medium, and high frequencies. Furthermore, there are minor dispersions such as the frequently noted δ dispersion. In its most basic representation, each of these relaxation segments signifies a polarization mechanism defined by a single time constant, τ. In a preliminary approximation, this leads to the subsequent formulation for the complex relative permittivity (ε) as a function of angular frequency (ω) [96].

$$\varepsilon(\omega) = \varepsilon'(\omega) - j\varepsilon''(\omega) = \varepsilon_\infty + \frac{\varepsilon_s - \varepsilon_\infty}{1 + j\omega\tau} \tag{2.33}$$

This is the renowned Debye formula, where the loss factor indicates the capability to absorb microwave energy, while the real part represents the ability to store it, ε_∞ represents the permittivity at frequencies associated with the field when $\omega\tau \gg 1$, ε_s denotes the permittivity at $\omega\tau \ll 1$, and j2 = -1. The dispersion's extent is quantified as $\Delta\varepsilon = \varepsilon_s - \varepsilon_\infty$.

In Hurt's 1985 study, the dielectric spectrum of muscle, describing its dielectric behavior from 10 Hz to 10 GHz, was represented by the sum of five Debye dispersions, accompanied by an additional term for conductivity. In this context, σ_i represents the static ionic conductivity, and ε_0 stands for the permittivity of free space [57]:

$$\varepsilon(\omega) = \sum_{n=1}^{5} \varepsilon_\infty + \frac{\Delta\varepsilon_n}{1 + j\omega\tau_n} + \frac{\sigma_i}{j\omega\varepsilon_0} \tag{2.34}$$

Nonetheless, the intricate nature of biological material in terms of both its structure and composition is such that numerous contributions may broaden each dispersion region. To accommodate this broadening empirically, a distribution parameter can be introduced, offering an alternative to the Debye equation, famously recognized as the Cole–Cole equation [96]:

$$\varepsilon(\omega) = \varepsilon_\infty + \frac{\Delta\varepsilon}{1 + (j\omega\tau)^{1-\alpha}} \tag{2.35}$$

In this case, the distribution parameter α serves as an indicator of how much the dispersion is widened. Consequently, describing the tissue's spectrum in terms of multiple Cole–Cole dispersions would be a more suitable approach [57].

$$\varepsilon(\omega) = \sum_{n} \varepsilon_\infty + \frac{\Delta\varepsilon_n}{1 + (j\omega\tau_n)^{1-\alpha_n}} + \frac{\sigma_i}{j\omega\varepsilon_0} \tag{2.36}$$

This method, using parameters specific to each tissue, allows for forecasting the dielectric response within the specified frequency range. The 4-Cole–Cole model, as introduced by Cole and Cole in 1941 and later discussed by Gabriel et al. in 1996, is utilized to derive isotropic material properties. Specifically, this model characterizes the frequency-dependent permittivity (ε) and conductivity (σ) of various biological tissues across a spectrum ranging from 10Hz to 100 GHz. Within this frequency range, the properties of each tissue are represented by a combination of terms that align with the primary polarization mechanisms, resulting in a distinctive spectrum showcasing four dispersion regions [75, 91].

$$\varepsilon(\omega) = \sum_{n=1}^{4} \varepsilon_\infty + \frac{\Delta\varepsilon_n}{1 + (j\omega\tau_n)^{1-\alpha_n}} + \frac{\sigma_i}{j\omega\varepsilon_0} \tag{2.37}$$

2.5.2 Numerical Body Phantoms

A numerical body phantom may consist of a singular component with uniform EM properties (homogeneous) or a multilayer, multi-component structure representing the diverse electromagnetic characteristics found in the human body (inhomogeneous), or more complex, such as voxel models. These are primarily employed at the initiation of the antenna design process, although they also find application in analytical evaluations for experimental validation and for comparing the performance of various antennas in identical scenarios. However, in specific instances, such as when assessing the distribution of SAR inside the human body, accurate

high-resolution human phantom models are essential.

As demonstrated in **Figures 2.5 to 2.10**, standard geometric shapes with diverse dimensions and varying dielectric properties of body tissues are frequently utilized in academic research to evaluate the performance of the antenna within a simulated human body model. The rectangular cuboid is the most frequently used phantom due to its ease of fabrication, making it particularly useful for validation purposes. Additionally, cylindrical and spherical phantoms find widespread application in various contexts, such as representing body parts like the neck, arm, eyeball, or head. In scenarios related to hyperthermia treatments and tumor detection, semispherical phantoms are utilized to mimic breast models. Moreover, a combination of these basic shapes to create models representing pregnant women is illustrated in **Figure 2.10**. It is possible to perform numerical modelling of the human body with simulation software such as Ansoft High Frequency Structure Simulator (HFSS), Feldberechnung bei Körpern mit beliebiger Oberfläche (FEKO), and Computer Simulation Technology (CST) design studio, etc.

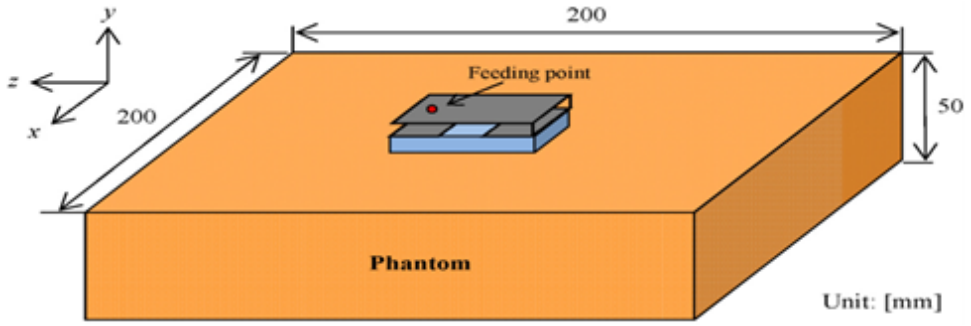

Figure 2.5: Rectangular cuboid homogeneous model. A part of chest phantom at 2.45 GHz ($\varepsilon_r = 35.2$ F/m, $\sigma = 1.16$ S/m)[102].

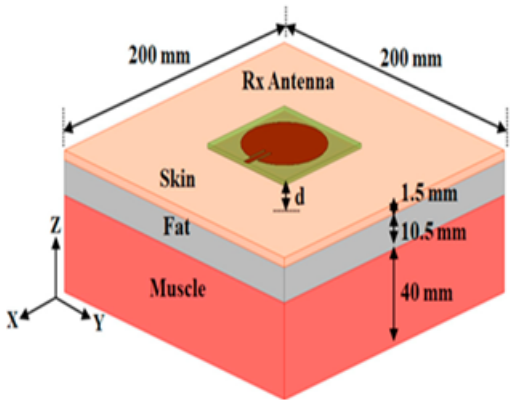

Electric property of human tissue model at 2.45 GHz

Tissue Model (Thickness)	Relative Permittivity (ε_r)	Conductivity σ (S/m)
Skin (1.5 mm)	38.0	1.46
Fat (10.5 mm)	5.28	0.104
Muscle (40 mm)	52.73	1.74

Figure 2.6: Rectangular cuboid inhomogeneous model. A 3-layer phantom tissue (muscle, fat, and skin) model was designed in the HFSS simulator[103].

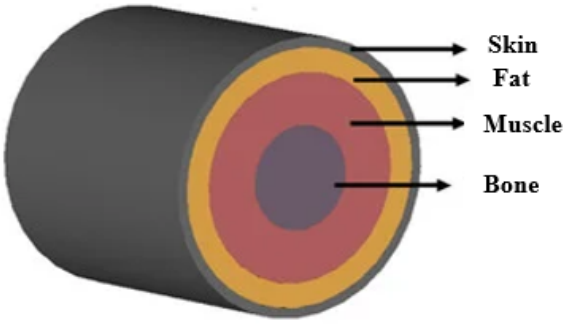

Figure 2.7: Cross-sectional view of the human tissue phantom with four layers, designed in CST Microwave Studio software. The dielectric constants at 2.43 GHz of the modeled bone, muscle, fat, and skin are approximately 11.4, 52, 5.3, and 37, respectively. The thicknesses of the bone, muscle, fat, and skin layers are 30, 15, 7, and 3 mm, respectively [104].

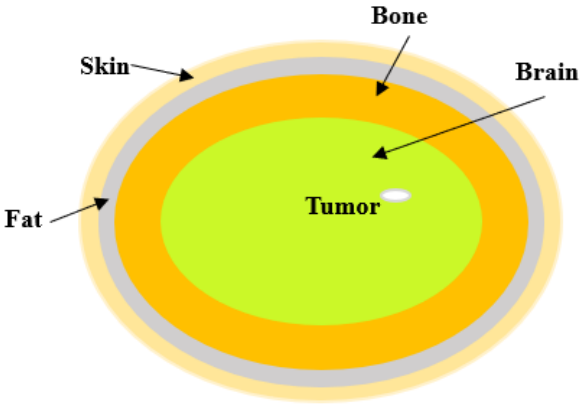

Information of phantom model at 2.39 GHz.

Tissues	Permittivity	Thickness (mm)	Conductivity (S/m)
Bone	5.6	5	0.03
Brain	43.22	35	1.29
Fat	5.54	2	0.04
Tumor	55	10	7
Skin	45	1	0.73

Figure 2.8: Spherical Phantom of human brain designed in CST microwave studio 2016[105].

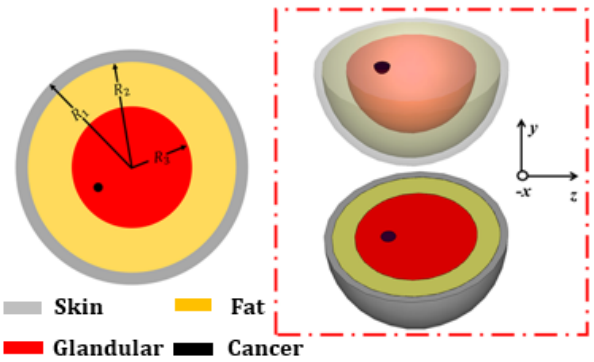

Dielectric properties of the breast tissues at 3 GHz

Fat		Glandular	
ε_r	$\sigma\ (S/m)$	ε_r	$\sigma\ (S/m)$
5	0.1	47	2.1
Skin		**Cancer**	
ε_r	$\sigma\ (S/m)$	ε_r	$\sigma\ (S/m)$
38	1.8	67	3.1

Figure 2.9: Hemispherical breast model designed in CST Studio Suite simulator [106].

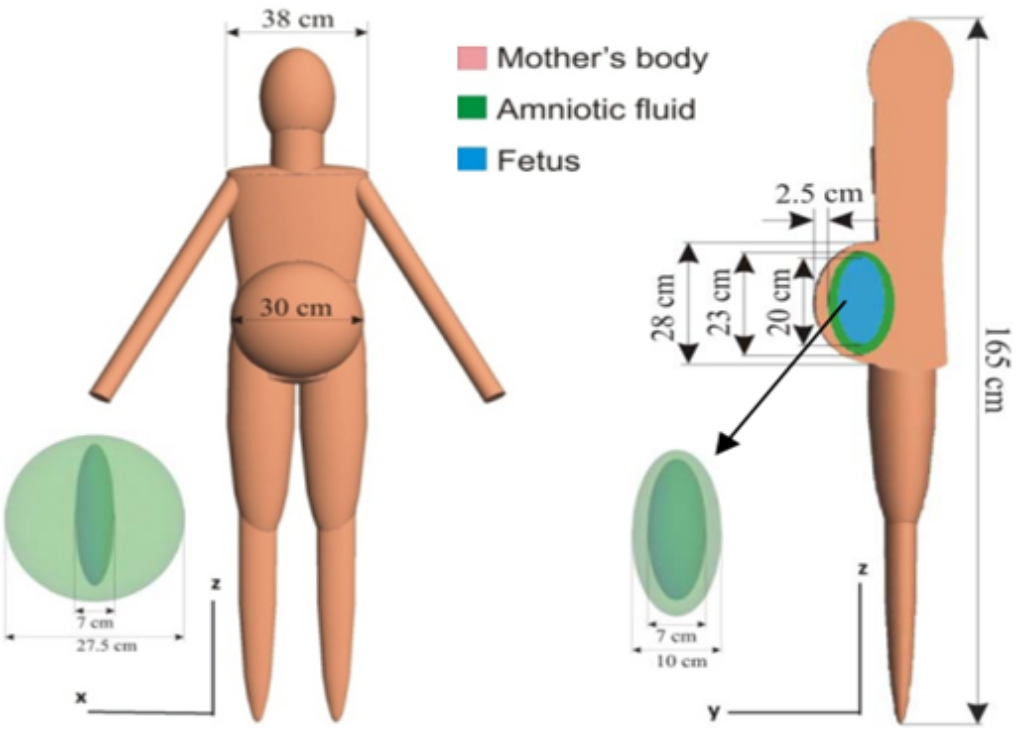

Figure 2.10: Model dimensions of a pregnant woman. FEKO treats electrically large and inhomogeneous dielectric bodies using the FEM approach [89].

Voxel phantoms refer to human models that accurately replicate the actual geometry and arrangement of biological tissues. Utilizing detailed data from medical imaging, these models can be integrated into simulation software to assess antenna prototypes in a more authentic setting compared to traditional phantoms. CST Studio Suite offers various 3D human models, including CST Voxel Family, CST Female Visible Human, and CST Surface Bio Models. The CST Voxel Family comprises eight human model voxel datasets derived from individuals of varying gender, age, and stature, as depicted in **Figure2.11**. Hugo is based on the US National Library of Medicine's Visible Human Project®, which involved dissecting and photographing a frozen corpse. This model is available in resolutions of 1, 2, and 5 mm. The 1 mm version is the most intricate, encompassing tissue types like Thyroid, CSF, Nerve, and Air within the body. Baby, Child, Emma, Donna, Gustav, Katja, and Laura are based on MRI and CT scans of real individuals, available in two resolutions.

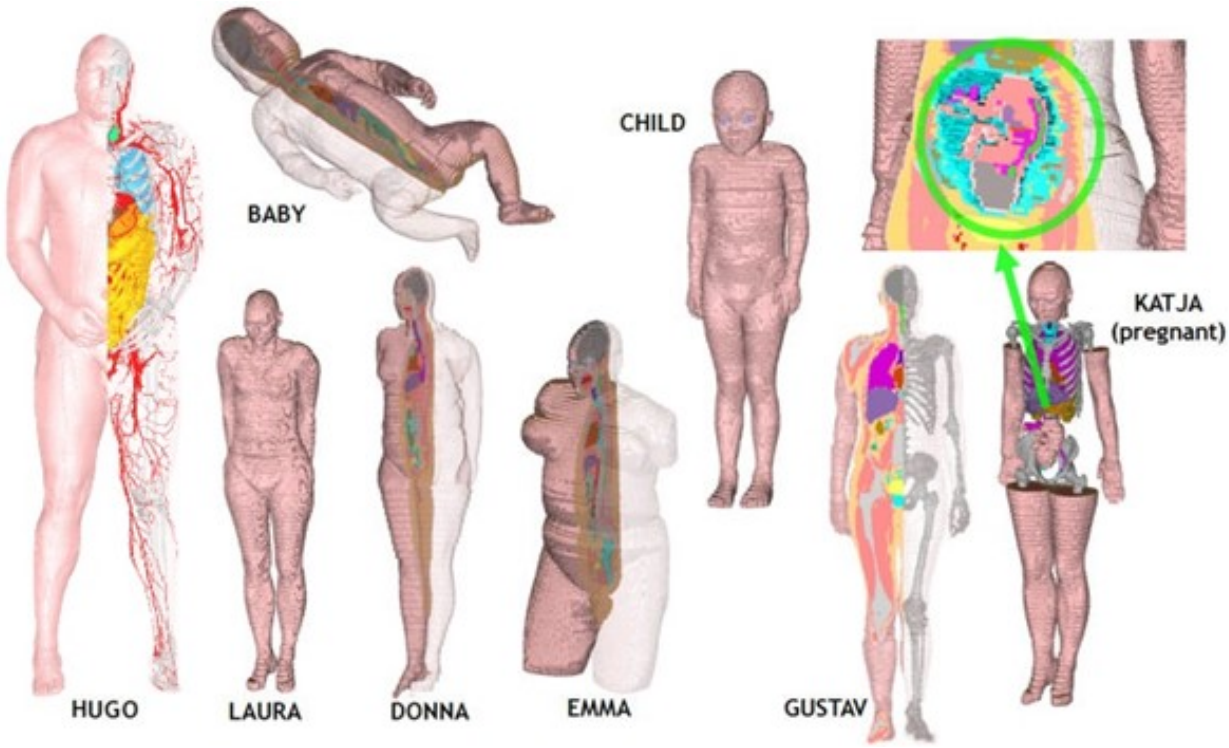

Figure 2.11: CST Voxel Family [107].

The CST Female Visible Human model "Nelly" has been optimized for tetrahedral meshing, as shown in **Figure 2.12**. It is based on the US National Library of Medicine's Visible Human Project®, for which a frozen female corpse was dissected and photographed.

Figure 2.12: CST Female Visible Human model [107].

The CST Surface Bio Models include characters named Tom, Ana, and four children (Baby, 4 years old, 8 years old, and 12 years old), illustrated in **Figure 2.13**.

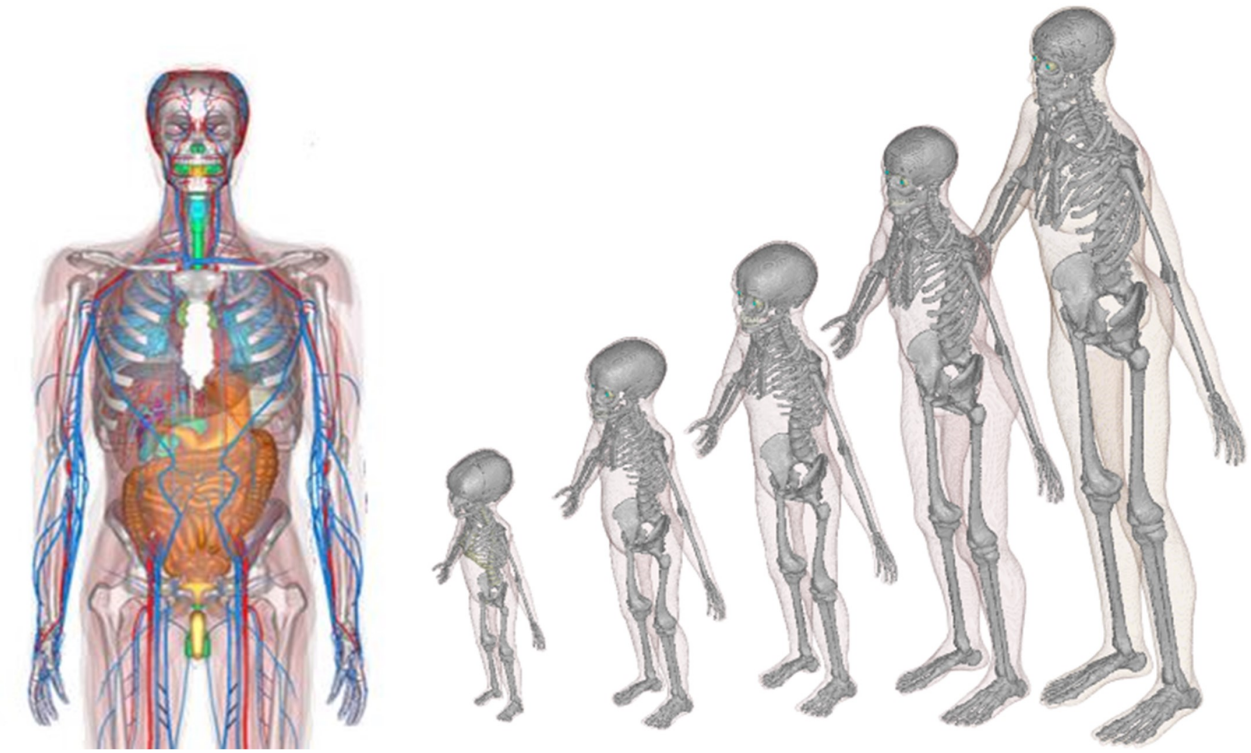

Figure 2.13: CST Surface Bio Models [107].

2.5.3 Experimental Phantoms

While numerical analysis offers a plethora of body phantoms, experimental phantoms pose an increased level of intricacy compared to simulated ones because of the fabrication or preparation procedure. They encompass both physically fabricated models and phantoms made from animal tissues.

Numerous types of physically manufactured models have been suggested to simulate human body tissues. These models can be broadly categorized into three groups depending on their physical state: liquid, semisolid, or solid phantoms, as shown in **Figure 2.14**. Each category has its own set of pros and cons.

Tissues with high water content, such as muscles and brain tissue, exhibit significant electrical properties. Liquid mixtures utilizing water can closely mimic these tissues and are often utilized in the fabrication of physical models due to their high permittivity. Liquid physical models offer the advantage of easy preparation by mixing components based on specific recipes. For physical models with low permittivity (e.g., fat and bone), a low water percentage or alternative mixtures are used.

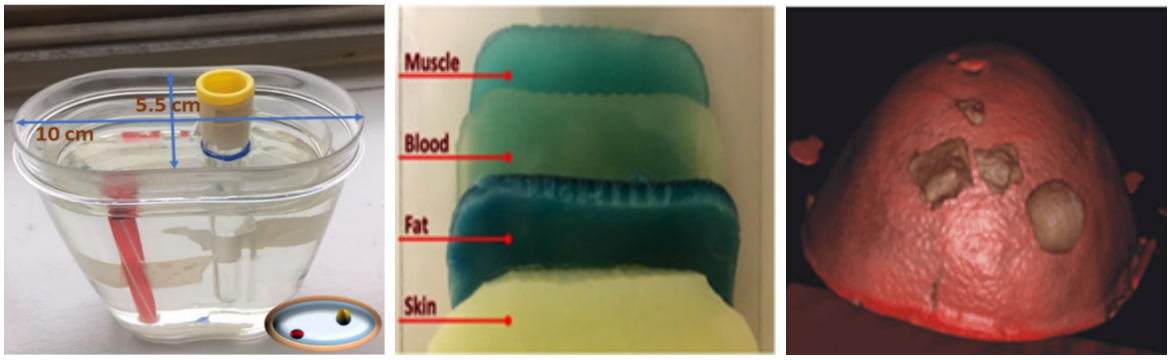

(a) (b) (c)

Figure 2.14: Types of physically manufactured models: (a) liquid tissue phantom (lung phantom with two inclusions) [108], (b) Realized multi-layer biological phantom [109], and (c) solid tissue phantom mimicking human breast with tumor [110].

Challenges include maintaining material consistency, considering the container's influence on measurements, and ensuring proper homogenization of components to achieve the desired electrical properties [108, 111]. Semi-solid physically manufactured models effectively replicate soft tissue shapes due to their castable nature. Their layered structure maintains stable electrical properties without osmosis, resembling human anatomy. The inclusion of gelatin, agar, or dough allows for adjustments in electrical properties during fabrication. These models offer a cost-effective means to replicate human tissues across a broad frequency range. However, they pose challenges for invasive experiments and lack the adjustability found in liquid and gel physically manufactured models [109, 111]. Dry physically manufactured models, crafted from ceramic powders, mitigate hydration issues found in their liquid, gel, and semi-solid counterparts. Ceramic powders offer a broad range of permittivity values but struggle to replicate human tissues' actual conductivity due to their low loss nature. By blending ceramic powders with conductivity-enhancing materials, control over permittivity and conductivity in solid physically manufactured models becomes feasible. The fabrication of solid physically manufactured models demands specialized production equipment and adhesive materials, affecting both cost and complexity. To address these challenges, soft and dry physically manufactured models utilize silicone rubber and carbon components, resulting in lightweight, enduring phantoms; however, invasive measurements can still present difficulties [110, 111].

Utilizing animal tissues for measurements is an efficient method to simulate the frequency-dependent properties of human body tissues. This approach provides an appropriate setting for conducting measurements involving wearable or implanted antennas. Measurements utilizing animal tissue may be performed by placing the antenna on tissue (ex-vivo) or within tissue samples (in-vivo) as shown in **Figure 2.15**. Alternatively, the antenna can be implanted into

a living model animal through surgical procedures as shown in **Figure 2.16**.

(a) (b)

Figure 2.15: Measurements using animal tissue: (a) An ex vivo tissue sample of bovine liver is enclosed in a plastic box. On top of the specimen, visible to the scanning system's arm, is the MWT antenna [112], and (b) Antenna tested inside minced meat [113].

(a) (b)

Figure 2.16: Continuous glucose monitoring using multi-layer implanted antenna sensor. (a) A rat with a sensor implanted; (b) the experimental setup [114].

2.6 Conclusion

In this chapter, We have conducted a comprehensive analysis of the theoretical aspects and challenges associated with the interaction between antennas and the human body. Additionally, we have explored the alterations in antenna performance that occur when a human body is nearby, as well as the effects of radiation emitted by antennas on the human body.

Furthermore, We have addressed the simulation of models for phantoms, which are utilized in both computational software and experimental validation. The existing literature reveals a wide array of phantom sizes, configurations, materials, and levels of realism, all influenced by factors like antenna placement within and in the vicinity of the body, accuracy requirements, and the available computational tools.

Chapter 3

Antennas for Biomedical Applications

Contents

3.1 Introduction

In the current era marked by rapid advancements in semiconductor technology and diverse signal processing methods, there is a growing focus on exploring and advancing medical applications centered around microwave techniques. Antennas assume a crucial role in the medical sector, with their applications categorized into three distinct domains: (a) diagnostic applications, illustrated by techniques such as MRI and MI; (b) the transmission of data, commonly known as biomedical telemetry; and (c) therapeutic applications, specifically in radiofrequency thermal ablation, with notable applications in cardiology and cancer (tumor) therapy [1]. A visual representation of these varied applications is presented in the flowchart illustrated in **Figure 3.1**.

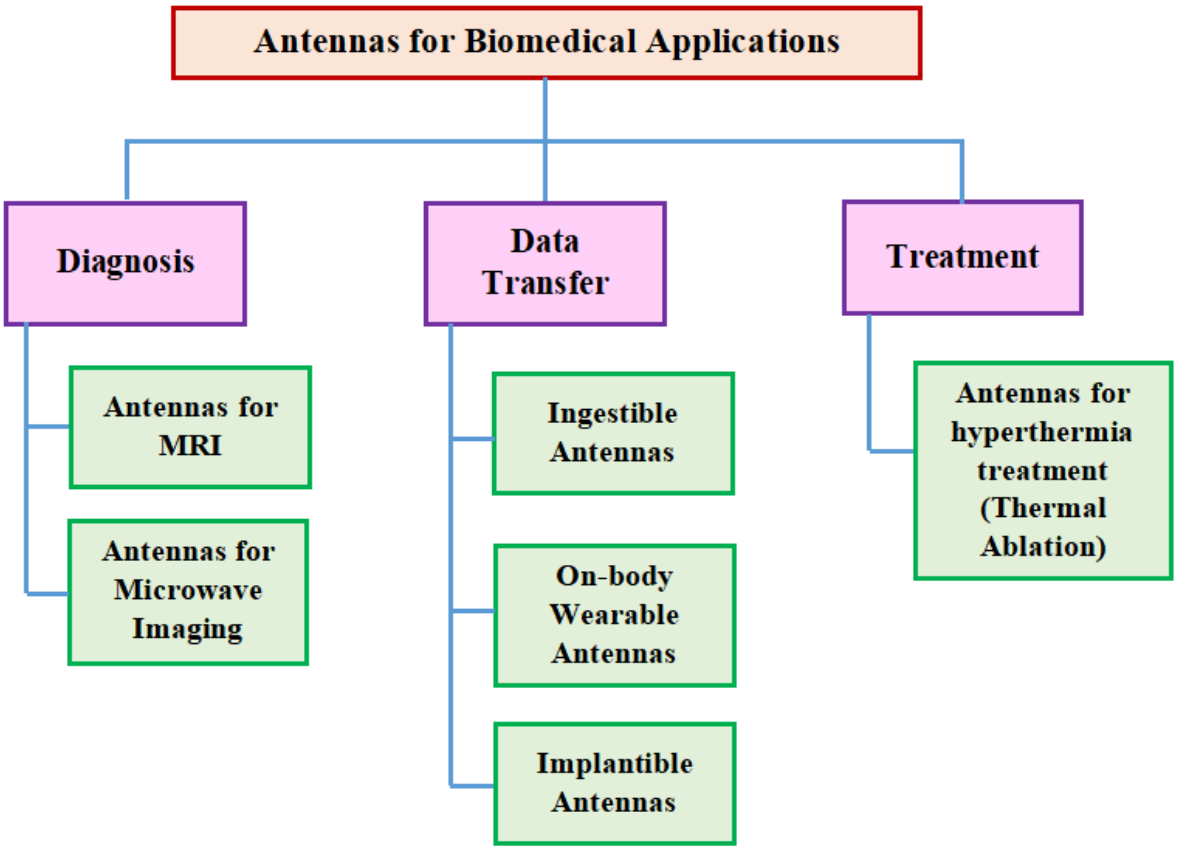

Figure 3.1: Applications of antennas in the medical domain.

Historically, technologies like MRI utilizing magnetic fields, mammography, CT scans employing X-rays, and sonography using ultrasound have been extensively employed in medical diagnosis, particularly for conditions such as cancer and bone imaging. While these methods excel in providing high sensitivity for distinguishing between various tissues and impressive spatial resolution in the sub-millimeter scale, the widespread accessibility of MRI systems in hospitals is limited due to bulky equipment, substantial manufacturing expenses, and comparatively lengthy examination durations. Mammography and CT scans, involving ionizing radiation, pose inherent risks and contribute to an elevated cancer risk, accompanied by the discomfort experienced by patients during mammography procedures. In contrast, ultrasound, operating without ionization, emerges as the preferred choice for medical diagnosis, despite its limitations in penetrating bones and air, resulting in acoustic shadows.

In stark contrast to the challenges associated with conventional technologies, the application of microwave techniques in medicine involves the use of non-ionizing EM waves, making it less detrimental to patients compared to CT scans and mammography. Microwaves at low frequencies and with circular polarization exhibit exceptional tissue penetration capabilities, including the ability to penetrate bones, presenting a challenge for ultrasound. Achieving

high-resolution medical imaging with microwaves becomes feasible through the utilization of wideband signals. Importantly, microwaves within this frequency range uniquely offer the capability to integrate diagnosis with wireless data transmission, a feature unattainable with other technologies in the medical field [51, 53, 115].

The medical application of microwaves extends beyond imaging, involving the utilization of microwave radiation-induced heat to elevate local temperatures and destroy abnormal tissues, particularly malignant tissues. This approach, marked by heightened sensitivity and efficacy in comparison to ionising radiation (e.g., X-rays) and chemical toxins (e.g., chemotherapy), finds applications in hyperthermia for breast cancer treatment [116], transurethral microwave thermotherapy [117], hepatocellular carcinoma (HCC), and microwave ablation [118].

As healthcare expenses rise and the aging demographic poses challenges for governments and providers of healthcare in developed nations, there is a notable attraction to leveraging emerging wireless technologies for unobtrusive, reliable, and cost-effective remote patient monitoring. WBANs emerge as a promising technology with the potential to considerably enhance healthcare services, disease tracking, diagnostic medical monitoring, and other medical processes. A key feature of WBANs lies in their capacity to establish extremely dependable communications for healthcare devices, particularly those inserted in the body of a human.

A WBAN comprises numerous inexpensive, lightweight, miniature sensors that can be strategically positioned on the human body as intelligent patch antennas, integrated into clothes, inserted beneath the skin, or embedded deeply within bodily tissues. The primary objective is to enable healthcare professionals to securely monitor patients' health status. WBAN technology offers economical and effective healthcare solutions, thereby enhancing the quality of life for individuals. Implanted or wearable wireless sensor nodes, strategically positioned, consistently monitor vital parameters including electroencephalogram (EEG), electrocardiogram (ECG), photoplethysmogram (PPG), electromyogram (EMG), blood pressure, blood oxygen saturation (SPO2), or essential environmental values such as humidity and temperature. The patient-related data collected across all WBANs can be transmitted to a centralized healthcare database for permanent storage. This data may be accessed remotely by physicians to evaluate the patient's health status, and patients can receive alerts through SMS, alarms, or reminders [119–121].

3.2 Medical Microwave Imaging Application

Medical imaging exploits physical processes, such as X-rays, ultrasound, magnetic resonance (MR), and radioactivity, to produce visual representations or images of the human anatomy, tissues, or organs. The primary imaging modalities in clinical medicine comprise X-ray radiography, CT, MRI, SPECT, ultrasound, and fluoroscopy. However, these screening methods are associated with significant costs, discomfort, and the use of ionizing radiation [122].

A different approach to medical imaging that is attracting the attention of numerous researchers is microwave imaging (MI). This method is becoming increasingly popular due to its use of nonionizing radiations, cost-effectiveness, safety, simplicity, and its capability to provide high-resolution images of scanned body tissues [51, 123].

In order to overcome the limitations inherent in current approaches, researchers have redirected their focus toward an alternate approach based on microwaves. MI is a method used for identifying concealed or embedded objects within a medium by utilizing microwave signals. An MI system comprises two primary components: (a) an antenna (hardware), responsible for emitting and capturing microwave signals reflected from the target object under test, such as breast and head tissues; and (b) software or post-processing algorithms tasked with reconstructing an image of the target object, as depicted in **Figure 3.2** [123].

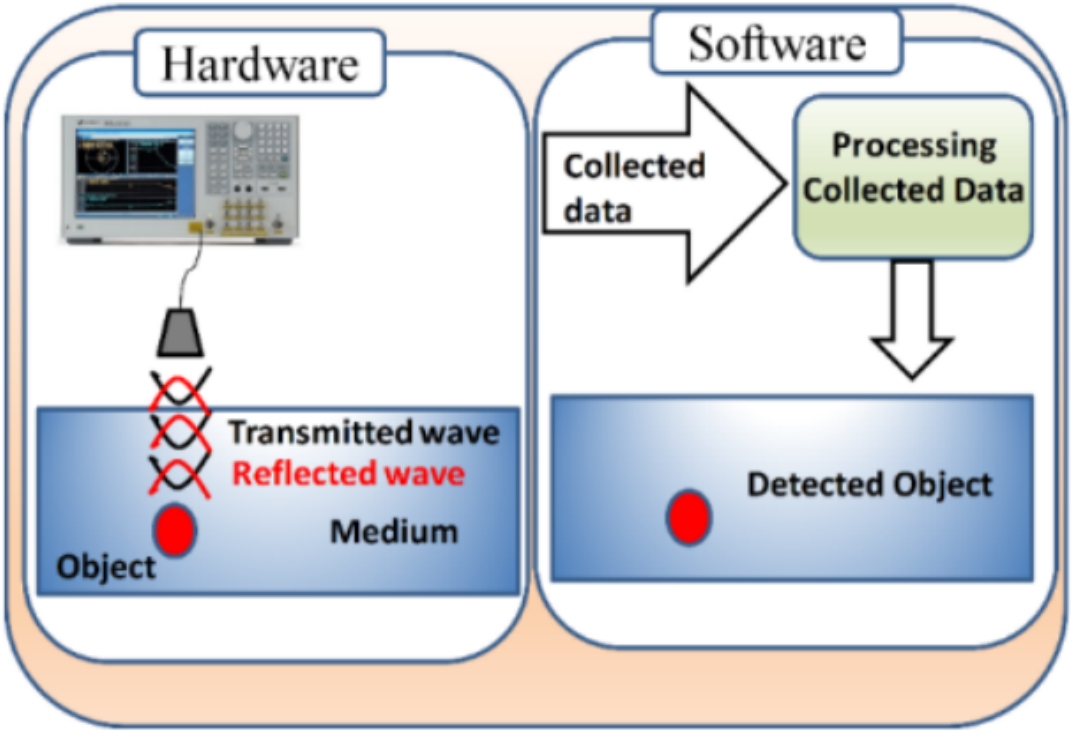

Figure 3.2: A visual illustration depicting the various components of the MI system [123].

MI operates on the basis of mono-static, bi-static, or multi-static radar-type measurements and capitalizes on the notable dielectric contrast between pathological and healthy tissues. [124].

The majority of research efforts aimed at determining the dielectric constants of various bodily organs and tissues rely on the relaxation model recognized as the Cole-Cole equation [Chapter 2]. This equation simplifies to the well-established Debye model [Chapter 2], widely recognized for assessing the dielectric properties of both malignant and normal breast tissues. According to the Debye model, **Figure 3.3** illustrates the dielectric properties of malignant and normal breast tissues at radio and microwave frequencies [125]. Furthermore, **Figure 3.4** depicts variations in skin, fat, oil, and tumour tissues across the frequency band of 0 to 7 GHz [126], highlighting that malignant tissues exhibit higher dielectric properties compared to healthy tissues.

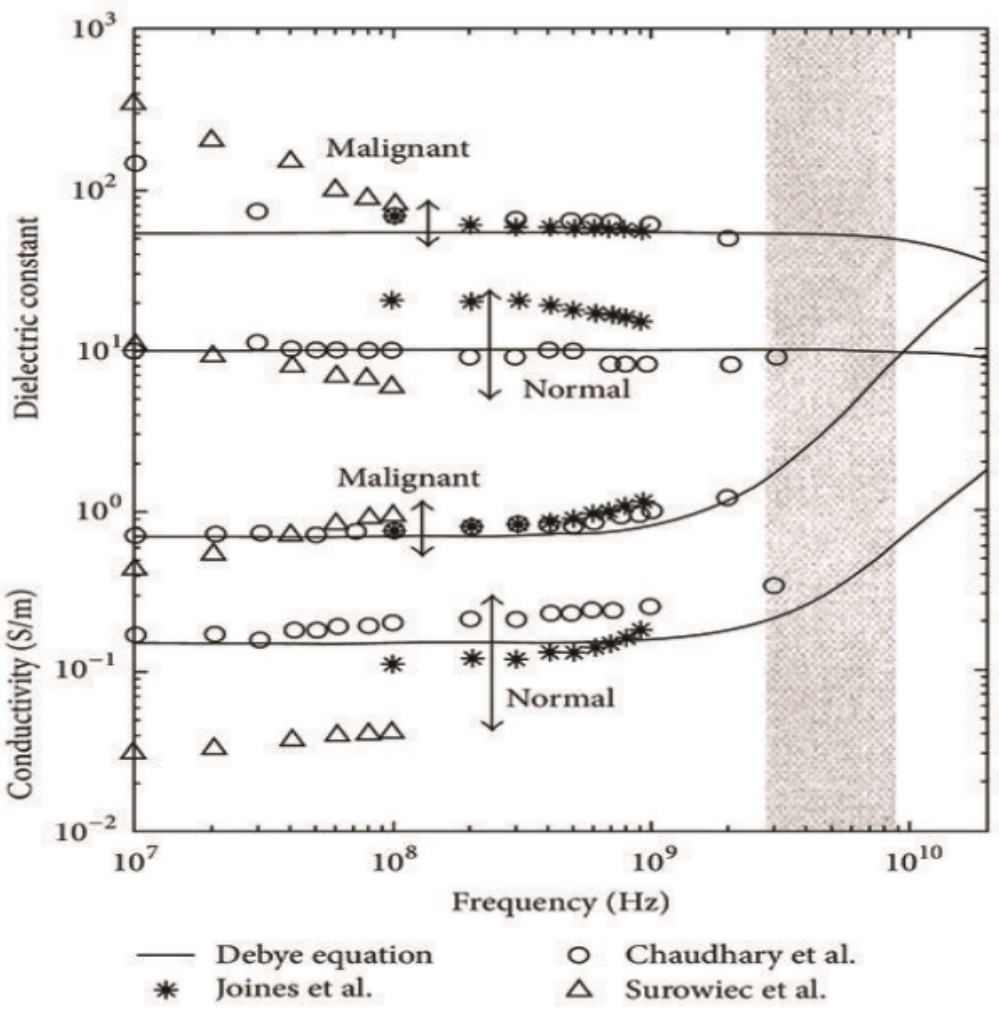

Figure 3.3: Data on the dielectric characteristics of normal and cancerous breast tissue at radio and microwave frequencies, as well as single-pole Fitting the Debye curve to the measured baseline [125].

Understanding the dielectric properties of body tissues is crucial for comprehending the interactions between EM fields, specifically microwaves, and the body tissue. In quantitative MI, the reconstruction of dielectric properties involves considering differences in complex permittivity. This applies specifically to non-metallic materials in biomedical applications and is defined by the following equation [Chapter 2]:

$$\varepsilon(\omega) = \varepsilon'(\omega) - j\varepsilon''(\omega) \tag{3.1}$$

with the real part denoting the material's capacity to store microwave energy, and the imaginary part, or the loss factor, indicating its ability to absorb microwave energy [Chapter 2].

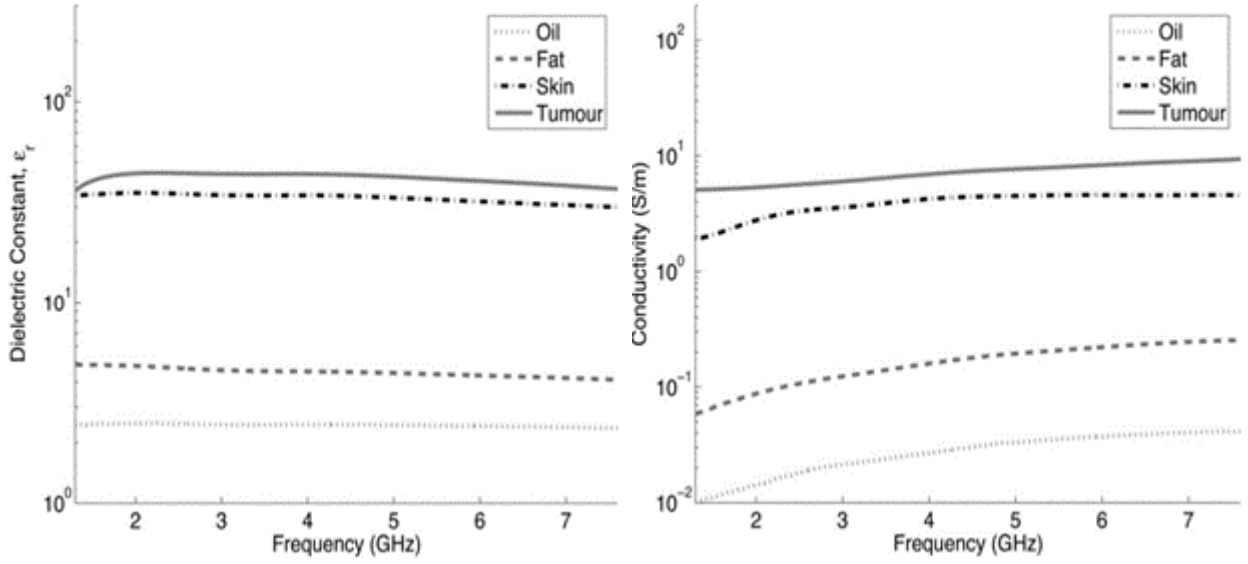

(a) (b)

Figure 3.4: Variations in (a) Relative permittivity, and (b) Conductivity of skin, fat, oil, and tumour tissues as frequency changes from 0 to 7 GHz [126].

Detection methods utilizing microwaves primarily rely on the significant variation in dielectric properties between healthy and abnormal tissues. MI utilizes brief pulses of low-power microwaves emitted from appropriate antennas directed at the human body. Consequently, microwaves scattered or reflected off body cells are expected to produce an image that enhances the contrast between diseased and normal cells.

The literature outlines three modalities studied for microwave-based body detection, as illustrated in **Figure 3.5**: active, passive, and hybrid methods [51, 123, 127, 128].

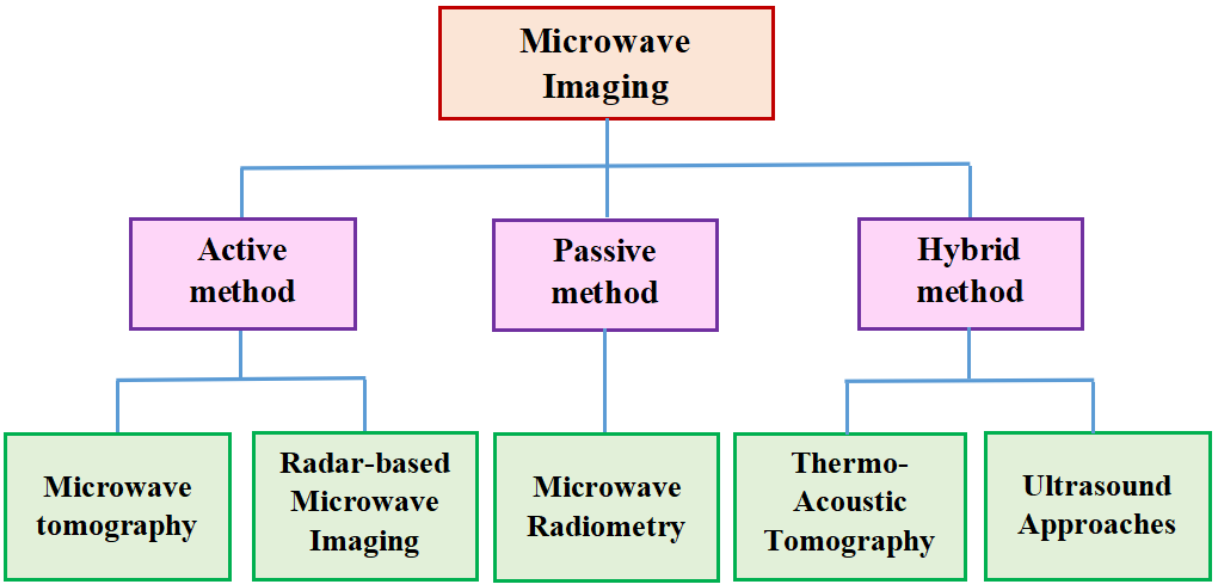

Figure 3.5: Diverse approaches and methods employed in MI.

3.2.1 Active Microwave Imaging

Active methods encompass procedures that depend on the notable electrical characteristics and distinctions between abnormal and normal body tissues when exposed to microwave frequencies. There are essentially two imaging methods, namely microwave tomography and radar-based MI techniques. Both employ low-power microwave signals to illuminate the body, and the analyzed backscattered signals are examined to interpret the dielectric properties of the body [51, 123, 127, 128].

- **Microwave Tomography Imaging Approach:**

  The initial active approach is transmission-reflection imaging, commonly known as microwave tomography (MWT). This approach utilizes a single antenna to emit microwave signals into the human body. Subsequently, multiple antennas, positioned equidistant from the body's surface at various locations, receive the transmitted signal. This iterative process involves changing the location of the transmitting antenna multiple times. Finally, signal processing is applied to the acquired data to generate a map illustrating the geometric distributions of the body's relative permittivity. For example, tumors typically diminish the intensity of the scattered signal, so regions displaying elevated relative permittivity (ε_r) and conductivity (σ) values indicate the presence of tumor cells. Employing various inverse scattering problems, the dielectric profile of the tested tissue is then inferred [51, 127].

MWT has been employed since the beginning of the 1970s, with many of the first accounts of its biomedical uses emerging in the early years of the 1980s. Various studies have investigated the application of MWT for detecting breast cancer [129].

The inaugural clinically tested MI system was documented by Meaney's team at Dartmouth College, and the setup is depicted in **Figure 3.6**. The group executed several iterations of the study, progressively refining each version. The initial MI prototype used a sixteen-element multi-static transmitter monopole antenna array that operated at frequencies ranging from 0.3 to 1 GHz [130]. Participants' breasts were subjected to imaging while lying prone on the exam table, with their breast immersed in a solution of saline. Every imaging session, lasting approximately fifteen minutes per breast, involved comprehensive tomographic information collection from seven different array locations, starting from the chest wall and advancing anteriorly toward the nipple, at seven different frequencies per array position. The preliminary outcomes of this investigation indicated a correlation between radiological breast density and breast permittivity [129].

During a later stage of their study, Meaney and colleagues utilized their MWT system but opted to replace the saline solution with a mixture of glycerin and water as the matching medium. This modification aimed to enhance the coupling liquid, as this mixture exhibited a more suitable match to the electrical impedance of the breast. The adjustment proved successful in minimising coupling noise among the array elements, leading to more precise images compared to the group's previous studies. The initial phase of the new experiment focused on imaging a series of cylindrical phantoms containing 2 tumour like inserts one centimetre and two centimetres in diameter, respectively) embedded in the imaging array.

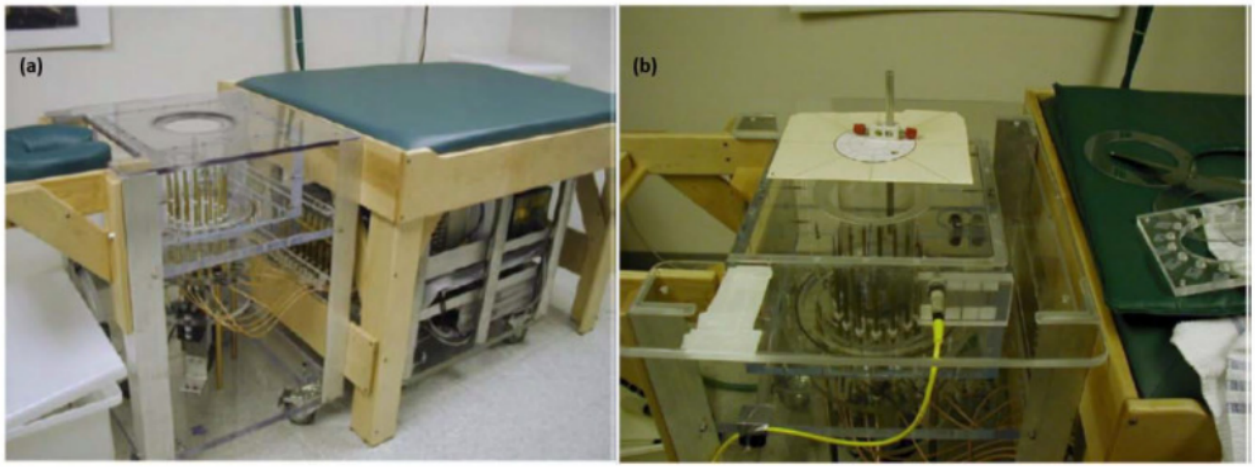

Figure 3.6: MWT imaging system prototype created by Meaney et al [130].

The objective of these phantom studies was to evaluate the system's precision in estimating the distribution of dielectric properties. The subsequent part of the research concentrated on assessing the established system's clinical viability and examining 43 female patients' in vivo normal breast microwave properties. Overall, this study's results were encouraging, especially in the clinical experiments where the system effectively identified tumours with a diameter as small as 1 cm. This underscores the potential of MI for early-stage breast cancer screening [131].

- **Radar-Based MI Approach:**

  In the field of radar-based MI, antennas play a crucial role in scanning multiple points on the body. The substantial difference in dielectric properties between healthy and pathological tissues results in a significant contrast in the scattered signals reflected from these tissues. This discrepancy in scattered signals is a key factor in radar-based MI [124]. MI is categorized into three types: Mono-static, Bi-static, and Multi-static, as shown in **Figure 3.7**.

  - **Mono-static MI** involves the use of a single antenna, serving both as a transmitter and a receiver.
  - In **Bi-static MI**, two antennas are employed, with one acting as a transmitter and the other as a receiver.
  - On the other hand, **Multi-static MI** utilizes an array of antennas, with one antenna operating as a transmitter at a given time while the others function as receivers.

  Patch antennas are extensively used in radar-based MI due to their cost-effectiveness, ease of fabrication, and accessibility.

  The proposal of the radar-based method for detecting breast cancer occurred independently in the late nineties, with Benjamin suggesting it in 1996 [132], and Hagness in 1998 [133]. Klemm et al. developed and executed a MI system based on UWB frequency-domain radar. The system comprised a set of UWB antennas arranged in an aperture array, strategically placed on a segment of a hemisphere to match the curved shape of the breast, as illustrated in **Figure 3.8.a**. The UWB antenna array was situated with the breast comfortably positioned on the spherical shell, as depicted in **Figure 3.8.b**. Signal data was acquired using a data acquisition module and then transmitted to a workstation. Clinical imaging outcomes demonstrated the system's capability to detect an 8 mm tumor, as illustrated in **Figure 3.9.b**.

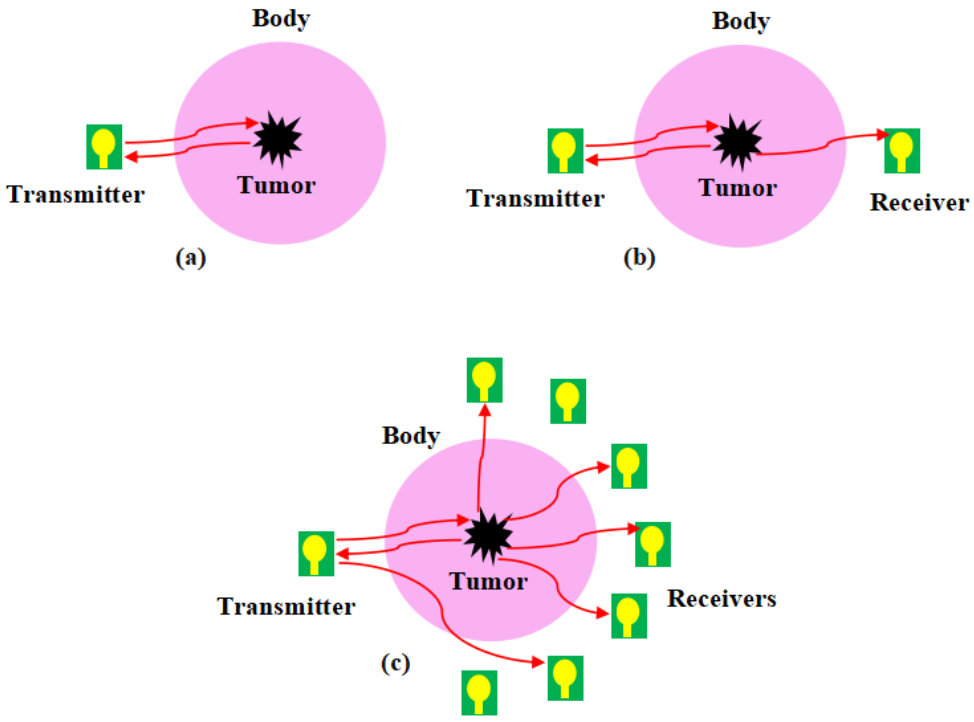

Figure 3.7: Types of Radar-Based Microwave Imaging - (a) Mono-static, (b) Bi-static, and (c) Multi-static.

Fear et al. created a prototype system for the detection of breast cancer, known as the 3D UWB Tissue Sensing Adaptive Radar (TSAR) MI. The setup included a patient interface featuring a cushioned table with an aperture, allowing the breast to descend within a cylindrical container, as illustrated in **Figure 3.10**[134] and **Figure 3.11**[134, 135]. Employing a mono-static approach for data collection, the system incorporated a filtering circuit to mitigate reflections from the skin tissues. Testing was conducted on a group of eight volunteers aged between 32 and 47 years. The system successfully identified breast tumors with a diameter as small as 5 mm, as shown in **Figure 3.12**[134].

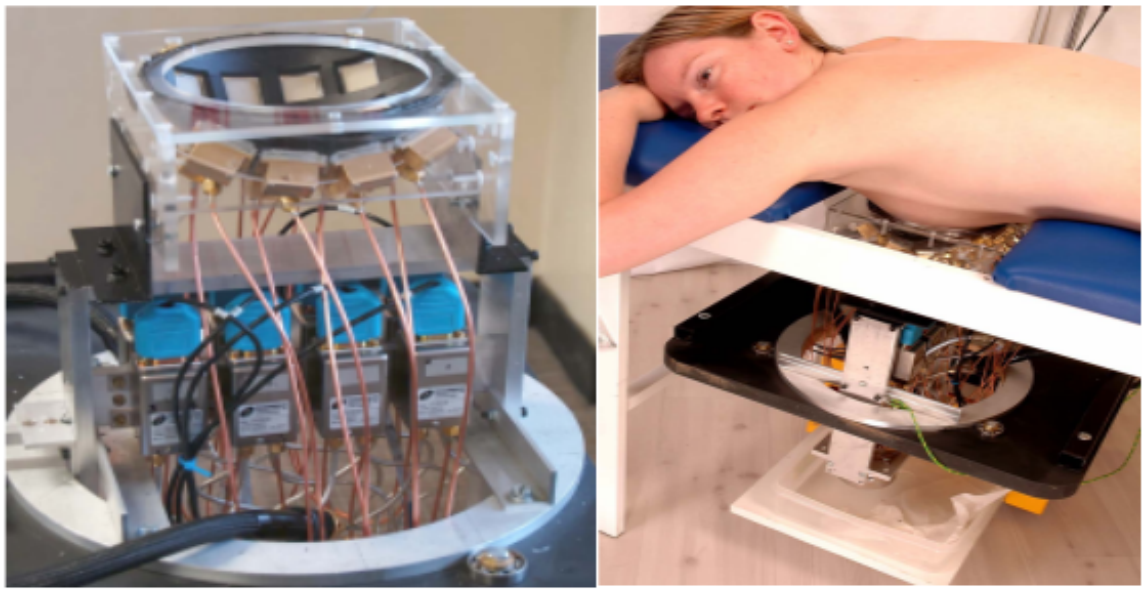

(a) (b)

Figure 3.8: UWB frequency-domain radar-based MI system prototype created by Klemm et al. (a) Array, feed, and switching, (b) Clinical configuration employing microwave radar for breast cancer detection, with the patient in a prone position [136].

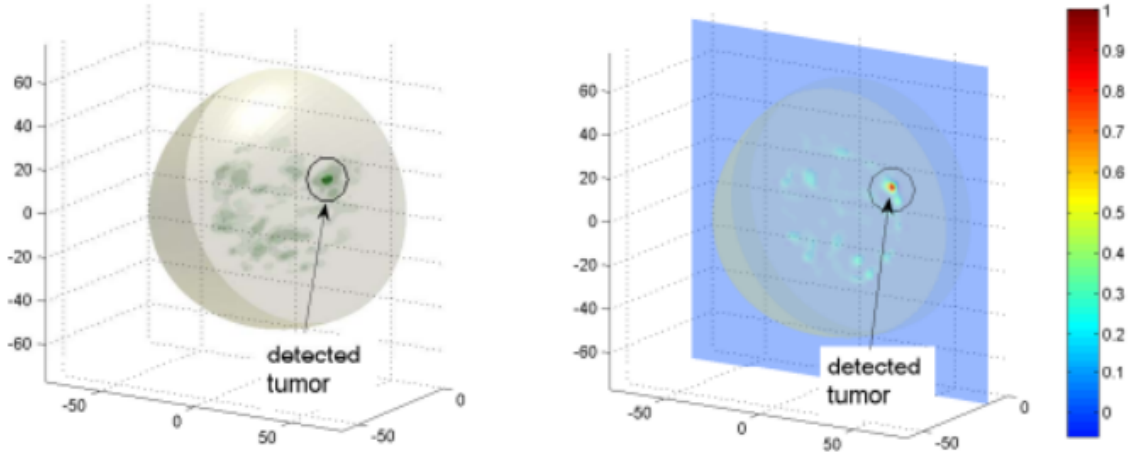

(a) (b)

Figure 3.9: Clinical imaging findings obtained with a radar-based UWB microwave system: (a) three-dimensional (3D) image, (b) two-dimensional (2D) image along a plane where the tumour was identified [136].

Figure 3.10: Prototype of the TSAR Radar-Based MI System for Breast Cancer Detection by Fear et al [135].

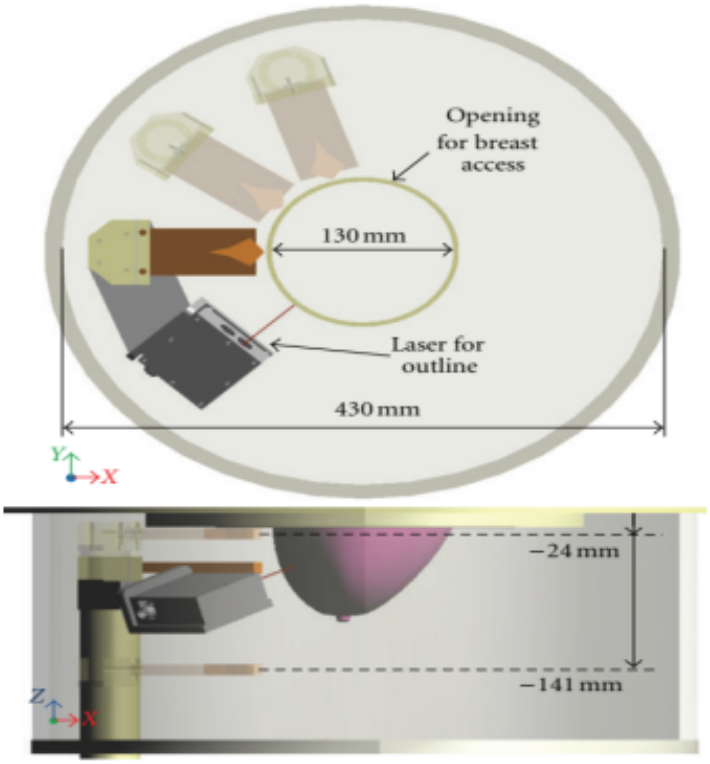

Figure 3.11: Top and lateral perspectives of the tank in the TSAR prototype system, featuring dimensional specifications [135].

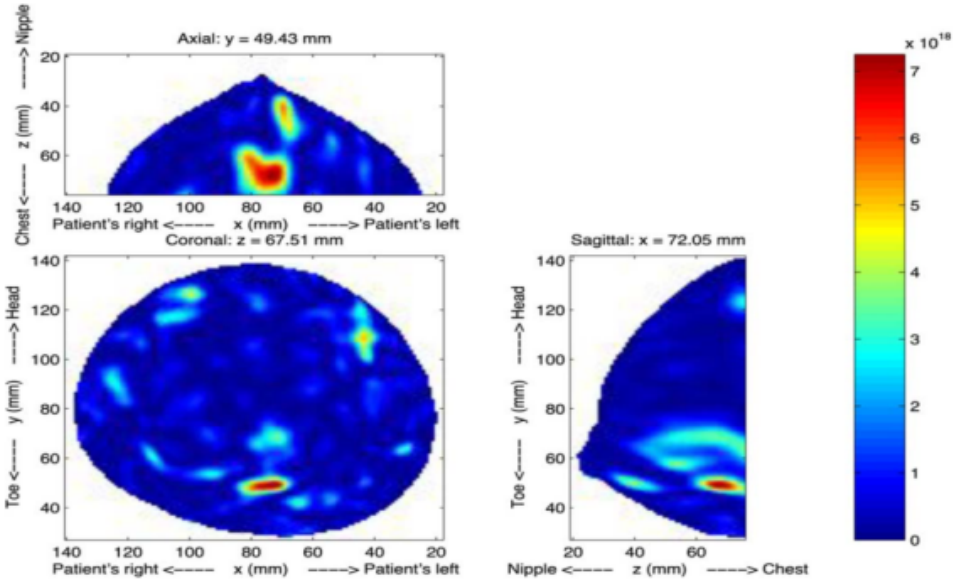

Figure 3.12: Images obtained through TSAR for patient 7 [134].

3.2.2 Passive Microwave Imaging

In the passive method, Microwave Radiometry (MWR) is used to illustrate the spatial temperature distribution within the body, encompassing both internal and surface areas. This technique assists in identifying the region affected by a pathological process and potentially discerning its qualitative characteristics,as illustrated in **Figure 3.13**. The fundamental principle of the biophysical noninvasive MWR method involves measuring the intrinsic EM radiation emitted by internal tissues to detect temperature irregularities in both the body's internal tissues and the skin [137]. Due to changes in electrical properties, abnormal tissues have a greater temperature compared to healthy tissues [123, 137].

In recent years, microwave radiometry technology has garnered increasing attention, with diverse medical applications targeting areas such as the breast [138], brain [139], carotid artery [140], juvenile idiopathic arthritis [141, 142], brown adipose tissue (BAT) activity [142], joints [143], synovial inflammation [144], veins [145], vesicoureteral reflux [146], the urogenital system [147], back pain [148], diabetic foot [149], and COVID-19 Pneumonia [150].

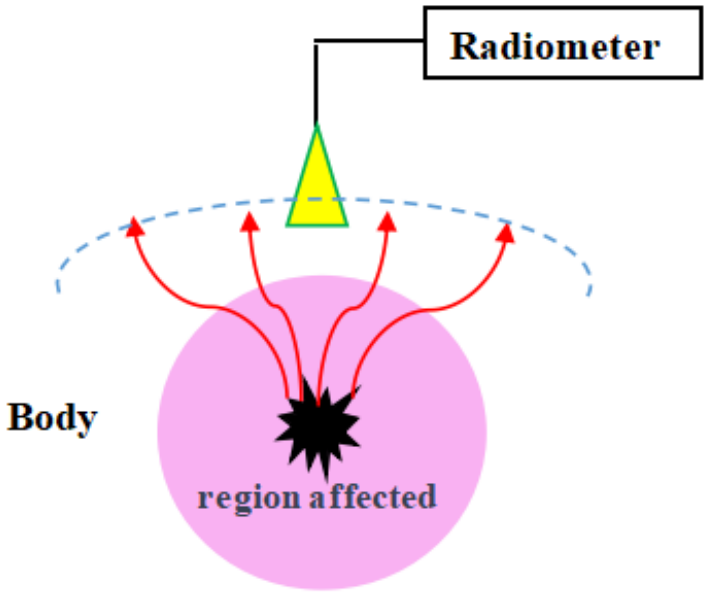

Figure 3.13: Passive microwave imaging.

3.2.3 Hybrid Microwave Imaging

In the 1980s, hybrid microwave-induced acoustic imaging techniques emerged, operating on a principle akin to passive MI. In this variation, microwaves are employed to selectively heat pathological cells. As these tissues absorb the heat, they expand, and any resulting acoustic waves are detected using an array of ultrasound transducers, as illustrated in **Figure 3.14**. Hybrid MI capitalizes on the fact that abnormal cells exhibit higher conductivity properties than healthy tissues, causing them to absorb greater microwave energy.

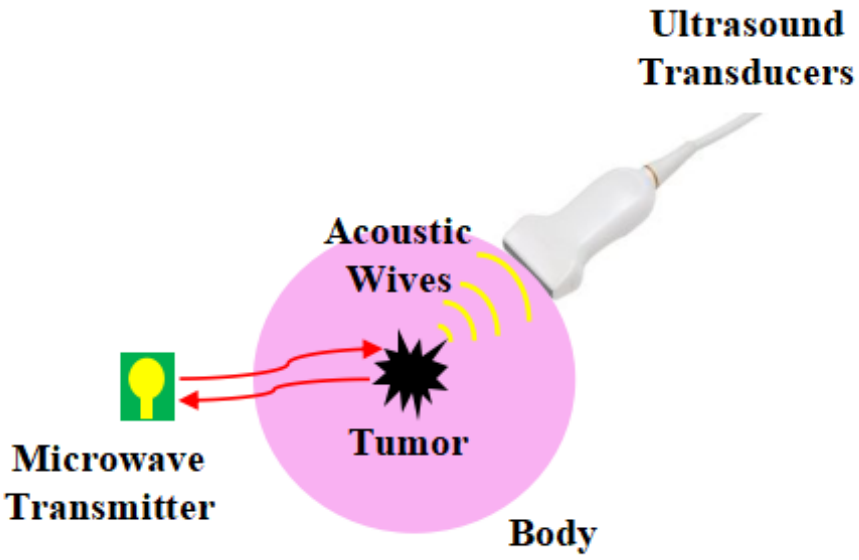

Figure 3.14: Hybrid microwave imaging.

Consequently, this absorption leads to the generation of more powerful acoustic and pressure waves. The induced acoustic signals are then captured by ultra-sensitive sensors. This method is remarkably responsive to tumors and yields images of superior resolution [51].

3.3 Biomedical Telemetry Applications

Wireless bio-telemetry involves the process of measuring signals originating from the body and transmitting them to a remote base station, such as a phone or PC, over an RF communication link. Subsequently, this data is sent over the internet to a doctor or relevant individual for diagnosis and guidance to the patient. **Figure 3.15** illustrates a remote healthcare monitoring system with either invasive or non-invasive sensor nodes deployed on the human body. Temperature, heart rate, EEG, ECG, EMG, PPG signals, glucose level, O2 saturation, and other essential data are transmitted to the monitoring unit for further analysis using the integrated antenna [1,119,120,151]. Antennas designed for bio-telemetry can be classified as body-centric (wearable antennas), implantable antennas, or ingestible antennas (used in capsule endoscopy), depending on the location of the sensor node on or inside the human body [1].

According to IEEE 802.15, a practical configuration utilized to characterize communications in Body Area Networks (BANs) concerning the transmission channel includes [152–154]:

- **On-body communications:** On-body communications involves the wireless exchange of data between devices mounted on the body.
- **In-body communications:** In-body communications involve the establishment of connections and relays that facilitate the exchange of data between implantable or ingestible devices and wearable, implantable or ingestible devices.
- **Off-body communications:** Off-body communications denote wireless connections between implantable, ingestible, or wearable devices and base units located in the surrounding environment (base station).

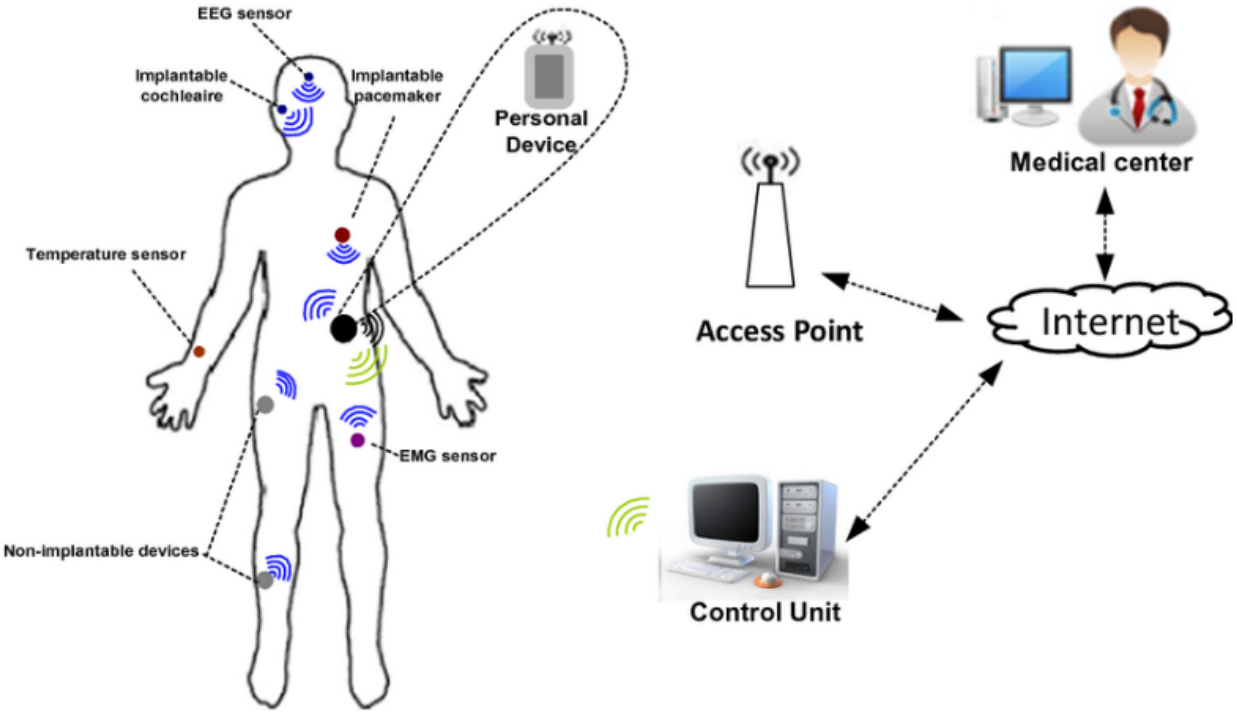

Figure 3.15: Communication architecture for WBANs [155].

Figure 3.16 illustrates the various forms of WBAN communication. In certain scenarios, incorporating a central node, referred to as a gateway, can prove advantageous as it functions as an intermediary between other devices and an external base station. One notable benefit of this network configuration is the ability to accommodate multiple small sensors operating at low bit rates, transmitting data to the gateway. Subsequently, the gateway assumes the role of a central node by storing information from the sensors and relaying it to a base station for in-depth analysis.

Additionally, in specific systems, the gateway may have the capability to power the passive sensors [151].

3.3.1 Wearable Antennas

Wearable antennas play a crucial role by being positioned on different body parts [5, 157], including the chest, back, legs, head, ankle, shoulder, torso, and arms, as shown in **Figure 3.16**. Such wearable monitoring can inform the wearer to any impending health threat, allowing for immediate helpful medical treatment (outside of a hospital environment). A strategy for seamless integration of electronics into the human body involves the use of skin mounted epidermal electronics systems. These systems enable non-invasive, continuous monitoring of crucial physiological signals, including skin temperature, blood pressure, pulse, heart rate, ECG, EEG,

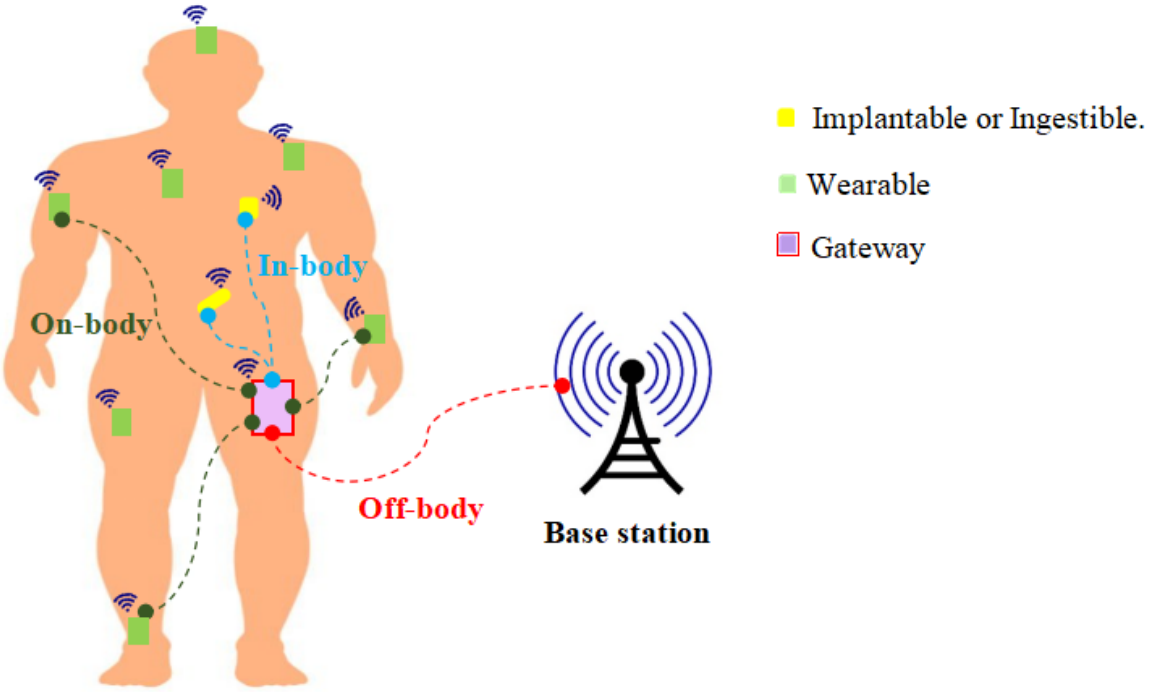

Figure 3.16: Depiction of the three classes of WBAN communication [156].

EMG, PPG signals, O2 saturation, glucose level, and respiration rate [1, 119, 120, 151]. The gathered information is then transmitted to both the patient and the physician. Beyond assessing clinically relevant physiological parameters, tears, saliva, and sweat contain various chemical constituents indicative of physiological conditions [158]. The utilization of such sensors shows significant potential in enhancing and preserving the quality of life, surpassing traditional systems. Unlike traditional systems with wires, cables, adhesive pads, clamps, or needles, epidermal electronics systems are more comfortable, less irritating, and less prone to inflammation. Traditional systems are also bulky and restrict mobility, typically monitoring only one physiological signal [159].

Wearable devices operate in two modes: off-body or on-body communication. In certain applications, a versatile wearable device acting as a gateway can combine multiple operation modes, such as in-/off-body or on-/off-body communication schemes [151]. Wearable antennas may face challenges due to body influence, similar to implants [Chapter 2]. However, this challenge can be addressed by using circular polarization, increasing ground plane dimensions, and employing multilayer or 3D structures. Unlike implants, wearable antennas have less strict requirements for biocompatibility, powering, and miniaturization techniques. Experimental evaluations often do not necessitate the use of phantoms. Nevertheless, certain design considerations for wearable antennas include proper impedance matching across the band of interest [see chapter 2], small and low-profile dimensions for seamless integration into daily life objects

or clothing, a stable radiation pattern independent of body presence, and specific considerations for off-body, on-body, and in-body communication antennas. Off-body communication antennas should prioritize radiation perpendicular to the body, on-body communication antennas should favor side-radiation for on-body propagation, and in-body communication wearable antennas should emphasize energy coupling into the body [151].

3.3.2 Implantable Antennas

The antenna is an integral part of the medical circuit; its shape is determined by the circuit, which, in turn, is influenced by the organs of the body or the location of use where the circuit is implanted.

An implantable medical device is commonly described as an electronic apparatus that is semi-permanently or permanently embedded within a patient, with the aim of addressing a health condition, enhancing the performance of a specific bodily part, or providing users with capabilities previously unavailable. Typically, these devices are surgically placed approximately 2–3 cm beneath the patient's skin and connected to the organ requiring monitoring or treatment, such as in the body, eyes, heart, brain, and blood. IMDs, or in-body electronic devices, are employed to observe the health status of individuals and investigate both normal and abnormal bodily functions by storing diverse physiological parameters like antibody levels, glucose levels, pH, intracorporeal temperature, hormones, pressure, and more. The four categorized instances of IMDs are [4]:

- **Implanted Cardiac Devices:**

  These devices comprise Implantable Cardioverter Defibrillators (ICD), as shown in **Figure 3.17**, Pacemakers, and cardiac resynchronization therapy (CRT) designed for treating cardiac conditions. Their function involves monitoring the electrical activity of the heart and delivering suitable electrical impulses to regulate the heart's pumping rate. Advanced models incorporate pressure sensors capable of actively monitoring changes indicative of potential heart failure. This feature enables the device to alert either the patient or medical personnel when an increase in ventricular pressure is detected, signifying a hazardous condition. Additionally, cardiac implants may feature accelerometers to gauge the level of physical activity in the patient. This information serves as an input parameter for the IMD controller, facilitating the adjustment of cardiac stimulation frequency to suit the specific needs of each moment [4, 160, 161].

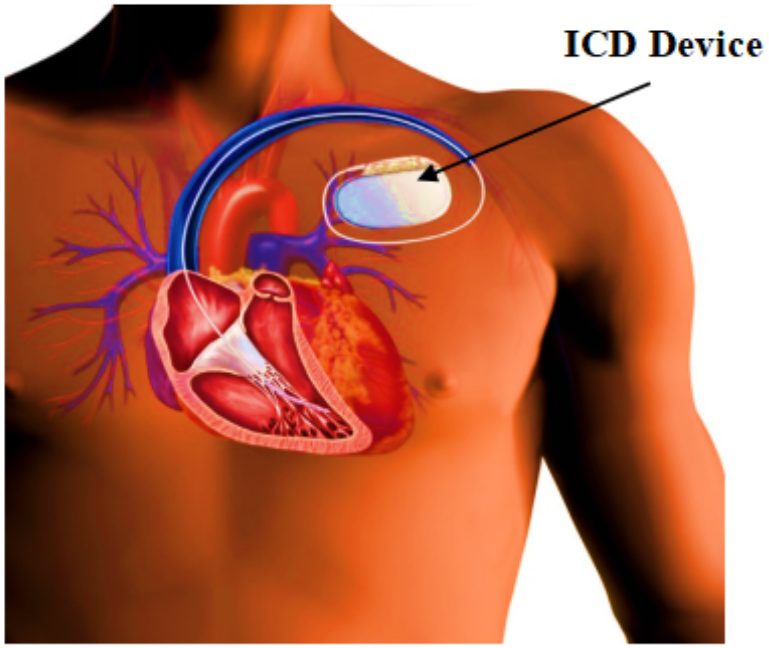

Figure 3.17: Cardiac implanted devices: Implantable Cardioverter Defibrillators (ICD) [162].

- **Biosensors:**

  Biosensors involve the use of an implant comprising sensors positioned within the human body for monitoring specific aspects. These sensors can measure various physiological parameters, utilizing the collected data to make informed decisions. Within such implants, a dedicated device serves as a control hub, establishing communication with both the sensors and outside entities, such as programmers. The combination of sensors and the control node is commonly referred to as a wireless biosensor network [4].

- **Neurostimulators:**

  Neurostimulators are devices that send low-amplitude electrical signals across one or more electrodes positioned at various points in the human brain, as illustrated in **Figure 3.18**. These electrodes are surgically inserted in certain regions tailored to the patient's condition. This procedure, referred to as Deep Brain Stimulation (DBS), is effective in treating various conditions like Parkinson's, dystonia, epilepsy, and even depression, particularly in cases where the conditions resist medication even after prolonged treatment [163].

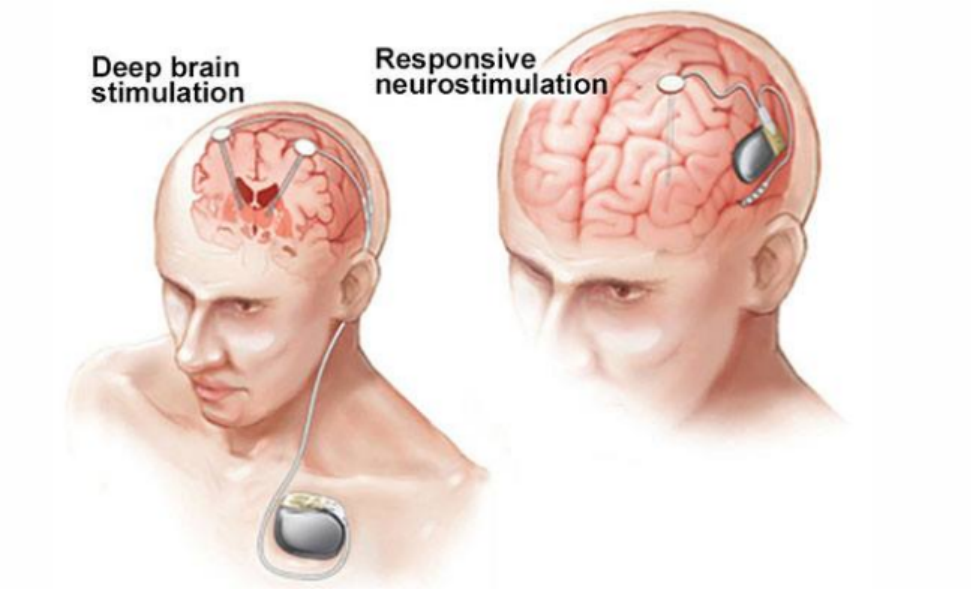

Figure 3.18: Application of Deep Brain Stimulation with the control of an implantable biosensor by a neurostimulator [164].

- **Drug Delivery Systems:**

  A Drug Delivery System comprises a surgically implanted pump and catheter beneath the skin, designed to deliver medication in a controlled, localized, and sustained manner.

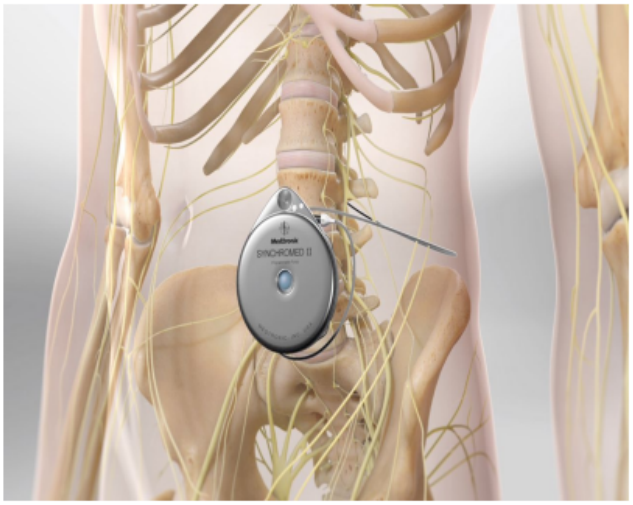

Figure 3.19: Intrathecal drug delivery system (pain pump implant) [165].

By directly administering the medication to the target area, an infusion pump offers significant control, enabling the use of lower doses compared to oral medication. For example, such implants have proven successful in alleviating pain in cases of cancer where conventional medication yields limited results [166].

3.3.3 Ingestible Antennas

Ingestible antennas, specifically in the context of capsule endoscopy, represent a widely recognized application for transmitting data from within the body to an external source. This technology involves capturing biological statistical data presented as images and videos through a camera embedded in a capsule. As the capsule traverses the digestive system, the antenna transmits this information. Wireless capsule endoscopy, in contrast to its wired counterpart, offers greater comfort, the ability to trace the concealed path, and effective visualization of the entire intricate route. It is utilized for examining the Gastro-Intestinal and digestive tract, facilitating the detection of various conditions such as Crohn's Disease, tumors, cancers, OGIB (Obscure Gastrointestinal Bleeding), and Celiac Disease. **Figure 3.20** illustrates the components integrated into the capsule, which typically includes an antenna, camera, battery, and light. When swallowed by the patient, the antenna becomes a crucial component for real-time wireless data transmission [1].

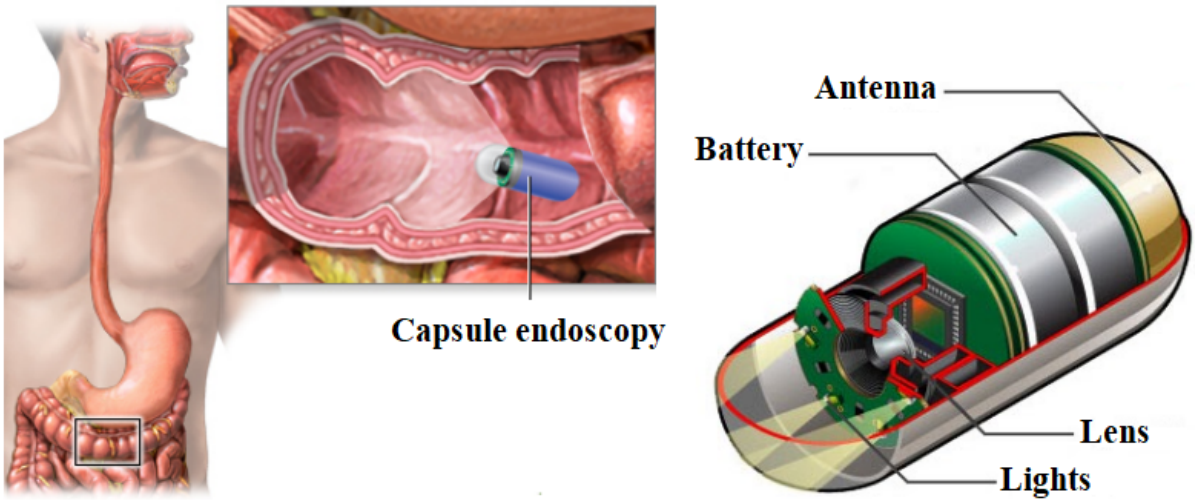

Figure 3.20: Capsule endoscopy [65, 167].

3.4 Treatment Applications

Currently, antennas serve as a successful method for treating a spectrum of diseases, encompassing various cancers such as breast, brain, prostate, lung, neck, esophagus, melanomas, and soft tissue sarcomas, along with hepatocellular carcinoma (HCC) and tumors, by employing image-guided thermal ablation, specifically through hyperthermia. Hyperthermia is a cancer treatment method involving the elevation of body temperature. Typically, tissues are heated

within the range of 41 to 45°C for 30 to 60 minutes [6]. Often, the focus is on directing energy to the tumor area, exploiting the tumor's greater sensitivity to heat compared to surrounding healthy tissues. This sensitivity may be due to the tumor's poor internal vasculature or its higher conductivity and permittivity resulting from increased water and ionic content. Hyperthermia has demonstrated the capability to enhance the effectiveness of radiation or chemotherapy. Frequencies commonly employed for hyperthermia include 2450, 915, and 433 MHz [Chapter 2]. The choice of an antenna or antenna array for hyperthermia is dependent on whether the treatment is intended to be administered superficially, interstitially, or deeply within the body.

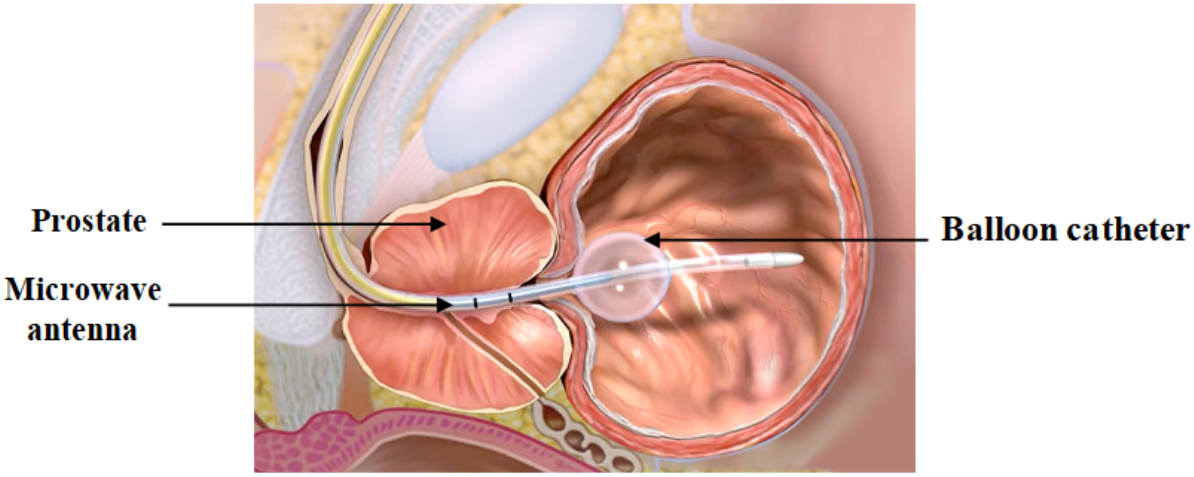

Figure 3.21: Transurethral microwave thermotherapy (TUMT)[168].

3.5 Conclusion

Biomedical antennas stand at the forefront of a rapidly advancing technology, holding immense promise to enhance the lives of patients and elevate the overall quality of healthcare. The advent of RF technology for medical devices brings forth a multitude of advantages for patients and healthcare providers alike. In the preceding chapter, we have elucidated fundamental concepts surrounding the application of antennas within the realm of biomedicine. Commencing with overarching insights into the utilization of biomedical antennas, we subsequently delved into their specific applications, encompassing medical microwave imaging, biomedical telemetry, and therapeutic interventions. This exploration underscores the transformative potential of biomedical antennas, paving the way for innovative advancements that can revolutionize patient care and medical practices.

Chapter 4

Design of a New Antenna for Medical Microwave Imaging and Health Monitoring Applications

Contents

4.1 Introduction

The widely employed medical imaging techniques for creating images of human tissues, anatomy, or organs comprise X-ray mammography, CT scans, MRI, ultrasound, and SPECT-CT. Nonetheless, all these diagnostic methods come with notable drawbacks, as they tend to be expensive, cause discomfort, and involve exposure to ionizing radiation [169].

Many biomedical researchers are interested in using MI to overcome the limitations of these technologies because of its appealing properties, which include high image resolution of the scanned bodily tissues,low cost, safety, simplicity, non-ionizing radiation, and non-invasiveness.

It makes use of the notable dielectric differential that exists between diseased and healthy tissues [123]. This imaging approach relies on mono-static, bi-static, or multi-static radar-type measurements and capitalizes on the noticeable dielectric contrast between normal and pathological tissues [Chapter 3]. The mono-static radar imaging system, employing a single antenna for body scanning with mechanical movement, provides a quick and better-performing solution. In contrast, bi-static and multi-static radar imaging systems, which use multiple antennas, are characterized by complexity, high cost, and time-consuming procedures [170].

CP antennas play a crucial role in improving the efficiency of medical MI radar systems. They effectively mitigate indoor multi-path effects and accommodate various body postures, minimizing polarization mismatch losses. CP antennas possess the ability to penetrate lossy dielectric materials in human body tissues, leading to robust tumor detection regardless of antenna orientation constraints [171]. While numerous antennas designed for biomedical applications have been documented in [172–184], the majority of these antennas are linearly polarized and serve a singular purpose, whether for medical surveillance, detection of cancer, or stroke detection. Consequently, there is a need for innovative antennas with superior performance suitable for diverse medical applications.

In this chapter, we introduce a mono-static CPPMA with dimensions measuring $34 \times 28 \times 1.5$ mm^3. The antenna is proposed for use in the ISM band, specifically designed for applications in medical MI and health-monitoring wearables. The CPPMA presented here is proficient in detecting brain strokes and breast tumors of varying sizes, positioned at various locations. Due to its operation within the ISM range and its circular polarization properties, this CPPMA holds potential for integration into remote health monitoring systems. These systems facilitate continuous monitoring of a patient's medical data while they are in the comfort of their home, simplifying the processes of diagnosis, treatment, and prediction of illness onset, as well as enhancing the regulation of their health condition.

This work introduces several additional contributions, which encompass: 1) the creation and construction of a straightforward and cost-effective antenna designed for various medical applications, including detection of breast cancer, brain stroke identification, and applications in health-monitoring and wearables; 2) the presentation and assessment of CP performance for tumor screening; 3) validation of the antenna's capability to detect brain strokes and extremely small breast tumours using phantom models; 4) experimental justification of the practicality of the fabricated prototype for health wearable applications; 5) the identification of brain strokes through the analysis of current density, H-field, and E-field; 6) an assessment of the SAR parameter on a human body phantom's arm, head, and breast. All simulations conducted in

this study utilize CST Microwave Studio software.

4.2 Design of the Antenna and Human Body Phantom Model

4.2.1 Design and Analysis of Antenna Evolution:

Figure 4.1 illustrates the geometry of the CPPMA that was designed. The optimized dimensions can be found in **Table 4.1**. The progression of the proposed CPPMA during the design process is illustrated in **Figure 4.2**, while **Figure 4.3** provides information on the Reflection coefficient and AR for the various designs.

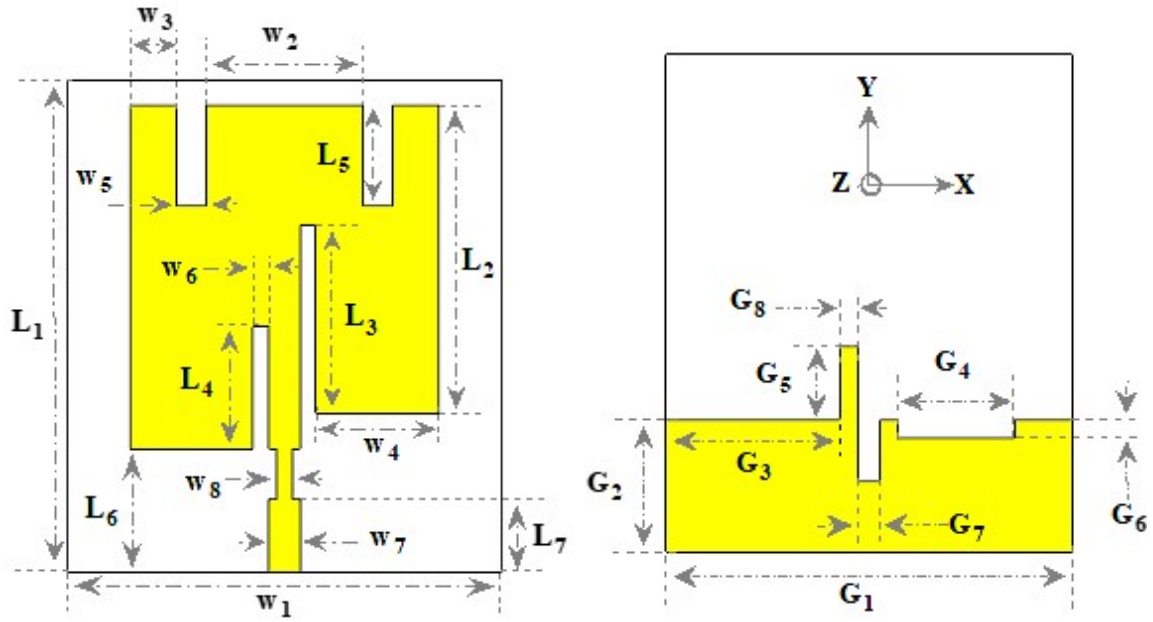

(a) (b)

Figure 4.1: Geometry of the designed CPPMA: (a) front view, (b) back view.

Table 4.1: Optimized dimensions of the proposed CPPMA

Parameter	W_1	L_1	W_2	W_3	W_4	W_5	W_6	W_7	W_8	L_2	L_3	L_4
Value (mm)	28	34	3	10	8	2	1	2	1	21.3	13	8.5
Parameter	L_5	L_6	L_7	G_1	G_2	G_3	G_4	G_5	G_6	G_7	G_8	
Value (mm)	7	8.7	5	28	9	12	8	5	1.25	1.6	1.2	

The generation of circular polarization (with an AR of 0.98 dB, less than 3 dB at a frequency of 2.45 GHz, and an AR bandwidth spanning from 2.4386 GHz to 2.4633 GHz.) is attributed to

the presence of a stub and two slots introduced into the ground plane. The circular polarization performance is evident in the surface current direction, where the phase increases over time. The current distributions for four distinct phases (0°, 90°, 180° and 270°) on the surface of the designed CPPMA at a frequency of 2.45 GHz are shown in **Figure 4.4**. According to the outcomes, the major current direction for 0° is in the -X direction, while for the 90°, it is in the +Y direction. Additionally, the major current directions for 180° and 270° are opposite of those at 0° and 90°, Consecutively. This indicates a clockwise trend in the main surface current, signifying the acquisition of LHCP in the direction of propagation using the proposed CPPMA.

Figure 4.5 displays the simulated far-field radiation patterns of the designed CPPMA at 2.45 GHz in the xz-plane (H-plane) and yz-plane (E-plane) for RHCP and LHCP emissions. It verifies that the CPPMA design emits LHCP in the propagation direction and RHCP in the opposite direction. The slight deviations in the radiation patterns in the H-plane result from the asymmetric geometry of the CPPMA design. Similar outcomes are reported in [185].

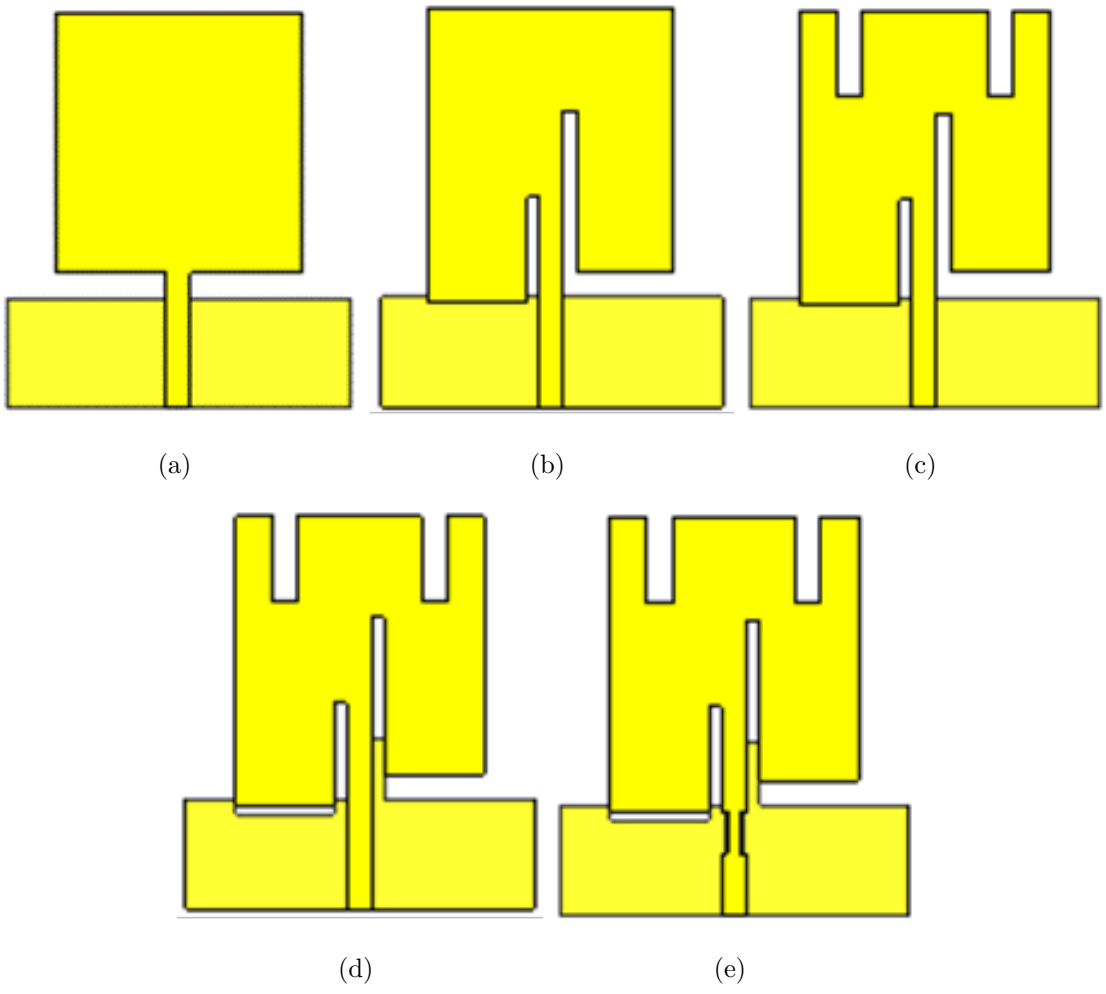

Figure 4.2: The development of the CPPMA design across its various stages: (a) Antenna 1, (b) Antenna 2, (c) Antenna 3, (d) Antenna 4, (e) Proposed CPPMA.

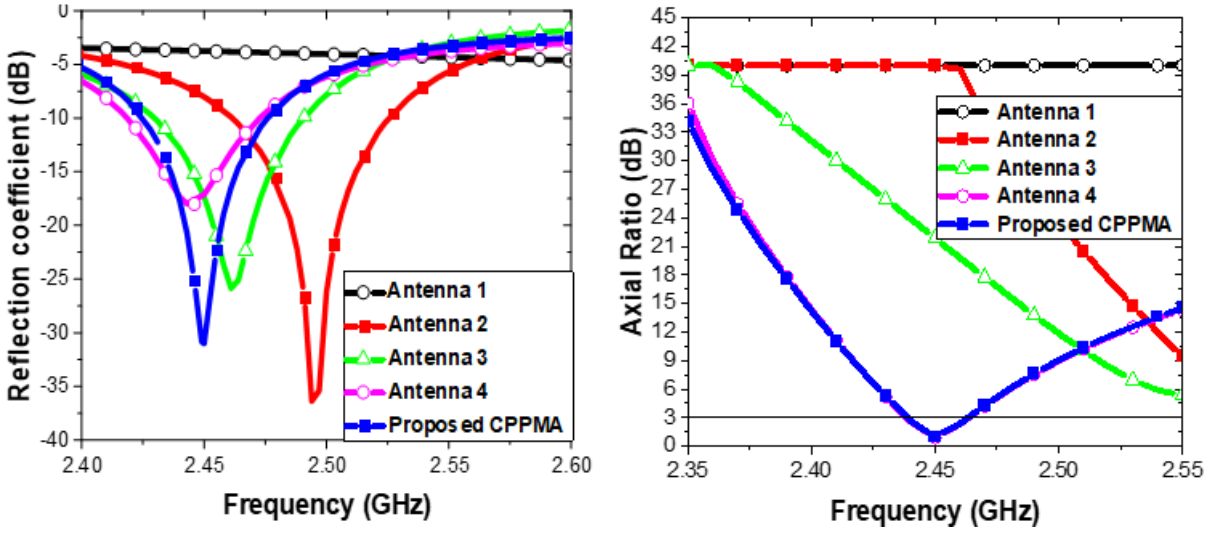

(a) (b)

Figure 4.3: (a) Reflection Coefficient, and (b) AR of the designed CPPMA in comparison to the preliminary reference antennas.

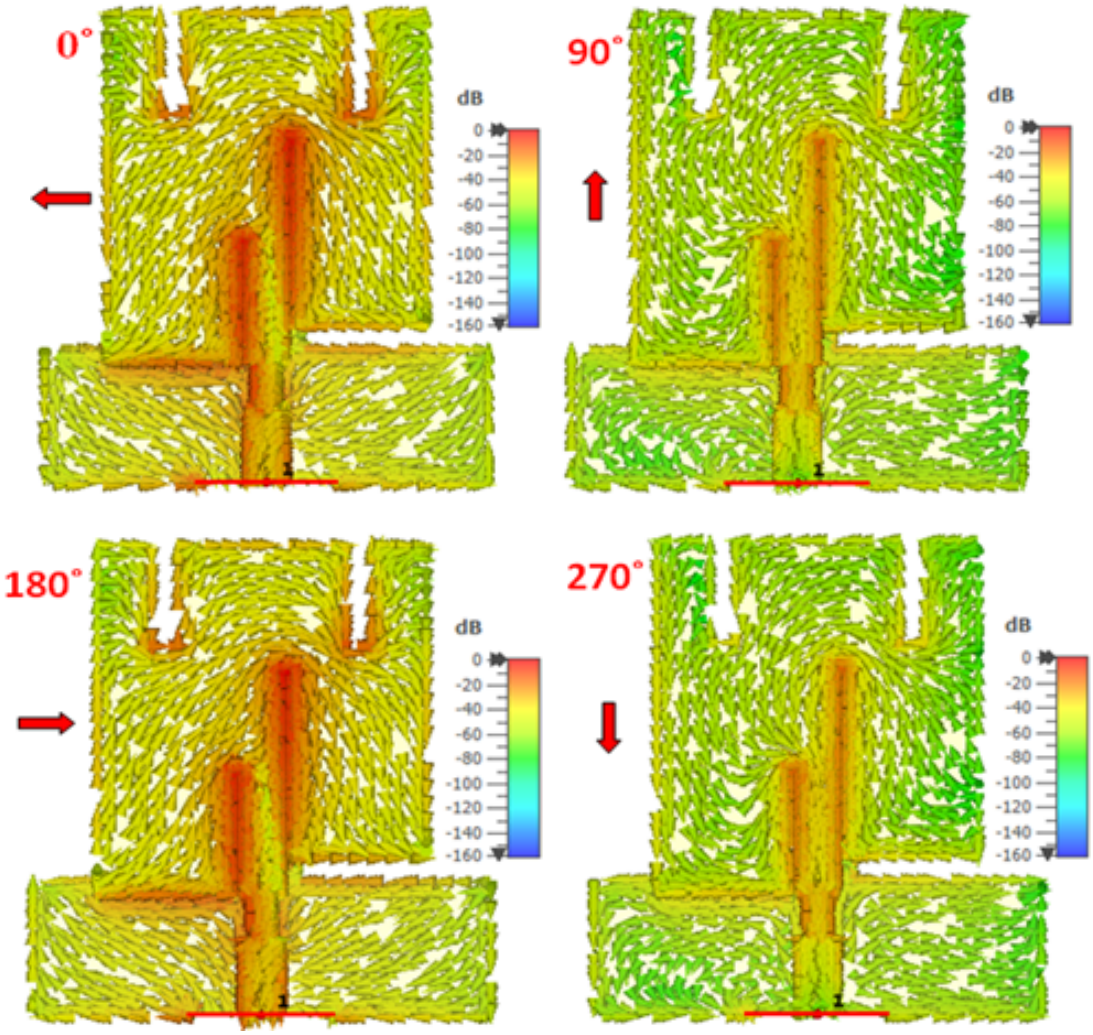

Figure 4.4: Surface current distribution for four different phases (0°, 90°, 180°, and 270°) on the proposed CPPMA at 2.45 GHz.

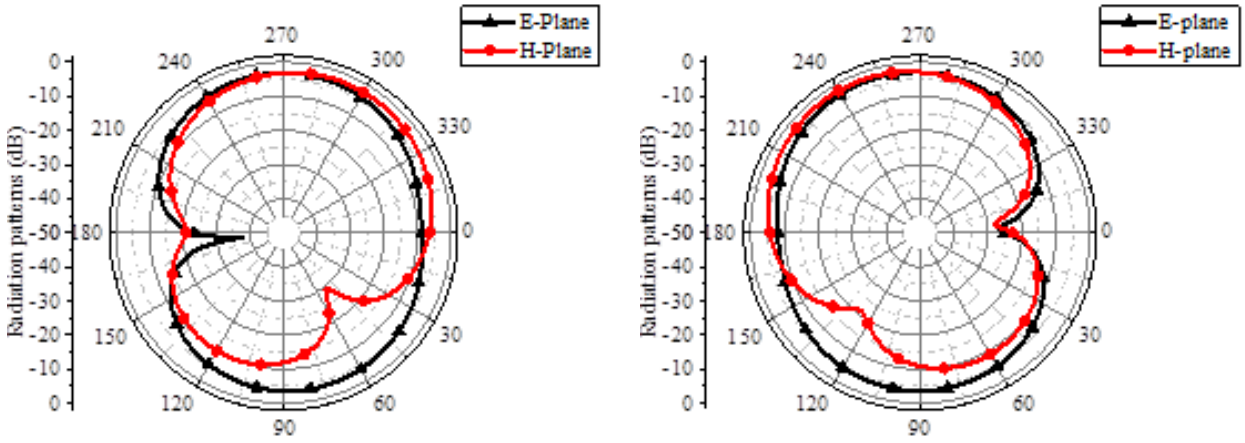

(a) (b)

Figure 4.5: Radiation patterns of the designed CPPMA at a frequency of 2.45 GHz: (a) LHCP, (b) RHCP.

Figure 4.6 illustrates the prototype of the proposed CPPMA fabricated on FR4 Epoxy with dimensions measuring 34 × 28 × 1.5 mm^3. The fabrication of the prototype was accomplished using the LPKF Proto Mat E44 PCB prototyping machine.

(a) (b)

Figure 4.6: Manufactured prototype of the designed CPPMA : (a) front view, (b) back view.

Figure 4.7 illustrates the reflection coefficient configuration measurement conducted with the R&S®ZNB Vector Network Analyzer. **Figure 4.8** indicates a favorable agreement between the simulated and measured reflection coefficients of the CPPMA. The simulated bandwidth fluctuates within 2.425 GHz and 2.475 GHz, whereas the measured impedance bandwidth spans from 2.32 GHz to 2.515 GHz.

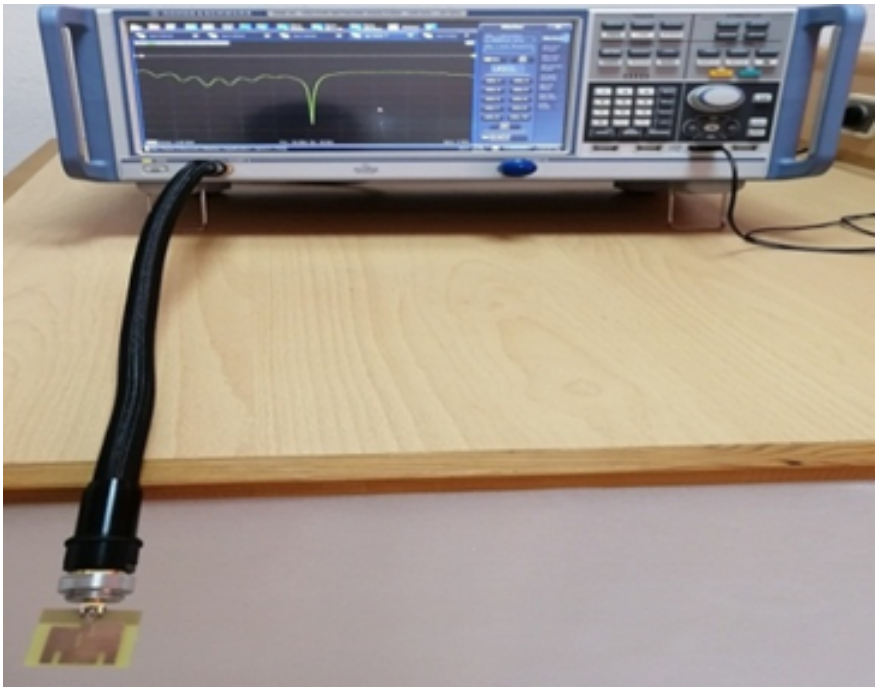

Figure 4.7: Measurement of the reflection coefficient configuration for the proposed CPPMA.

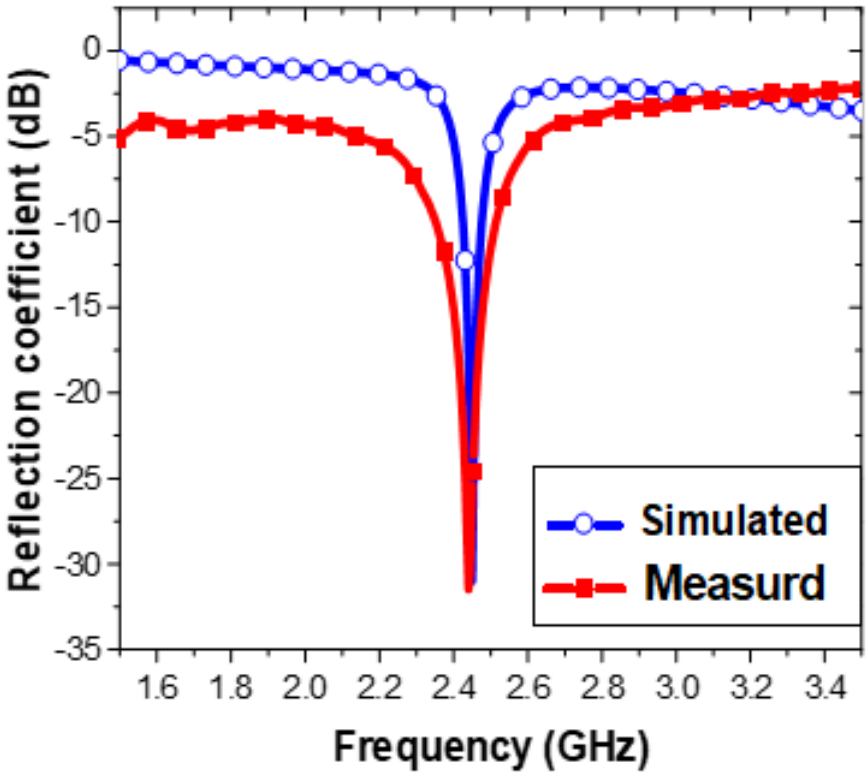

Figure 4.8: Simulated and measured reflection coefficients for the proposed CPPMA.

4.2.2 Phantom Models of Human Bodies

Several arm, head, and breast phantoms have been suggested in existing literature [chapter 2]. The absorption of microwaves varies among tissues with distinct electrical properties, and

shifts in the frequency spectrum significantly impact the dielectric properties of biological tissues [57, 186].

Quantitative MI relies on reconstructing dielectric properties by leveraging variations in complex permittivity. To address the intricate structure and composition of biological tissues, Gabriel et al. employed the 4-Cole-Cole model. This model provides a parametric representation of 4 types of dispersion in biological tissues, offering a description of the frequency-dependent conductivity and permittivity across various biological tissues within the frequency range from 10 Hz to 100 GHz, as shown in equation 2.37[187, 188].

The fundamental concept behind employing microwaves in breast imaging for the identification of malignant cells relies on the substantial contrast in dielectric properties between pathological tissues and healthy tissues. In the context of breast cancer detection, a monostatic radar imaging system utilizes a single antenna that serves as a transceiver to identify and localize tumors within the breast more conveniently and distinctly. This antenna emits microwave pulses directed towards the breast, systematically scanning various locations within the human phantom.

Subsequently, the antenna captures signals from the human breast, manifesting as either reflected or scattered signals. It is essential to emphasise that variations in the back-scattered signal reveal differences in the tissue's dielectric properties. Consequently, the back-scattered signal may be utilized for detecting tumour tissues within the human breast, as these cells have greater dielectric properties compared to healthy breast tissues [189, 190].

- **Phantom Model of the Human Breast:**

  In this study, we have simulated a hemispherical-shaped breast model with three layerss i.e fibro-glandular, fat, and skin, as illustrated in **Figure 4.9**. **Table 4.2** provides the properties of the female breast phantom model [187, 191] and the tumor model [192, 193].

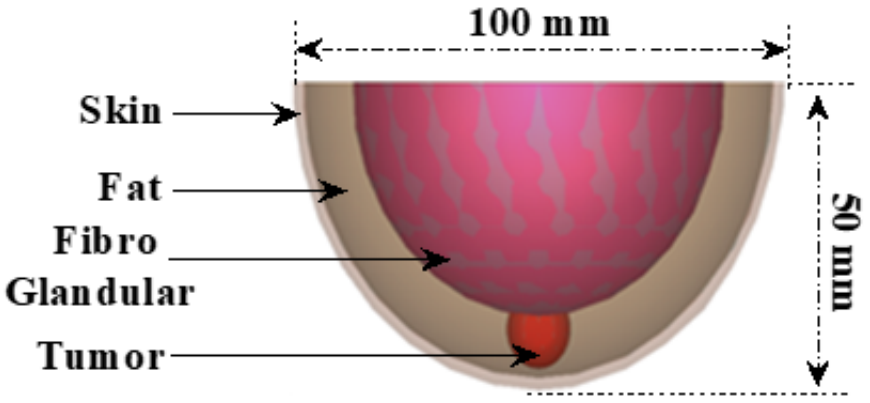

Figure 4.9: Hemispherical model of the human breast phantom.

Table 4.2: Properties of the three-layer woman's breast phantom model and tumour model at a frequency of 2.45 GHz

Tissues	$\varepsilon[F/m]$	$\sigma[S/m]$	$\rho[kg/m^3]$	$Radius[mm]$
Skin	38.0067	1.46407	1100	50
Fat	5.14667	0.137039	900	48
Fibro-Glandular	20.1	0.5	1040	38
Tumor	55.2566	2.7015	1050	/

- **Phantom Model of the Human Head:**

  This study incorporates a spherical-shaped human head model, as shown in **Figure 4.10**, comprising seven layers: brain, cerebrospinal fluid, dura, muscle, skull, fat, and dry skin. The characteristics of the stroke model (blood clot) and the specified human head phantom model can be found in **Table 4.3**.

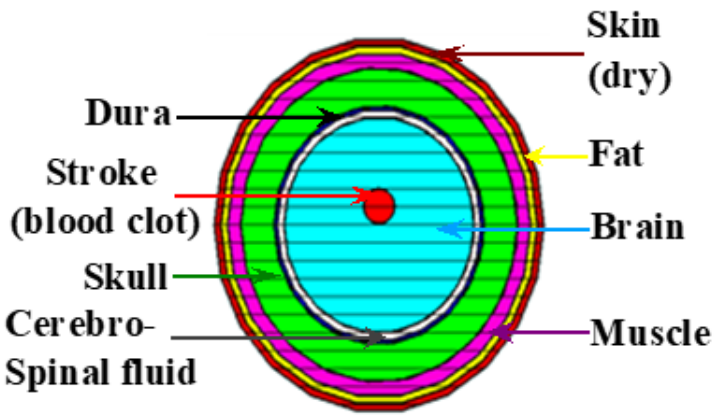

Figure 4.10: Phantom human head spherical model.

Table 4.3: Characteristics of the brain stroke model (blood clot) and the seven-layer human head phantom model at a frequency of 2.45 GHz [187, 194]

Tissues	$\varepsilon[F/m]$	$\sigma[S/m]$	$\rho[kg/m^3]$	$Radius[mm]$
Skin	38.0067	1.46407	1100	50
Fat	5.14667	0.137039	900	48
Muscle	53.573540	1.810395	1040.0	46
Skull	14.965101	0.599694	1850.0	42
Dura	42.035004	1.668706	1130	32
Cerebrospinal fluid	66.243279	3.457850	1006	31
Brain	42.538925	1.511336	1030.0	29
Stroke (blood clot)	58.263756	2.544997	/	/

- **Phantom Model of the Human Arm:**

  A section of a phantom model representing a human arm has been created. The model consists of four layers: bone, muscle, fat, and skin, as illustrated in **Figure 4.11**. The properties of this human arm phantom model are detailed in **Table 4.4** [195].

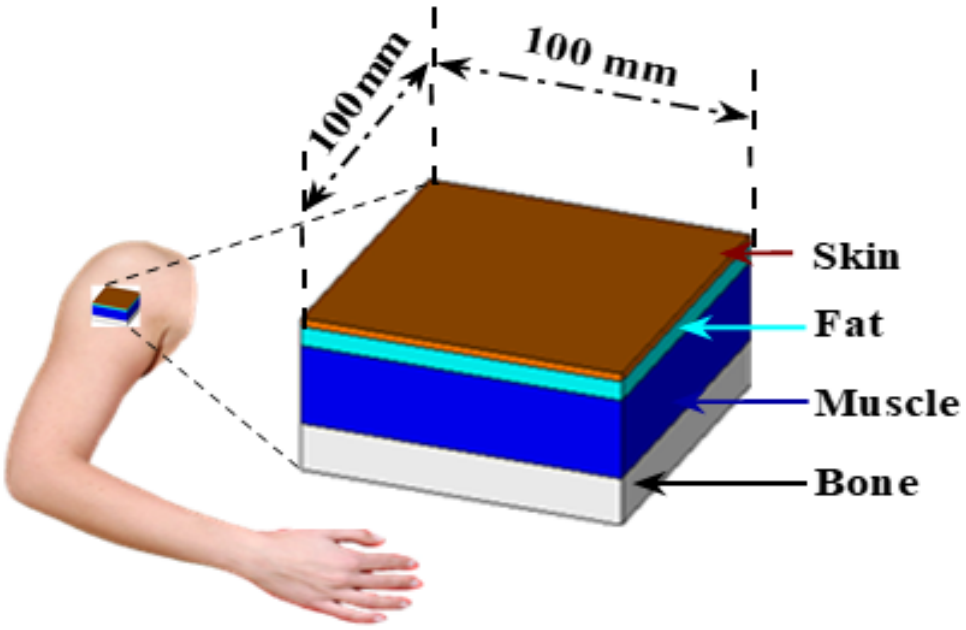

Figure 4.11: Section of a phantom model representing the human arm.

Table 4.4: Characteristics of the four-layer arm phantom model at a frequency of 2.45 GHz [195]

Tissues	$\varepsilon[F/m]$	$\sigma[S/m]$	$\rho[kg/m^3]$	$Thickness[mm]$
Skin	37.95	1.49	1001	2
Fat	5.27	0.11	900	5
Muscle	52.67	1.77	1006	20
Bone	18.49	0.82	1008	13

4.3 Simulation and Results

4.3.1 Detection of Breast Cancer

In this subsection, we investigate the impact of radiation on a woman's breast model. Initially, the designed CPPMA was positioned near a healthy woman's breast phantom model at a secure distance of 10 mm, as illustrated in **Figure 4.12(a)**. Subsequently, a spherical tumour with a radius of 2.5 mm was implanted at four different locations within the healthy human breast phantom, as apparent in **Figure 4.12(b)**. **Figure 4.13** illustrates the reflection coefficient of the proposed CPPMA with a phantom model of a woman's breast containing a tumor (Radius = 2.5 mm) at 4-various locations: (x = 0, y = 0, z = 15), (x = 25, y = 15, z = 30), (x = 0, y = 0, z = 40), (x = 30, y = 30, z = 50), and without a tumour. The shift in the resonant frequency is clearly inversely proportional to the distance between the proposed CPPMA and the tumour.

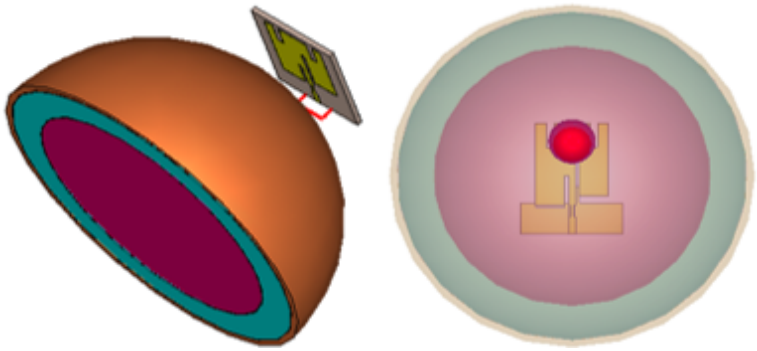

(a) (b)

Figure 4.12: CPPMA positioned at a 10 mm distance from the phantom model of a woman's breast: (a) not having a tumour and (b) having a tumour.

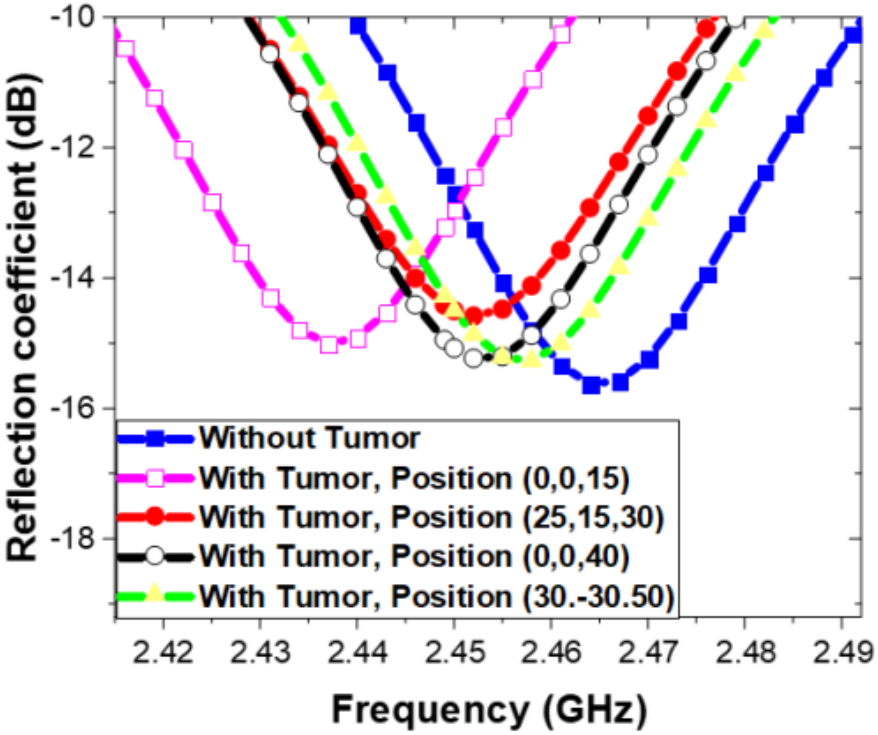

Figure 4.13: Simulated reflection coefficient for the phantom model of a woman's breast with a tumour of radius 2.5 mm at four various locations.

Afterward, as illustrated in **Figure 4.12(b)**, tumours of three distinct sizes (Radius = 9 mm, 7 mm, and 4 mm) were implanted within the healthy woman's breast phantom at a fixed location. **Figure 4.14** illustrates the reflection coefficient of the proposed CPPMA and a phantom model of a woman's breast both without and with a tumour. The results indicate that for larger tumour sizes, there is a more noticeable shift in resonance frequency and adaptation level. As a result, the tumour becomes easier to detect as it increases in size.

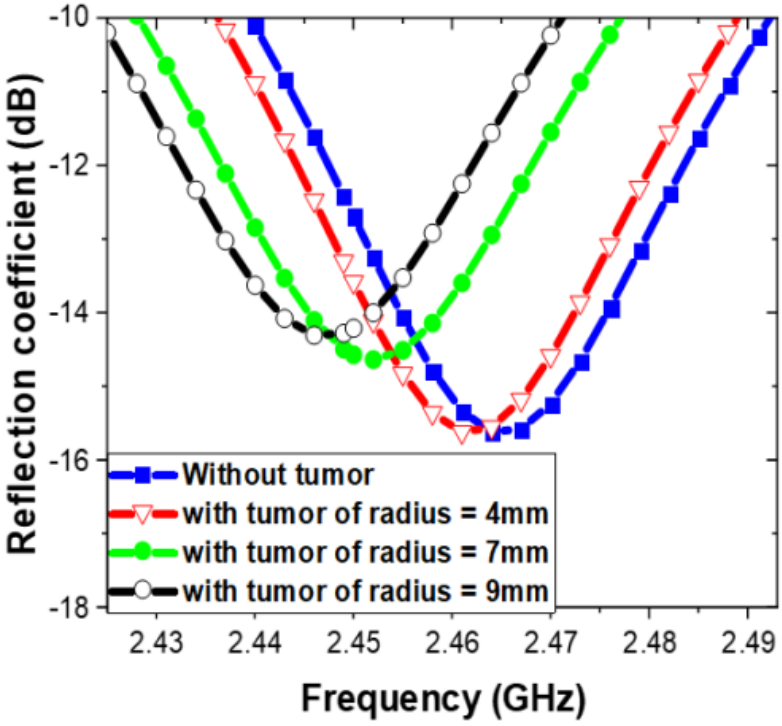

Figure 4.14: Simulated reflection coefficient for the detection of breast tumors of three different sizes at a consistent location.

4.3.2 Detecting Brain Strokes

In this subsection, we explore the impact of radiation on the phantom model of the human head. Initially, the proposed CPPMA was placed near a healthy human head phantom model at a secure distance of 5 mm, as illustrated in **Figure 4.15(a)** . Subsequently, a brain stroke (blood clot) of two various radii, 13 mm and 5 mm, characterised by the dielectric properties listed in **Table 4.3**, was inserted into the healthy human brain, as shown in **Figure 4.15(b)**.

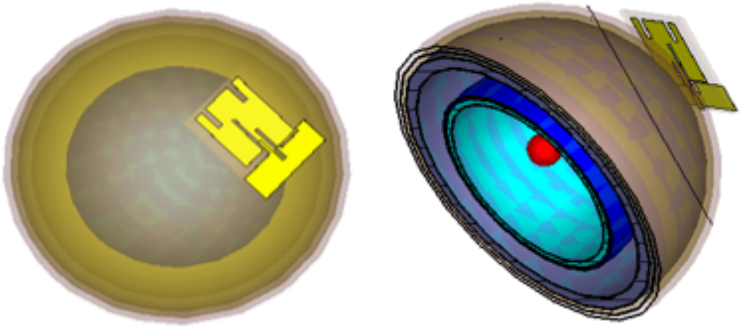

(a) (b)

Figure 4.15: CPPMA placed at a 5 mm distance from the phantom model of the human head: (a) not having a blood clot, and (b) having a blood clot.

Figure 4.16 depicts the reflection coefficient of the proposed CPPMA and the phantom model of the human head both without and with a brain stroke (blood clot). In both normal and brain stroke cases, a noticeable shift in the resonance frequency of the proposed CPPMA is observed. Consistent with intuition, the reflected wave increases as the size of the blood clots grows.

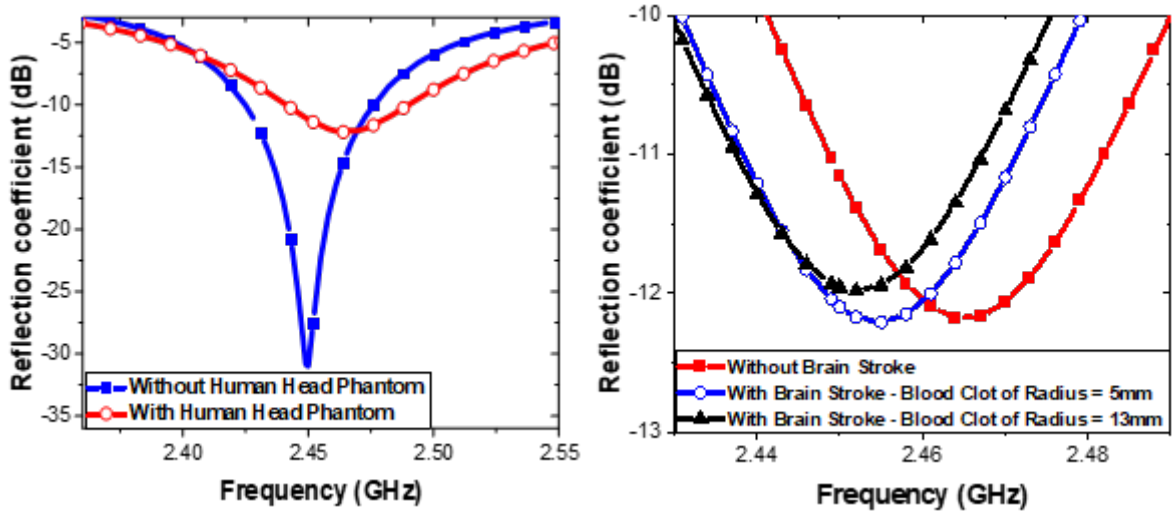

(a) (b)

Figure 4.16: Simulated reflection coefficients: (a) without and with a phantom model of the human head ; (b) for identifying two distinct sizes of brain strokes.

In **Figures 4.17-4.19**,the CPPMA and the phantom model of the human head without and with a blood clot are simulated in terms of their E-field, H-field, and current density at a frequency of 2.45 GHz. According to **Table4.5**, the E-field, H-field, and current density values reduce when a brain stroke is present, indicating its presence inside the human head.

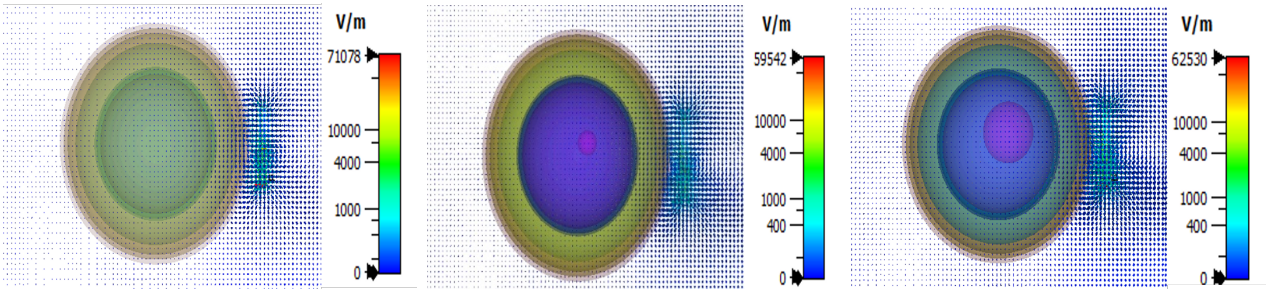

(a) (b) (c)

Figure 4.17: E-Field: (a) without blood clot, (b) with a blood clot of radius 5 mm, and (c) with a blood clot of radius 13 mm.

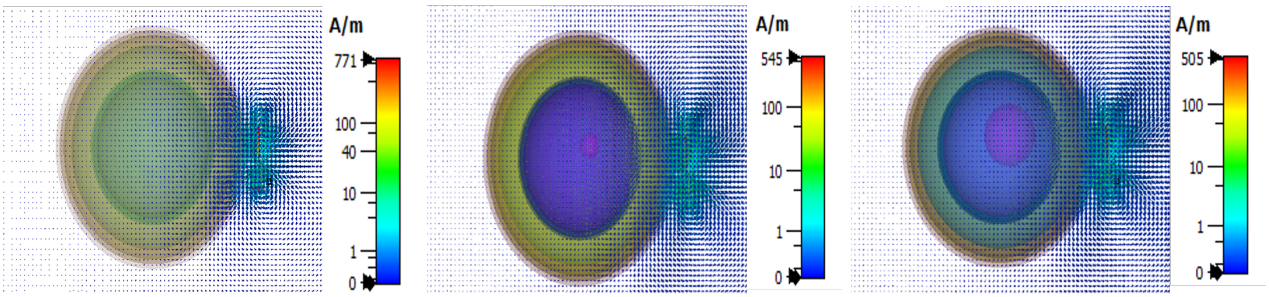

(a) (b) (c)

Figure 4.18: H-Field: (a) without blood clot, (b) with a blood clot of radius 5 mm, and (c) with a blood clot of radius 13 mm.

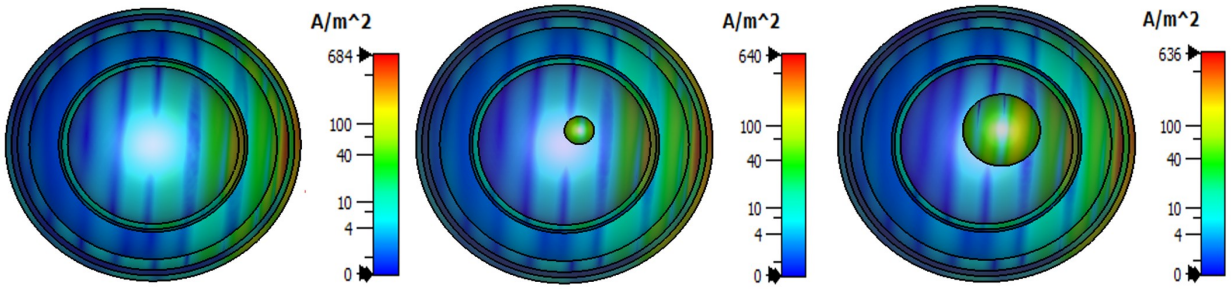

(a) (b) (c)

Figure 4.19: Current density: (a) without blood clot, (b) with a blood clot of radius 5 mm, and (c) with a blood clot of radius 13 mm.

Table 4.5: Comparison of simulated outcomes at a frequency of 2.45 GHz without and with the brain stroke models.

	Without blood clot	**With blood clot R=5mm**	**With blood clot R=13mm**
Resonance frequency (GHz)	2.464	2.455	2.452
Reflection coefficient (dB)	-12.142075	-12.207286	-11.97995
Current Density A/m^2	683.562	639.836	636.324
E Field V/m	71078.5	59542.3	62530
H Field A/m	770.724	545.151	505.475

The LP antenna depicted in **Figure 4.2(b)** was simulated both without and with a blood clot model (Radius = 5 mm and 13 mm) to demonstrate the benefits of CP in detecting brain

strokes. Minor modifications were made to the antenna dimensions to shift the resonance frequency to 2.45 GHz.

Figure4.20 illustrates the reflection coefficient of a simulated linearly polarised printed monopole antenna (LPPMA).

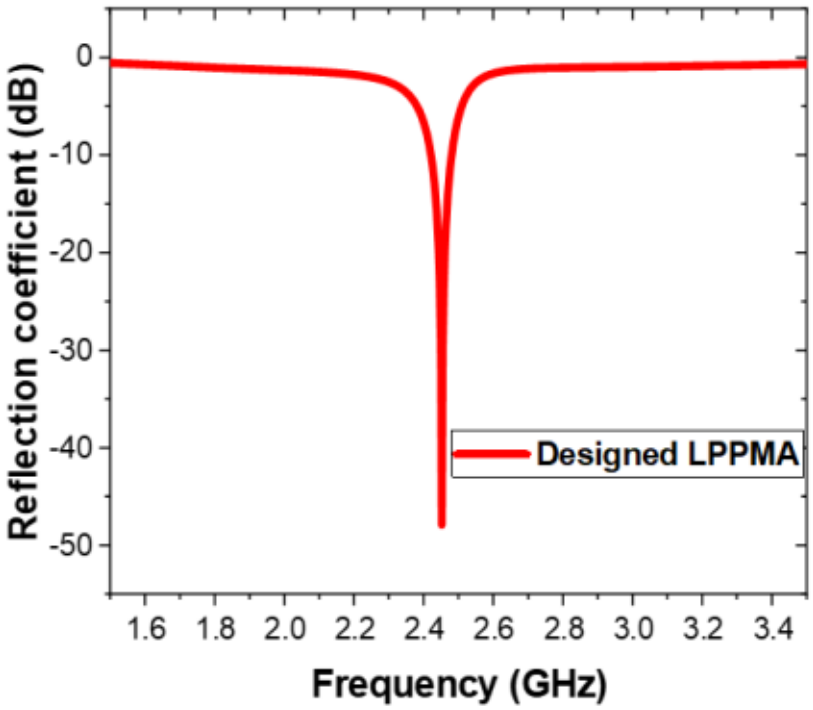

Figure 4.20: Simulated reflection coefficient of the LPPMA.

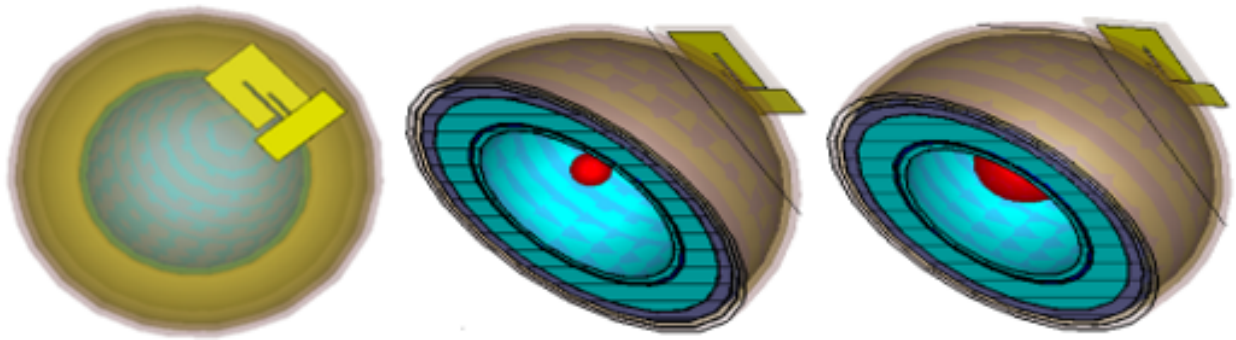

(a) (b) (c)

Figure 4.21: LPPMA positioned near the human head phantom model at a distance of 5 mm: (a) without a blood clot, (b) with a blood clot of radius 5 mm, and (c) with a blood clot of radius 13 mm.

Figure4.22 illustrates the reflection coefficient of the LPPMA and the human head model without and with a blood clot model. It indicates that the resonance frequency remains constant in comparison with the outcomes obtained when using the designed CPPMA (**Figure**

4.16(b)).**Table 4.3** demonstrates that the proposed CPPMA is more successful than the LPPMA in diagnosing brain strokes due to the deeper penetration of CP waves into the body.

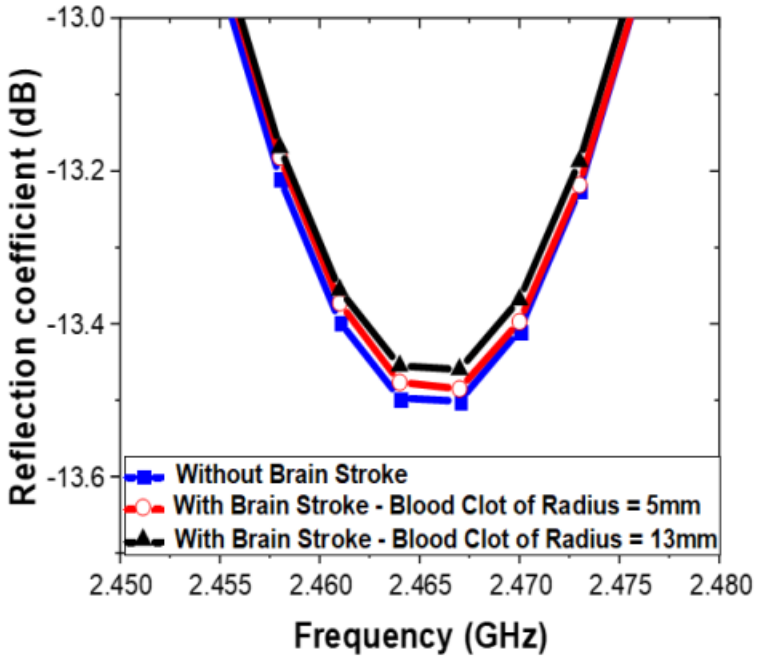

Figure 4.22: Simulated LPPMA reflection coefficient for the detection of two various sizes of the blood clot model.

Table 4.6: Comparison of simulated outcomes without and with the brain stroke model at a frequency of 2.45 GHz.

		Without brain stroke	With blood clot Radius = 5 mm	With blood clot Radius = 13 mm
CPPMA	Resonance frequency (GHz)	2.464	2.455	2.452
	Reflection coefficient (dB)	-12.14207	-12.207286	-11.97995
LPPMA	Resonance frequency (GHz)	2.467	2.467	2.467
	Reflection coefficient (dB)	-13.50134	-13.485089	-13.45988

4.4 Application for Wearable Devices

In this part, we conducted simulations to evaluate the CPPMA's performance on a phantom model of the human arm as well as on a real human arm, with the goal of determining its

suitability for wearable health monitoring applications. Initially, the CPPMA was placed near a phantom model of the human arm at a secure distance of 10 mm, as illustrated in **Figure 4.23(a)**. **Figure 4.23(b)** reveals that the CPPMA's resonant frequency on a phantom model of the human arm experiences slight shifts in comparison to the CPPMA without the phantom, attributed to the higher dielectric properties of body tissues. Nevertheless, the proposed CPPMA, in the vicinity of a phantom of the human arm, exhibits an impedance band ranging from 2.438 GHz to 2.489 GHz and a reflection coefficient level of -13.28 dB, successfully covering the required ISM range.

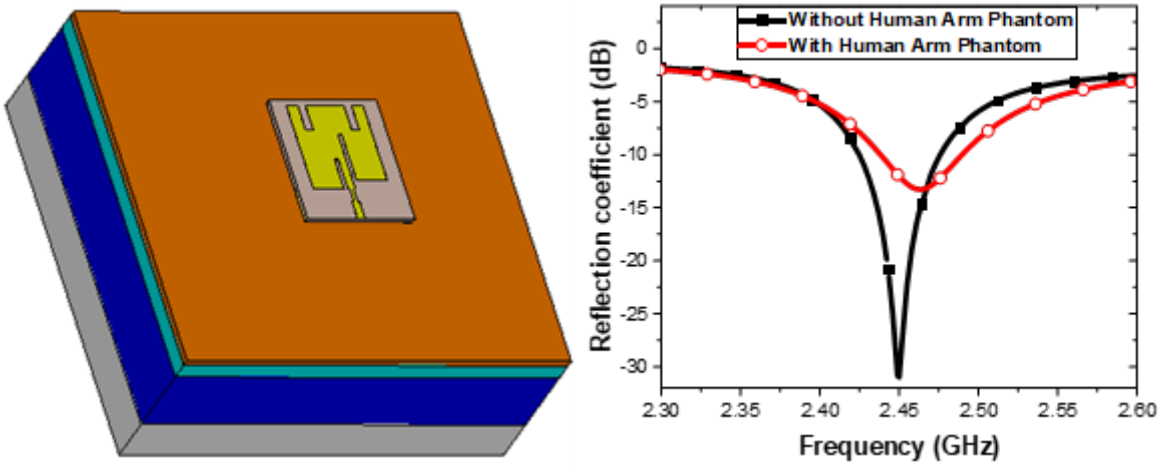

(a) (b)

Figure 4.23: (a) CPPMA positioned at a 10 mm distance from a section of a phantom model of the human arm, and (b) Simulated reflection coefficient without and with a section of an arm phantom.

The effectiveness of the designed CPPMA for health wearable applications was verified through experimental testing, involving the placement of the manufactured prototype on a real human arm, as demonstrated in **Figure 4.24**.

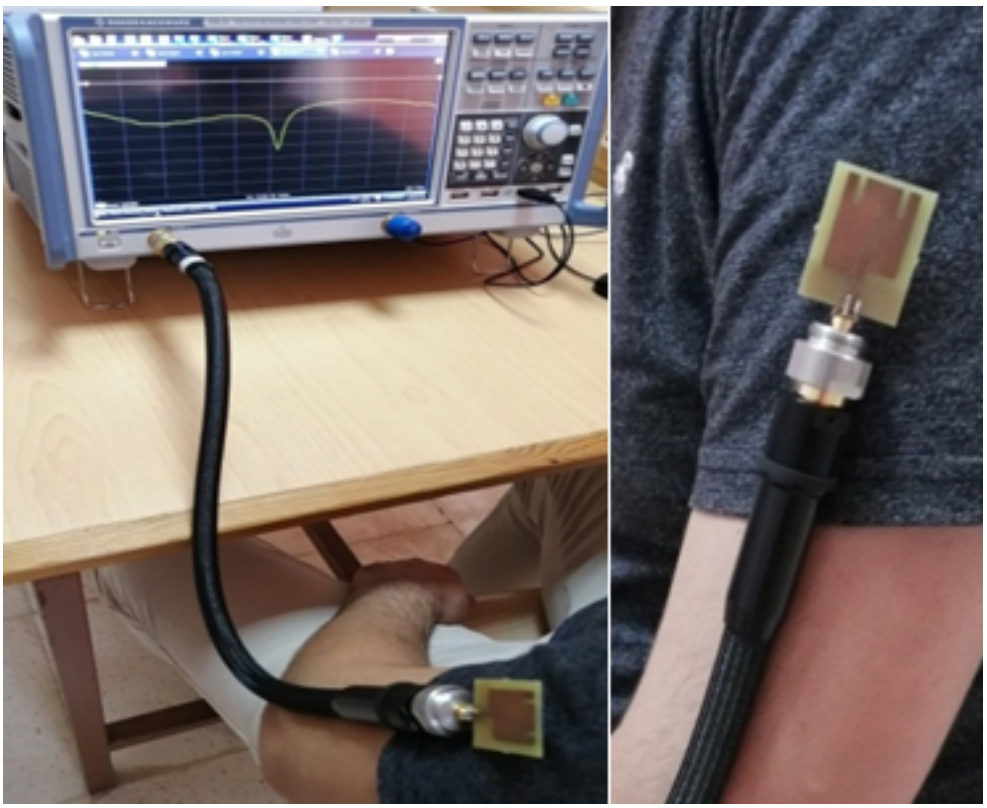

Figure 4.24: Measurement of the reflection coefficient for the manufactured prototype on a real human arm.

The comparison of simulated and measured reflection coefficient outcomes for the designed CPPMA positioned on a human arm is illustrated in **Figure 4.25**.

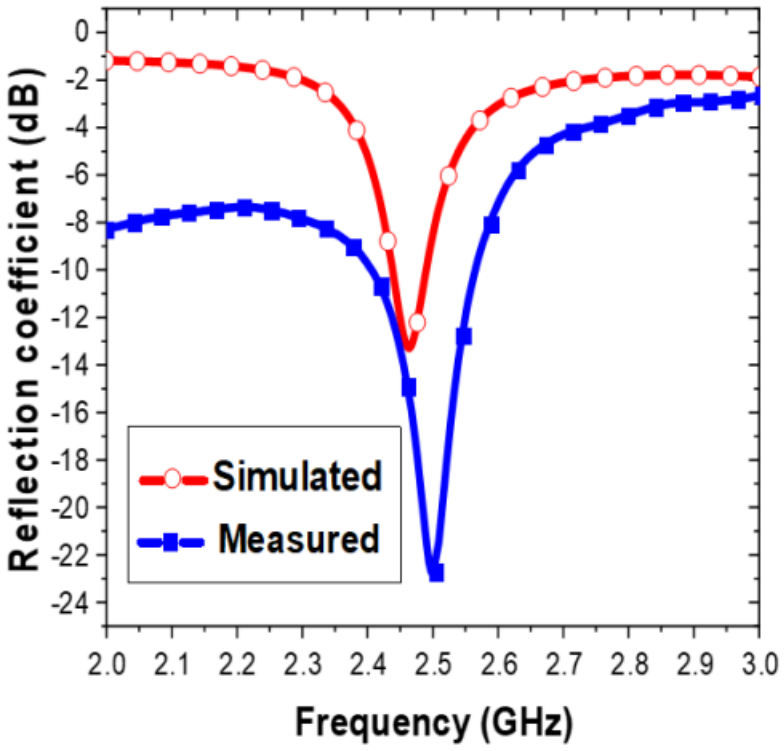

Figure 4.25: The designed CPPMA's reflection coefficient in the vicinity of a human arm.

The disparity that exists between on-arm measurements and the simulation results can be attributed to several factors, such as the size of the human arm, the distance between the proposed CPPMA and the human arm, and SMA losses. Despite these variations, the results indicate that the designed CPPMA is well-suited for wearable medical monitoring devices.

4.5 SAR Calculations

As elaborated in Chapter 2, the SAR characterizes the amount of power absorbed per kilogram of human body tissue, denoted in Watts per Kilogram (W/Kg). Generally, SAR is averaged over a small tissue volume, typically 1 gram or 10 grams, and its computation is determined by the equation 2.30.

In this part, we evaluated the SAR parameter of the developed CPPMA in the vicinity of the arm, head, and breast of a human body phantom. The values of SAR represent the power normalised over 10 grams of tissues. To adhere to the stringent SAR regulation (i.e., $SAR_{10g} < 2W/kg$), the input powers must be restricted as per **Table 4.7**.

The simulated SAR_{10g} on the head, breast, and section of a human arm is illustrated in **Figure 4.26**.

Table 4.7: Thresholds for input power ensuring acceptable SAR_{10g} values at a frequency of 2.45 GHz

	gap [mm]	**Input power [mW]**	$SAR_{10g}[W/kg]$
Breast	10	110	1.84
Head	5	68	1.9
Arm	10	170	1.92

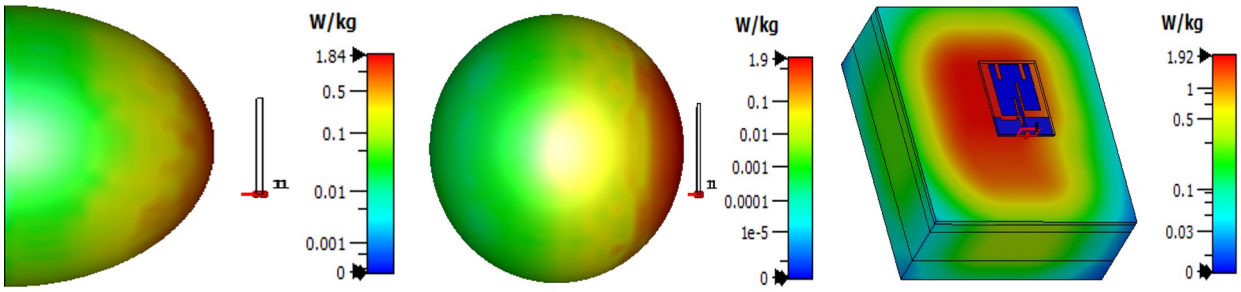

(a) (b) (c)

Figure 4.26: Simulated SAR_{10g} at a frequency of 2.45 GHz: (a) Breast phantom model, (b) Head phantom model, and (c) arm phantom model.

Table 4.8: A comparison between the CPPMA proposed in the current research and some recently published antennas

Ref.	**Application**	**The used technique for pathological tissues detection**	**Substrate and dimensions (mm^3)**	**Circular Polar.**	**Frequency band (GHz)**	**SAR evaluation**
[196]	Body centric communications	-	RO4003 $42 \times 30 \times 0.813$	No	2.4 - 12	Not reported
[197]	Breast tumors detection	Scattering imaging	Air-gap $40 \times 25 \times 10.5$	No	1.67 - 1.74	Not reported
[198]	Breast tumors detection	-	RO4003 $40 \times 40 \times 1.54$	No	0.49 - 0.56	Not reported
[199]	Wireless body area network	-	RT-Duroid 5880 $34.4 \times 34.4 \times 4$	Yes	5.27 - 6.37	SAR evaluated on human body
[200]	Head imaging	Scattering parameters and Near field directivity	RO4350B $50 \times 44 \times 1.524$	No	1.70 - 3.71	SAR evaluated on head
[201]	Wireless body area network	-	Denim $50 \times 44 \times 0.7$	No	2.27 - 3.42	SAR evaluated on human body arm
This work	**Tumor detection, Brain stroke detection and Health monitoring remote**	**Resonance frequency shift, current density, E-Field and H-Field distribution**	**FR-4 $34 \times 28 \times 1.5$**	**Yes**	**2.425 - 2.475**	**SAR evaluated on breast, head, and human body arm**

4.6 Conclusion

A monostatic narrow-band CPPMA designed for medical MI and health-monitoring applications is presented in this chapter. The CPPMA prototype, measuring $34 \times 28 \times 1.5$ mm^3,

has been successfully created and printed on an economical FR-4 substrate. Experimental measurements reveal that the manufactured prototype operates within a narrow-band of 195 MHz (2.32–2.515 GHz). Furthermore, the CPPMA design demonstrates CP within the band of 2.4386-2.4633 GHz. Several phantom models were used to validate CPPMA's capability to detect brain strokes and breast cancers.

Additionally, the practical applicability of the designed CPPMA for health-monitoring wearable applications was experimentally validated. The comprehensive outcomes validate the efficacy and versatility of the designed CPPMA for a variety of biomedical applications.

General Conclusion

Continuous innovation characterizes the development of antennas in medical applications, driven by the demand for more accurate, less invasive, and patient-oriented healthcare solutions. With ongoing technological progress, we anticipate further improvements in antenna design and applications, significantly influencing the future landscape of medical diagnostics, treatments, and monitoring.

Numerous antennas have been documented for use in biomedical applications; however, these antennas exhibit linear polarization and are specifically designed for singular purposes, such as stroke detection, cancer screening, or health monitoring. Consequently, there is a need for innovative, high-performance antennas suitable for various biomedical applications. The primary goal of this thesis is to develop a new CP antenna crafted specifically for biomedical purposes, including applications like microwave medical imaging and health monitoring. This antenna is distinguished by its compact size, consistent radiation pattern ensuring optimal gain and efficiency, heightened sensitivity for precise detection of tumor and stroke locations and sizes, as well as the ability to penetrate the body to the greatest possible depth.

In the initial chapter, fundamental principles regarding antennas have been presented, encompassing attributes such as radiation pattern, reflection coefficient, directivity, gain, and more. There is a general description of microstrip antennas, exploring their strengths and limitations, applications, feeding techniques, and radiation mechanisms. The chapter concludes with a brief summary of various methods for analyzing microstrip antennas.

In the second chapter, a thorough examination of the theoretical aspects and challenges linked to the interaction between antennas and the human body has been carried out. Moreover, we investigated how antenna performance changes when a human body is in close proximity, along with exploring the effects of radiation emitted by antennas on the human body. Additionally, we delved into the simulation of models for phantoms, which find applications in both computational software and experimental validation. The existing body of literature reveals a diverse range of phantom sizes, configurations, materials, and levels of realism. These varia-

tions are influenced by factors such as antenna placement within and near the body, precision requirements, and the computational tools available.

In the third chapter, we have clarified basic principles related to the use of antennas in the field of bio-medicine. Starting with broad insights into the application of biomedical antennas, we then examined their particular uses, including medical microwave imaging, biomedical telemetry, and therapeutic interventions. This exploration highlights the transformative possibilities of biomedical antennas, opening the door to innovative advancements that have the potential to revolutionize patient care and medical procedures.

In the fourth chapter, we have introduced a monostatic narrow-band CPPMA tailored for applications in medical MI and health-monitoring. The designed CPPMA, with dimensions of $34 \times 28 \times 1.5$ mm^3, has been successfully manufactured and printed using a cost-effective FR-4 substrate. The obtained measurements reveal that the prototype operates within a narrow bandwidth of 195 MHz (2.32 – 2.515 GHz). Additionally, the CPPMA, as envisioned, displays CP within the frequency band of 2.4386 - 2.4633 GHz. The ability of the CPPMA to detect brain strokes and breast tumors was confirmed using various phantom models. diverse phantom models. Moreover, the practicality of deploying the proposed CPPMA in health-monitoring wearable applications was experimentally affirmed. The overall findings confirm the efficacy and versatility of the proposed CPPMA across various biomedical applications.

Perspectives

The progress achieved in this thesis should be seen as an advancement in implementing novel medical devices. However, numerous opportunities for future research exist in the domains of both medical microwave imaging and health monitoring applications. Encouraging perspectives can be envisioned for further exploration:

- The integration of antennas with other advanced technologies, such as artificial intelligence and machine learning, could lead to more intelligent and responsive medical devices. This could improve real-time data analysis, diagnostics, and personalized healthcare.
- Integration with other imaging modalities, such as MRI or PET, may provide a more comprehensive understanding of physiological processes. Combining multiple modalities can enhance diagnostic capabilities.
- Development of flexible and stretchable antenna designs could enhance comfort and versatility in wearable health monitoring devices. Such antennas could conform to the body's

shape and movement, enabling continuous monitoring without discomfort.

- The integration of antennas with 5G technology is expected to provide faster and more reliable communication in health monitoring applications. This could support high-bandwidth data transmission, enabling seamless connectivity between medical devices and healthcare systems.

Bibliography

[1] Anupma Gupta, Ankush Kansal, and Paras Chawla. "a survey and classification on applications of antenna in health care domain: data transmission, diagnosis and treatment". *Sādhanā*, 46:1–17, 2021.

[2] Koichi Ito. "compelling challenges in antenna technologies for future medical applications". *Engineering*, 11:15–17, 2022.

[3] Wenyi Shao and Todd McCollough. "advances in microwave near-field imaging: Prototypes, systems, and applications". *IEEE microwave magazine*, 21(5):94–119, 2020.

[4] Carmen Camara, Pedro Peris-Lopez, and Juan E Tapiador. "security and privacy issues in implantable medical devices: A comprehensive survey". *Journal of biomedical informatics*, 55:272–289, 2015.

[5] Silvia Gallucci, Marta Bonato, Emma Chiaramello, Serena Fiocchi, Gabriella Tognola, and Marta Parazzini. "human exposure assessment to wearable antennas: Effect of position and interindividual anatomical variability". *International Journal of Environmental Research and Public Health*, 19(10):5877, 2022.

[6] John Leonidas Volakis and John Leonidas Volakis. *"Antenna engineering handbook"*, volume 1755. McGraw-hill New York, 2007.

[7] Constantine A Balanis. *"Antenna theory: analysis and design"*. John wiley & sons, 2016.

[8] Mohammed GUERROUI. *"Conception d'une nouvelle antenne pour une application GPR"*. PhD thesis, Université 8 Mai 1945 Guelma, 2022.

[9] Steven Shichang Gao, Qi Luo, and Fuguo Zhu. *"Circularly polarized antennas"*. John Wiley & Sons, 2014.

[10] David M Pozar. *"Microwave engineering"*. John wiley & sons, 2011.

[11] Elham Ebrahimi. *"Wideband and reconfigurable antennas for emerging wireless networks"*. PhD thesis, University of Birmingham, 2012.

[12] Abdelhalim Chaabane. *"Conception d'une antenne bip large bande a fort gain"*. PhD thesis, Université Ferhat Abbas, 2017.

[13] Irfan Ali Tunio. *"Study of impedance matching in antenna arrays"*. PhD thesis, Université de Nantes, 2020.

[14] Hubregt J Visser. *"Antenna theory and applications"*. John Wiley & Sons, 2012.

[15] Nicolas Mézières. *"Contributions to fast and accurate antenna characterization"*. PhD thesis, Université Rennes 1, 2021.

[16] JEM Engineering. "introduction to antenna polarization", October 2020. Accessed: 22/06/2023.

[17] Anuj Mehta. "microstrip antenna". *International Journal of Scientific and Technology Research*, 4, 03 2015.

[18] Nasimuddin Nasimuddin. *"Microstrip antennas"*. BoD–Books on Demand, 2011.

[19] R. B. Waterhouse. *"Microstrip Patch Antennas: A Designer's Guide"*. Kluwer Academic Publishers Boston, 2003.

[20] David R Jackson and Stuart A Long. "history of microstrip and dielectric resonator antennas". In *2020 14th European Conference on Antennas and Propagation (EuCAP)*, pages 1–5. IEEE, 2020.

[21] Udit Raithatha and S Sreenath Kashyap. "microstrip patch antenna parameters, feeding techniques & shapes of the patch–a survey". *International Journal of Scientific & Engineering Research*, 6(4), 2015.

[22] Anushi Arora, Aditya Khemchandani, Yash Rawat, Shashank Singhai, and Gaurav Chaitanya. "comparative study of different feeding techniques for rectangular microstrip patch antenna". *International Journal of Innovative research in electrical, electronics, instrumentation and control Engineering*, 3(5):32–35, 2015.

[23] S Sibi Chakravarthy, N Sarveshwaran, S Sriharini, and M Shanmugapriya. "comparative study on different feeding techniques of rectangular patch antenna". In *2016 Thirteenth International Conference on Wireless and Optical Communications Networks (WOCN)*, pages 1–6. IEEE, 2016.

[24] T Kshitija, S Ramakrishna, Suhas B Shirol, and Priyatam Kumar. "micro-strip patch antenna using various types of feeding techniques: An implementation". In *2019 International Conference on Intelligent Sustainable Systems (ICISS)*, pages 318–322. IEEE, 2019.

[25] Ali Giuma F Esseid. *"A Novel Design of Broadband Antennas with a Defected Radiating Patch Structure for Wireless Communication Systems"*. PhD thesis, Florida Institute of Technology, 2020.

[26] Hemant Kumar Varshney, Mukesh Kumar, AK Jaiswal, Rohini Saxena, and Komal Jaiswal. "a survey on different feeding techniques of rectangular microstrip patch antenna". *International Journal of Current Engineering and Technology*, 4(3):1418–1423, 2014.

[27] Muneer Khan and Anil Chaurasia. "design of ultra-wideband microstrip patch antenna". In *Conference Paper. November*, 2018.

[28] Dalia M Elsheakh, Esmat A Abdallah, et al. "different feeding techniques of microstrip patch antennas with spiral defected ground structure for size reduction and ultra-wide band operation". *Journal of Electromagnetic Analysis and Applications*, 4(1):410–418, 2012.

[29] S.M. Bahloul and Mehadji Abri. *"Étude et conception de réseaux d'antennes imprimées larges bandes à polarisation diverse par l'utilisation d'architectures log périodiques"*. PhD thesis, Université Aboubakr Belkaïd,Tlemcen, 02 2017.

[30] DSS Satyanarayana and A Bathula. "aperture coupled microstrip antenna design and analysis using matlab". *Int. J. Eng. Res. Technol.(IJERT)*, 8(06):2278–0181, 2019.

[31] David M Pozar et al. "a review of aperture coupled microstrip antennas: History, operation, development, and applications". *University of Massachusetts at Amherst*, pages 1–9, 1996.

[32] Djelloul AISSAOUI. *"Etude et Conception d'Antennes Fractales pour des Applications Ultra-Large-Bande"*. PhD thesis, Université de Tlemcen-Abou Bekr Belkaid.

[33] Amit Kumar, Jaspreet Kaur, and Rajinder Singh. "performance analysis of different feeding techniques". *International journal of emerging technology and advanced engineering*, 3(3):884–890, 2013.

[34] Debajyoti Chatterjee and Anjan Kumar Kundu. "performance analysis and comparative study of microstrip patch antenna using aperture coupled and proximity coupled feeding methodology". In *2017 International Conference on Computer, Communication and Signal Processing (ICCCSP)*, pages 1–7. IEEE, 2017.

[35] Aissa ATTOUI. *"Contribution A L'étude Des Déphaseurs Micro Rubans Applications Aux Réseaux D'antennes Imprimées"*. PhD thesis, Université 8 Mai 1945 Guelma, 2018.

[36] Anil Pandey. *"Practical microstrip and printed antenna design"*. Artech House, 2019.

[37] Rashmi Roges and Praveen Kumar Malik. "planar and printed antennas for internet of things-enabled environment: Opportunities and challenges". *International Journal of Communication Systems*, 34(15):e4940, 2021.

[38] Nageswara Lalam and Maitri Somani Bangard. "wireless reception for microcontroller based sensor networks". *International Journal of Advanced Computational Engineering and Networking*, 1(10):2320–2106, 2013.

[39] Murthy S Chavali and Maria P Nikolova. "metal oxide nanoparticles and their applications in nanotechnology". *SN applied sciences*, 1(6):607, 2019.

[40] C. A. Balanis. "microstrip antennas: Analysis, design, and application". In *Modern Antenna Handbook*, pages 157–200. Wiley, 2008.

[41] Girish Kumar and Kamala Prasan Ray. *"Broadband microstrip antennas"*. Artech house, 2002.

[42] Y Lo, D Solomon, and W Richards. "theory and experiment on microstrip antennas". *IEEE transactions on Antennas and Propagation*, 27(2):137–145, 1979.

[43] Keith Carver and James Mink. "microstrip antenna technology". *IEEE transactions on antennas and propagation*, 29(1):2–24, 1981.

[44] Ranjan Mishra. "an overview of microstrip antenna". *HCTL Open International Journal of Technology Innovations and Research (IJTIR)*, 21(2):39–55, 2016.

[45] A Habibzadeh Sharif and M Soleimani. "accurate analysis and design of circularly polarized dual-feed microstrip array antenna using multiport network model". In *2005 Asia-Pacific Conference on Applied Electromagnetics*, pages 5–pp. IEEE, 2005.

[46] Goker Sener, Lale Alatan, and Mustafa Kuzuoglu. "design of irregularly shaped patch antennas by using the multiport network model". In *2008 IEEE Antennas and Propagation Society International Symposium*, pages 1–4. IEEE, 2008.

[47] Yi Huang and Kevin Boyle. "from theory to practice", 2008.

[48] Adnan Saghir. *"Contribution à la caractérisation des structures rayonnantes. Application aux études en champ proche de rayonnement électromagnétique"*. PhD thesis, Institut National Polytechnique de Toulouse-INPT, 2013.

[49] Govind Arora, Paramjot Maman, Ameya Sharma, Nitin Verma, and Vivek Puri. "systemic overview of microstrip patch antenna's for different biomedical applications". *Advanced Pharmaceutical Bulletin*, 11(3):439, 2021.

[50] Sarmad Nozad Mahmood, Asnor Juraiza Ishak, Alyani Ismail, Azura Che Soh, Zahriladha Zakaria, and Sameer Alani. "on-off body ultra-wideband (uwb) antenna for wireless body area networks (wban): a review". *IEEE Access*, 8:150844–150863, 2020.

[51] Daphne Anne Pollacco. "microwave medical imaging". *May*, 2016.

[52] Md Mohiuddin Soliman, Muhammad EH Chowdhury, Amith Khandakar, Mohammad Tariqul Islam, Yazan Qiblawey, Farayi Musharavati, and Erfan Zal Nezhad. "review on medical implantable antenna technology and imminent research challenges". *Sensors*, 21(9):3163, 2021.

[53] Xuyang Li. *"Body matched antennas for microwave medical applications"*, volume 72. KIT Scientific Publishing, 2014.

[54] Leena Ukkonen, Lauri Sydänheimo, Toni Björninen, and Shubin Ma. "antennas and wireless power transfer for brain-implantable sensors". *Antenna and Sensor Technologies in Modern Medical Applications*, pages 91–143, 2021.

[55] Francesco Merli. "implantable antennas for biomedical applications". Technical report, EPFL, 2011.

[56] Aleix Garcia Miquel. "antenna design and characterization for biomedical applications". Phd thesis, University of Barcelona, 2018.

[57] Camelia Gabriel, Sami Gabriel, and YE Corthout. "the dielectric properties of biological tissues: I. literature survey". *Physics in medicine & biology*, 41(11):2231, 1996.

[58] Parisa Zakavi, Nemai Chandra Karmakar, and Ian Griggs. "wireless orthopedic pin for bone healing and growth: Antenna development". *IEEE transactions on antennas and propagation*, 58(12):4069–4074, 2010.

[59] Rula Alrawashdeh. *"Implantable antennas for biomedical applications"*. PhD thesis, University of Liverpool, 2015.

[60] Asimina Kiourti and Konstantina S Nikita. "miniature scalp-implantable antennas for telemetry in the mics and ism bands: Design, safety considerations and link budget analysis". *IEEE Transactions on antennas and propagation*, 60(8):3568–3575, 2012.

[61] Nabeel Ahmed Malik. "design of implantable antennas for biomedical applications". Phd thesis, University of Bedfordshire, 2022.

[62] Simon R Saunders and Alejandro Aragón-Zavala. *"Antennas and propagation for wireless communication systems"*. John Wiley & Sons, 2007.

[63] R Moore. "effects of a surrounding conducting medium on antenna analysis". *IEEE Transactions on Antennas and Propagation*, 11(3):216–225, 1963.

[64] C Tsao. "radiation resistance of antennas in lossy media". *IEEE Transactions on Antennas and Propagation*, 19(3):443–444, 1971.

[65] Sung Chae, Sang Won Choi, and Sae-Young Chung. Optimal multiplexing gain of k-user line-of-sight interference channels with polarization. pages 288 – 293, 11 2009.

[66] Wen-Tzu Chen and H-R Chuang. "human body coupling effects on radiation characteristics of superquadric loop antennas for pagers' application". In *IEEE Antennas and Propagation Society International Symposium 1997. Digest*, volume 2, pages 1190–1193. IEEE, 1997.

[67] Masood Ur-Rehman, Qammer Hussain Abbasi, Xiaodong Chen, and Zhinong Ying. "numerical modelling of human body for bluetooth body-worn applications". *Progress In Electromagnetics Research*, 143:623–639, 2013.

[68] Anas Abdu, Hong-Xing Zheng, and Adamu Halilu Jabire. "examining the effect of human body to the performance of antenna in wireless body area network". *ATBU Journal of Science, Technology and Education*, 7(2):202–209, 2019.

[69] Usman Ali, Sadiq Ullah, Babar Kamal, Ladislau Matekovits, Amir Altaf, et al. "design, analysis and applications of wearable antennas: A review". *IEEE ACCESS*, 11:14458–14486, 2023.

[70] Naoto Kogo and Tetsuomi Ikeda. "effect of human body on antenna performance of transceiver for push-to-talk communication line in vhf and uhf bands". In *2012 IEEE International Workshop on Antenna Technology (iWAT)*, pages 197–200. IEEE, 2012.

[71] Nikta Pournoori. "antenna development in brain-implantable biotelemetric systems for next-generation of human healthcare". Phd thesis, Faculty of Medicine and Health Technology of Tampere University, Finland, 2023.

[72] Denys Nikolayev, Maxim Zhadobov, and Ronan Sauleau. "impact of tissue electromagnetic properties on radiation performance of in-body antennas". *IEEE Antennas and Wireless Propagation Letters*, 17(8):1440–1444, 2018.

[73] International Agency for Research on Cancer, International Agency for Research on Cancer, et al. "non-ionizing radiation, part 2: radiofrequency electromagnetic fields". *IARC monographs on the evaluation of carcinogenic risks to humans*, 102(PT 2):1–460, 2013.

[74] Md Kamal Hosain, Abbas Z Kouzani, Susannah J Tye, Osama A Abulseoud, Andrew Amiet, Amir Galehdar, Akif Kaynak, and Michael Berk. "development of a compact rectenna for wireless powering of a head-mountable deep brain stimulation device". *IEEE journal of translational engineering in health and medicine*, 2:1–13, 2014.

[75] Bilal Guetaf, Abdelhalim Chaabane, Abderrezak Khalfallaoui, and Hussein Attia. "narrow-band circularly polarized antenna for medical microwave imaging and health monitoring applications". *Applied Computational Electromagnetics Society Journal*, 38(6), 2023.

[76] Tayaallen Ramachandran, Mohammad Rashed Iqbal Faruque, and Mohammad Tariqul Islam. "specific absorption rate reduction for sub-6 frequency range using polarization dependent metamaterial with high effective medium ratio". *Scientific reports*, 12(1):1803, 2022.

[77] Brogan T McWilliams, Emily E Schnell, Sergio Curto, Thomas M Fahrbach, and Punit Prakash. "a directional interstitial antenna for microwave tissue ablation: Theoretical and experimental investigation". *IEEE Transactions on Biomedical Engineering*, 62(9):2144–2150, 2015.

[78] Harry H Pennes. "analysis of tissue and arterial blood temperatures in the resting human forearm". *Journal of applied physiology*, 1(2):93–122, 1948.

[79] Arthur W Astrin, Huan-Bang Li, and Ryuji Kohno. "standardization for body area networks". *IEICE transactions on communications*, 92(2):366–372, 2009.

[80] Eric Y Chow, Milton M Morris, and Pedro P Irazoqui. "implantable rf medical devices: The benefits of high-speed communication and much greater communication distances in biomedical applications". *IEEE Microwave Magazine*, 14(4):64–73, 2013.

[81] Huseyin S Savci, Ahmet Sula, Zheng Wang, Numan S Dogan, and Ercument Arvas. "mics transceivers: regulatory standards and applications [medical implant communications service]". In *Proceedings. IEEE SoutheastCon, 2005.*, pages 179–182. IEEE, 2005.

[82] Mohd Noor Islam and Mehmet R Yuce. "review of medical implant communication system (mics) band and network". *Ict Express*, 2(4):188–194, 2016.

[83] Shuoliang Ding. *"Design of a Power-Efficient Radiative Wireless System for Autonomous Biomedical Implants"*. PhD thesis, Université Paris-Saclay, 2021.

[84] Fish & Richardson. *"Wireless Medical Technologies: Navigating Government Regulation in the New Medical Age"*. Fish & Richardson, Boston, MA, USA, 2017.

[85] Electronic Communications Committee. "erc recommendation (70-03) on relating to the use of short range devices (srd), subsequent amendments 12 february 2021", 2021. Accessed on 08 October 2023.

[86] Gurveer Kaur, Amandeep Kaur, Gurpreet Kaur Toor, Balwinder S Dhaliwal, and Shyam Sundar Pattnaik. "antennas for biomedical applications". *Biomedical Engineering Letters*, 5:203–212, 2015.

[87] Botswana Communications Regulatory Authority. "technical specification for medical applications". Document Number: TS0048, Revision: Original V1, 2015. Accessed on 09 October 2023.

[88] Electronic Communications Committee Working Group Spectrum Engineering (WG SE). "ecc report 267: Coexistence of wideband ultra-low power wireless medical capsule endoscopy application operating in the frequency band 430-440 mhz". Approved 29 September 2017, 2017. Accessed on 09 October 2023.

[89] Zlatko Živković, Ema Vujević, Dragan Poljak, Khalil El Khamlichi Drissi, and Antonio Šarolić. "computation of sar in the simplified model of a pregnant woman exposed to rf radiation from 10 mhz to 1800 mhz". In *2013 21st International Conference on Software, Telecommunications and Computer Networks-(SoftCOM 2013)*, pages 1–5. IEEE, 2013.

[90] Asimina Kiourti and Konstantina S Nikita. "detuning issues and performance of a novel implantable antenna for telemetry applications". In *2012 6th European Conference on Antennas and Propagation (EUCAP)*, pages 746–749. IEEE, 2012.

[91] Samah Mustafa, Amin M Abbosh, and Phong Thanh Nguyen. "modeling human head tissues using fourth-order debye model in convolution-based three-dimensional finite-difference time-domain". *IEEE Transactions on Antennas and propagation*, 62(3):1354–1361, 2014.

[92] Andrew K Martusevich, Elena S Golygina, Vladimir V Nazarov, Ivan V Bocharin, Inessa A Minenko, and Mikhail Yu Artamonov. "dielectric properties of the tissues with different histological structure: Ex vivo study". *Journal of Experimental Biology and Agricultural Sciences*, 10(2):451–455, 2022.

[93] Ronald Pethig. "dielectric properties of body tissues". *Clinical Physics and Physiological Measurement*, 8(4A):5, 1987.

[94] Yongjun Lu, Hongming Cui, Jue Yu, and Satoru Mashimo. "dielectric properties of human fetal organ tissues at radio frequencies". *Bioelectromagnetics: Journal of the Bioelectromagnetics Society, The Society for Physical Regulation in Biology and Medicine, The European Bioelectromagnetics Association*, 17(5):425–426, 1996.

[95] C. Gabriel. "dielectric properties of biological tissue: variation with age". *Bioelectromagnetics*, Suppl 7:S12–S18, 2005.

[96] Camelia Gabriel and Azadeh Peyman. "dielectric properties of biological tissues; variation with age". *Conn's Handbook of Models for Human Aging*, pages 939–952, 2018.

[97] S Cruciani, V De Santis, M Feliziani, and Francescaromana Maradei. "cole-cole vs debye models for the assessment of electromagnetic fields inside biological tissues produced by wideband emf sources". In *2012 Asia-Pacific Symposium on Electromagnetic Compatibility*, pages 685–688. IEEE, 2012.

[98] Mohammed A Eleiwa and Atef Z Elsherbeni. "debye constants for biological tissues from 30 hz to 20 ghz". *Applied Computational Electromagnetics Society Journal*, 16(3):202–213, 2001.

[99] Koichi Ito, Chia-Heisn Lin, and Ho-Yu Lin. "evaluation of wearable and implantable antennas with human phantoms". In *Handbook of antenna technologies*, pages 2239–2268. Springer, 2016.

[100] Leslie A Geddes and Lee E Baker. "the specific resistance of biological material—a compendium of data for the biomedical engineer and physiologist". *Medical and biological engineering*, 5:271–293, 1967.

[101] K. R. Foster and H. P. Schwan. "dielectric properties of tissues and biological materials: a critical review". *Critical Reviews in Biomedical Engineering*, 17(1):25–104, 1989.

[102] Chia-Hsien Lin and Koichi Ito. "a compact dual-mode wearable antenna for body-centric wireless communications". *Electronics*, 3(3):398–408, 2014.

[103] Tarakeswar Shaw, Gopinath Samanta, Debasis Mitra, Bappaditya Mandal, and Robin Augustine. "design of metamaterial based efficient wireless power transfer system utilizing antenna topology for wearable devices". *Sensors*, 21(10):3448, 2021.

[104] Md Amanath Ullah, Mohammad Tariqul Islam, Touhidul Alam, and Farhad Bin Ashraf. "based flexible antenna for wearable telemedicine applications at 2.4 ghz ism band". *Sensors*, 18(12):4214, 2018.

[105] Tejinderpal Singh, Simranjit Singh, Mandeep Singh, and Rajbir Kaur. "design of patch antenna to detect brain tumor". In *2019 International Conference on Issues and Challenges in Intelligent Computing Techniques (ICICT)*, volume 1, pages 1–6. IEEE, 2019.

[106] Kabir Hossain, Thennarasan Sabapathy, Muzammil Jusoh, Shen-Han Lee, Khairul Shakir Ab Rahman, and Muhammad Ramlee Kamarudin. "negative index metamaterial-based frequency-reconfigurable textile cpw antenna for microwave imaging of breast cancer". *Sensors*, 22(4):1626, 2022.

[107] "mit space, cst online: Common tools for bio-models". `https://space.mit.edu/RADIO/CST_online/mergedProjects/3D/common_tools/common_tools_biomodels.htm`. Accessed on [01/11/2023].

[108] Banafsheh Khalesi, Bilal Khalid, Navid Ghavami, Giovanni Raspa, Mohammad Ghavami, Sandra Dudley-McEvoy, and Gianluigi Tiberi. "a microwave imaging procedure for lung lesion detection: Preliminary results on multilayer phantoms". *Electronics*, 11(13):2105, 2022.

[109] Sandra Costanzo, Vincenzo Cioffi, Adil Masoud Qureshi, and Antonio Borgia. "gel-like human mimicking phantoms: Realization procedure, dielectric characterization and experimental validations on microwave wearable body sensors". *Biosensors*, 11(4):111, 2021.

[110] Sara Azizian Amiri, Pieter Van Berckel, Marco Lai, Jenny Dankelman, and Benno HW Hendriks. "tissue-mimicking phantom materials with tunable optical properties suitable for assessment of diffuse reflectance spectroscopy during electrosurgery". *Biomedical Optics Express*, 13(5):2616–2643, 2022.

[111] Ahmed T Mobashsher and Amin M Abbosh. "artificial human phantoms: Human proxy in testing microwave apparatuses that have electromagnetic interaction with the human body". *IEEE Microwave Magazine*, 16(6):42–62, 2015.

[112] Rosa Scapaticci, Vanni Lopresto, Rosanna Pinto, Marta Cavagnaro, and Lorenzo Crocco. "monitoring thermal ablation via microwave tomography: An ex vivo experimental assessment". *Diagnostics*, 8(4):81, 2018.

[113] Abdullah J Alazemi and Amjad Iqbal. "a compact and wideband mimo antenna for high-data-rate biomedical ingestible capsules". *Scientific Reports*, 12(1):14290, 2022.

[114] Khaled Aliqab, Iram Nadeem, and Sadeque Reza Khan. "a comprehensive review of in-body biomedical antennas: Design, challenges and applications". *Micromachines*, 14(7):1472, 2023.

[115] Umair Rafique, Stefano Pisa, Renato Cicchetti, Orlandino Testa, and Marta Cavagnaro. "ultra-wideband antennas for biomedical imaging applications: A survey". *Sensors*, 22(9):3230, 2022.

[116] Minu Sethi and SK Chakarvarti. "hyperthermia techniques for cancer treatment: A review". *Int. J. PharmTech Res*, 8(6):292–299, 2015.

[117] Nathaniel D Kwok, Dominique Thomas, and Bilal Chughtai. "transurethral microwave thermotherapy for treatment of benign prostatic hyperplasia". In *A Comprehensive Guide to the Prostate*, pages 131–141. Elsevier, 2018.

[118] Punit Prakash. "microwave ablation: Physical principles and technology". In *Principles and Technologies for Electromagnetic Energy Based Therapies*, pages 139–167. Elsevier, 2022.

[119] Rim Negra, Imen Jemili, and Abdelfettah Belghith. "wireless body area networks: Applications and technologies". *Procedia Computer Science*, 83:1274–1281, 2016.

[120] GK Ragesh and K Baskaran. "an overview of applications, standards and challenges in futuristic wireless body area networks". *International Journal of Computer Science Issues (IJCSI)*, 9(1):180, 2012.

[121] Muhammad Aamir Panhwar, Samiullah Jatoi, KA Memon, and Salahuddin Saddar. "wireless body area networks: architecture, standards, challenges, and applications". *International Journal of Computer Science and Network Security*, 19(12):173–178, 2019.

[122] Mark A Haidekker. "medical imaging technology", Springer Briefs in Physics ,2013. https://doi.org/10.1007/978-1-4614-7073-1.

[123] Maged A Aldhaeebi, Khawla Alzoubi, Thamer S Almoneef, Saeed M Bamatraf, Hussein Attia, and Omar M Ramahi. "review of microwaves techniques for breast cancer detection". *Sensors*, 20(8):2390, 2020.

[124] Deepshikha Bhargava and Phadungsak Rattanadecho. "microwave imaging of breast cancer: Simulation analysis of sar and temperature in tumors for different age and type". *Case Studies in Thermal Engineering*, 31:101843, 2022.

[125] Xu Li and Susan C Hagness. "a confocal microwave imaging algorithm for breast cancer detection". *IEEE Microwave and wireless components letters*, 11(3):130–132, 2001.

[126] Jeff M Sill and Elise C Fear. "tissue sensing adaptive radar for breast cancer detection—experimental investigation of simple tumor models". *IEEE Transactions on Microwave theory and Techniques*, 53(11):3312–3319, 2005.

[127] Zubaida Abdul-Sattar. *"Experimental analysis on effectiveness of confocal algorithm for radar based breast cancer detection"*. PhD thesis, Durham University, 2012.

[128] Ali Recai Celik, Muhammed Bahaddin Kurt, and Selcuk Helhel. "design of an elliptical planar monopole antenna for using in radar-based and ultra-wideband microwave imaging system". *International Research Journal of Engineering and Technology*, 4(11):1978–1983, 2017.

[129] Nour AlSawaftah, Salma El-Abed, Salam Dhou, and Amer Zakaria. "microwave imaging for early breast cancer detection: Current state, challenges, and future directions". *Journal of Imaging*, 8(5):123, 2022.

[130] Paul M Meaney, Margaret W Fanning, Timothy Raynolds, Colleen J Fox, Qianqian Fang, Christine A Kogel, Steven P Poplack, and Keith D Paulsen. "initial clinical experience with microwave breast imaging in women with normal mammography". *Academic radiology*, 14(2):207–218, 2007.

[131] Paul M Meaney, Margaret W Fanning, Roberta M di Florio-Alexander, Peter A Kaufman, Shireen D Geimer, Tian Zhou, and Keith D Paulsen. "microwave tomography in the context of complex breast cancer imaging". In *2010 Annual International Conference of the IEEE Engineering in Medicine and Biology*, pages 3398–3401. IEEE, 2010.

[132] R Benjamin. "synthetic, post-reception focusing in near-field radar". EUREL International Conference (Conf. Publ. No. 431) The Detection of Abandoned Land Mines: A Humanitarian Imperative Seeking a Technical Solution, pp. 133-137. October 1996.

[133] Susan C Hagness, Allen Taflove, and Jack E Bridges. "two-dimensional fdtd analysis of a pulsed microwave confocal system for breast cancer detection: Fixed-focus and antenna-array sensors". *IEEE transactions on biomedical engineering*, 45(12):1470–1479, 1998.

[134] Elise C Fear, Jeremie Bourqui, Charlotte Curtis, Daphne Mew, B Docktor, and C Romano. "microwave breast imaging with a monostatic radar-based system: A study of application to patients". *IEEE transactions on microwave theory and techniques*, 61(5):2119–2128, 2013.

[135] Jeremie Bourqui, Jeff M Sill, and Elise C Fear. "a prototype system for measuring microwave frequency reflections from the breast". *Journal of Biomedical Imaging*, 2012:9–9, 2012.

[136] Maciej Klemm, Ian Craddock, Jack Leendertz, Alan Preece, and Ralph Benjamin. "experimental and clinical results of breast cancer detection using uwb microwave radar". In *2008 IEEE Antennas and Propagation Society International Symposium*, pages 1–4. IEEE, 2008.

[137] Alexander V Tarakanov, Elena S Ladanova, Alexander A Lebedenko, Tatyana D Tarakanova, Sergey G Vesnin, Tatyana Kharybina, and Igor I Goryanin. "passive microwave radiometry as a component of imaging diagnostics in juvenile idiopathic arthritis". *Rheumato*, 2(3):55–68, 2022.

[138] Sergey Vesnin, Arran K Turnbull, J Michael Dixon, and Igor Goryanin. "modern microwave thermometry for breast cancer". *J. Mol. Imaging Dyn*, 7(2):1000136, 2017.

[139] Evangelos Groumpas, Maria Koutsoupidou, Irene S Karanasiou, Charalabos Papageorgiou, and Nikolaos Uzunoglu. "real-time passive brain monitoring system using near-field microwave radiometry". *IEEE Transactions on Biomedical Engineering*, 67(1):158–165, 2019.

[140] Maria Drakopoulou, Carmen Moldovan, Konstantinos Toutouzas, and Dimitris Tousoulis. "the role of microwave radiometry in carotid artery disease. diagnostic and clinical prospective". *Current opinion in pharmacology*, 39:99–104, 2018.

[141] Katerina Laskari, Elias Siores, Maria G Tektonidou, and Petros P Sfikakis. "microwave radiometry for the diagnosis and monitoring of inflammatory arthritis". *Diagnostics*, 13(4):609, 2023.

[142] John P Crandall, Prateek Gajwani, Jeffrey P Leal, Daniel D Mawhinney, Fred Sterzer, Richard L Wahl, et al. "measurement of brown adipose tissue activity using microwave radiometry and 18f-fdg pet/ct". *Journal of Nuclear Medicine*, 59(8):1243–1248, 2018.

[143] George Pentazos, Katerina Laskari, Kleanthis Prekas, John Raftakis, Petros P Sfikakis, and Elias Siores. "microwave radiometry-derived thermal changes of small joints as additional potential biomarker in rheumatoid arthritis: a prospective pilot study". *JCR: Journal of Clinical Rheumatology*, 24(5):259–263, 2018.

[144] Evangelia Zampeli, Ioannis Raftakis, Archontoula Michelongona, Chara Nikolaou, Antonia Elezoglou, Konstantinos Toutouzas, Elias Siores, and Petros P Sfikakis. "detection of subclinical synovial inflammation by microwave radiometry". *PLoS One*, 8(5):e64606, 2013.

[145] TV Zamechnik, SI Larin, and AG Losev. "kombinirovannaya radiotermometriya kak metod issledovaniya venoznogo krovoobrashcheniya nizhnikh konechnostey [combined radio thermometry as a method of investigating of venous circulation of the lower limbs]". *Volgograd, Izd-vo VolgGMU*, 2015.

[146] Paul R Stauffer, Paolo F Maccarini, Kavitha Arunachalam, Valeria De Luca, Sara Salahi, Alina Boico, Oystein Klemetsen, Yngve Birkelund, Svein K Jacobsen, Fernando Bardati, et al. "microwave radiometry for non-invasive detection of vesicoureteral reflux (vur) following bladder warming". In *Energy-based Treatment of Tissue and Assessment VI*, volume 7901, pages 284–294. SPIE, 2011.

[147] AD Kaprin, AA Kostin, MI Andryukhin, KV Ivanenko, SV Popov, PV Shegai, DP Kruglov, F Sh Mangutov, V Yu Leushin, and SV Agasieva. "microwave radiometry in the diagnosis of various urological diseases". *Biomedical Engineering*, 53:87–91, 2019.

[148] AV Tarakanov, AA Tarakanov, S Vesnin, VV Efremov, I Goryanin, and N Roberts. "microwave radiometry (mwr) temperature measurement is related to symptom severity in patients with low back pain (lbp)". *Journal of Bodywork and Movement Therapies*, 26:548–552, 2021.

[149] Stavros Spiliopoulos, Vasiliki Theodosiadou, Nikolaos Barampoutis, Konstantinos Katsanos, Periklis Davlouros, Lazaros Reppas, Panagiotis Kitrou, Konstantinos Palialexis, Chrysostomos Konstantos, Elias Siores, et al. "multi-center feasibility study of microwave radiometry thermometry for non-invasive differential diagnosis of arterial disease in diabetic patients with suspected critical limb ischemia". *Journal of Diabetes and its Complications*, 31(7):1109–1114, 2017.

[150] Berik Emilov, Aleksander Sorokin, Meder Seiitov, Binsei Toshi Kobayashi, Tulegen Chubakov, Sergey Vesnin, Illarion Popov, Aleksandra Krylova, and Igor Goryanin. "diagnostic of patients with covid-19 pneumonia using passive medical microwave radiometry (mwr)". *Diagnostics*, 13(15):2585, 2023.

[151] Muhammad Shadi Hajar, M Omar Al-Kadri, and Harsha Kumara Kalutarage. "a survey on wireless body area networks: Architecture, security challenges and research opportunities". *Computers & Security*, 104:102211, 2021.

[152] João Manuel de Almeida Monteiro Felício. *"Antennas for Biomedical Applications: Wireless Body Area Networks and Medical Microwave Imaging"*. PhD thesis, Universidade de Lisboa, Instituto Superior Técnico, 2018.

[153] Saadat Hanif Dar. *"Optimal Flexible Antenna Designs for Future WBAN"*. PhD thesis, Department of electrical engineering, riphah international university, 2018.

[154] NHM Rais, Ping Jack Soh, F Malek, S Ahmad, NBM Hashim, and PS Hall. "a review of wearable antenna". In *2009 Loughborough antennas & propagation conference*, pages 225–228. IEEE, 2009.

[155] Dalila Laouej, Houda Daoud, and Mourad Loulou. "an ultra-low power hybrid 2nd order feed forward $\delta\sigma$ modulator design for implantable medical devices". *Analog Integrated Circuits and Signal Processing*, 108(2):277–289, 2021.

[156] Mohamad Jaafar Ali, Hassine Moungla, Mohamed Younis, and Ahmed Mehaoua. *"Interference Mitigation Techniques in Wireless Body Area Networks"*, pages 677–718. Springer International Publishing, Cham, 2019.

[157] Amor Smida, Amjad Iqbal, Abdullah J Alazemi, Mohamed I Waly, Ridha Ghayoula, and Sunghwan Kim. "wideband wearable antenna for biomedical telemetry applications". *IEEE Access*, 8:15687–15694, 2020.

[158] Amay J Bandodkar, Wenzhao Jia, and Joseph Wang. "tattoo-based wearable electrochemical devices: a review". *Electroanalysis*, 27(3):562–572, 2015.

[159] Shaimaa Mohamed Farghaly Sayed. *"Low-Power Dual-band on-body Antenna for Wireless Body Sensor Networks"*. University of Salford (United Kingdom), 2020.

[160] M. Haghjoo. "cardiac implantable electronic devices". In *Practical Cardiology*, pages 251–260. 2018.

[161] Alessandro Russo, Riccardo Serraino, Francesca Serapide, Enrico Maria Trecarichi, and Carlo Torti. "new advances in management and treatment of cardiac implantable electronic devices infections". *Infection*, pages 1–14, 2023.

[162] "icd image". `https://www.washingtonhra.com/wp-content/uploads/Figure-4-ICD-image2.jpg`. Accessed: 09/12/2023.

[163] Andres M Lozano, Nir Lipsman, Hagai Bergman, Peter Brown, Stephan Chabardes, Jin Woo Chang, Keith Matthews, Cameron C McIntyre, Thomas E Schlaepfer, Michael Schulder, et al. "deep brain stimulation: current challenges and future directions". *Nature Reviews Neurology*, 15(3):148–160, 2019.

[164] National Institute of Neurological Disorders and Stroke (NINDS). "application of deep brain stimulation with the control of an implantable biosensor by a neurostimulator". `https://www.ninds.nih.gov/about-ninds/what-we-do/impact/ninds-contributions-approved-therapies/brain-stimulation-therapies-epilepsy`. Accessed: 10/12/2023.

[165] "intrathecal drug delivery system (pain pump implant)". `https://www.soundpainalliance.com/interventional-pain-management/intrathecal-pump-implantation/`. Accessed: 11/12/2023.

[166] Marcos Luciano Bruschi. *"Strategies to modify the drug release from pharmaceutical systems"*. Woodhead Publishing, 2015.

[167] "medical illustration of a knee joint". `https://medlineplus.gov/ency/images/ency/fullsize/24352.jpg`. Accessed: 12/12/2023.

[168] "transurethral microwave therapy (tumt) image". `https://www.saintjohnscancer.org/urology/wp-content/uploads/sites/2/2022/09/Transurethral-microwave-therapy-TUMT.jpg`. Accessed: 13/12/2023.

[169] K Lalitha and J Manjula. "non-invasive microwave head imaging to detect tumors and to estimate their size and location". *Physics in Medicine*, 13:100047, 2022.

[170] Gagandeep Kaur and Amanpreet Kaur. "monostatic radar-based microwave imaging of breast tumor detection using a compact cubical dielectric resonator antenna". *Microwave and Optical Technology Letters*, 63(1):196–204, 2021.

[171] Wei He, Yejun He, Sai-Wai Wong, and Chao-Hsiang Liao. "a wideband circularly polarized s-shaped slot antenna". *International Journal of RF and Microwave Computer-Aided Engineering*, 31(5):e22612, 2021.

[172] Navneet Sharma, Anubhav Kumar, Asok De, and Rakesh K Jain. "design of compact hexagonal shaped multiband antenna for wearable and tumor detection applications". *Progress In Electromagnetics Research M*, 105(2021):205–217, 2021.

[173] R Alagee and A Assalem. "brain cancer detection using u-shaped slot vivaldi antenna and confocal radar based microwave imaging algorithm". *Am. Sci. Res. J. Eng. Technol. Sci*, 66:1–13, 2020.

[174] Md Samsuzzaman, Khalid A Fakeeh, Md Siam Talukder, Md Mahedi Hasan, Md Hasanur Rahman, Md Mottahir Alam, Mahaboob Sharief Shaik, and Mohammad Tariqul Islam. "a double hollow rectangular-shaped patch and with the slotted ground plane monopole wideband antenna for microwave head imaging applications". *International Journal of Communication Systems*, 34(16):e4958, 2021.

[175] BS Srikanth, Stuttee Bellona Gurung, S Manu, GNS Gowthami, Tanweer Ali, Sameena Pathan, et al. "a slotted uwb monopole antenna with truncated ground plane for breast cancer detection". *Alexandria Engineering Journal*, 59(5):3767–3780, 2020.

[176] Amit Baran Dey, Soumya Sundar Pattanayak, Debasis Mitra, and Wasim Arif. "investigation and design of enhanced decoupled uwb mimo antenna for wearable applications". *Microwave and Optical Technology Letters*, 63(3):845–861, 2021.

[177] Umhara Rasool Khan, Javaid A Sheikh, Shahid Bashir, and Suhaib Ahmed. "metamaterial inspired wideband on-body antenna design for bio-medical applications". *Materials Today: Proceedings*, 80:1772–1776, 2023.

[178] Hari Singh, Kunal Srivastava, Sachin Kumar, and Binod Kumar Kanaujia. "a planar dual-band antenna for ism/wearable applications". *Wireless Personal Communications*, 118:631–646, 2021.

[179] Kim Ho Yeap, Eileen Mei Foong Tan, Takefumi Hiraguri, Koon Chun Lai, and Kazuhiro Hirasawa. "a multi-band planar antenna for biomedical applications". *Frequenz*, 75(5-6):221–228, 2021.

[180] Sourav Roy and Ujjal Chakraborty. "metamaterial based dual wideband wearable antenna for wireless applications". *Wireless Personal Communications*, 106(3):1117–1133, 2019.

[181] Kai Zhang, Ping Jack Soh, and Sen Yan. "design of a compact dual-band textile antenna based on metasurface". *IEEE Transactions on Biomedical Circuits and Systems*, 16(2):211–221, 2022.

[182] Xiaoyou Lin, Yifan Chen, Zheng Gong, Boon-Chong Seet, Ling Huang, and Yilong Lu. "ultrawideband textile antenna for wearable microwave medical imaging applications". *IEEE Transactions on Antennas and Propagation*, 68(6):4238–4249, 2020.

[183] Kai Zhang, Guy AE Vandenbosch, and Sen Yan. "a novel design approach for compact wearable antennas based on metasurfaces". *IEEE Transactions on biomedical circuits and systems*, 14(4):918–927, 2020.

[184] Ondrej Fiser, Vojtech Hruby, Jan Vrba, Tomas Drizdal, Jan Tesarik, Jan Vrba Jr, and David Vrba. "uwb bowtie antenna for medical microwave imaging applications". *IEEE transactions on Antennas and Propagation*, 70(7):5357–5372, 2022.

[185] Abdelhalim Chaabane and Mohammed Guerroui. "circularly polarized ultra wideband antenna with question mark-shaped patch for ground penetrating radar applications". *Journal of applied research and technology*, 20(3):274–283, 2022.

[186] Lourdes Farrugia, P Schembri Wismayer, L Zammit Mangion, and Charles V Sammut. "accurate in vivo dielectric properties of liver from 500 mhz to 40 ghz and their correlation to ex vivo measurements". *Electromagnetic biology and medicine*, 35(4):365–373, 2016.

[187] C Garbriel. "compilation of the dielectric properties of body tissues at rf and microwave frequencies". *the US Air Force Report AFOSR-TR*, 96, 1997.

[188] Nele De Geeter, Guillaume Crevecoeur, Luc Dupré, Wim Van Hecke, and Alexander Leemans. "a dti-based model for tms using the independent impedance method with frequency-dependent tissue parameters". *Physics in Medicine & Biology*, 57(8):2169, 2012.

[189] I Rexiline Sheeba and T Jayanthy. "design and analysis of a flexible softwear antenna for tumor detection in skin and breast model". *Wireless Personal Communications*, 107:887–905, 2019.

[190] Rakesh Singh, Naina Narang, Dharmendra Singh, and Manoj Gupta. "compact wideband microstrip patch antenna design for breast cancer detection". *Defence Science Journal*, 71(3), 2021.

[191] Zahra Katbay, Sawsan Sadek, Raafat Lababidi, André Pérennec, and Marc Le Roy. "miniature antenna for breast tumor detection". In *2015 IEEE 13th International New Circuits and Systems Conference (NEWCAS)*, pages 1–4. IEEE, 2015.

[192] Rocío Ortega-Palacios, Lorenzo Leija, Arturo Vera, and MFJ Cepeda. "measurement of breast-tumor phantom dielectric properties for microwave breast cancer treatment evaluation". In *2010 7th International conference on electrical engineering computing science and automatic control*, pages 216–219. IEEE, 2010.

[193] Merih Palandoken, Caner Murat, Adnan Kaya, and Bing Zhang. "a novel 3-d printed microwave probe for ism band ablation systems of breast cancer treatment applications". *IEEE Transactions on Microwave Theory and Techniques*, 70(3):1943–1953, 2022.

[194] Md Ashikur Rahman, Md Foisal Hossain, Manjurul Ahsan Riheen, and Praveen Kumar Sekhar. "early brain stroke detection using flexible monopole antenna". *Progress In Electromagnetics Research C*, 99:99–110, 2020.

[195] Sina Kiani, Pejman Rezaei, and Mina Fakhr. "a cpw-fed wearable antenna at ism band for biomedical and wban applications". *Wireless Networks*, 27:735–745, 2021.

[196] Amin Darvazehban and Taraneh Rezaee. "ultra-wideband microstrip antenna for body centric communications". *The Applied Computational Electromagnetics Society Journal (ACES)*, pages 355–358, 2018.

[197] Md Amanath Ullah, Touhidul Alam, Mohammed Shamsul Alam, Salehin Kibria, and Mohammad Tariqul Islam. “a unidirectional 3d antenna for biomedical microwave imaging based detection of abnormality in human body”. *Microsystem Technologies*, 24:4991–4996, 2018.

[198] Maged A Aldhaeebi, Thamer S Almoneef, Hussein Attia, and Omar M Ramahi. “electrically small magnetic probe with pca for near-field microwave breast tumors detection”. *Progress In Electromagnetics Research M*, 84:177–186, 2019.

[199] Youcef Braham Chaouche, Mourad Nedil, Ismail Ben Mabrouk, and Omar M Ramahi. “a wearable circularly polarized antenna backed by amc reflector for wban communications”. *IEEE Access*, 10:12838–12852, 2022.

[200] Mohammad Islam, Muhammad Chowdhury, Amran Hossain, and Md Samsuzzaman. “a grounded coplanar waveguide-based slotted inverted delta-shaped wideband antenna for microwave head imaging”. *IEEE Access*, 8:185698 – 185724, 10 2020.

[201] Dattatreya Gopi, Phaninder Vinay Kokilagadda, Shipli Gupta, and Venkata Rama Koti Reddy Dodda. “asymmetric coplanar strip-fed textile-based wearable antenna for mban and ism band applications”. *International Journal of Numerical Modelling: Electronic Networks, Devices and Fields*, 34(6):e2920, 2021.

.